

2020:01325- Unrestricted

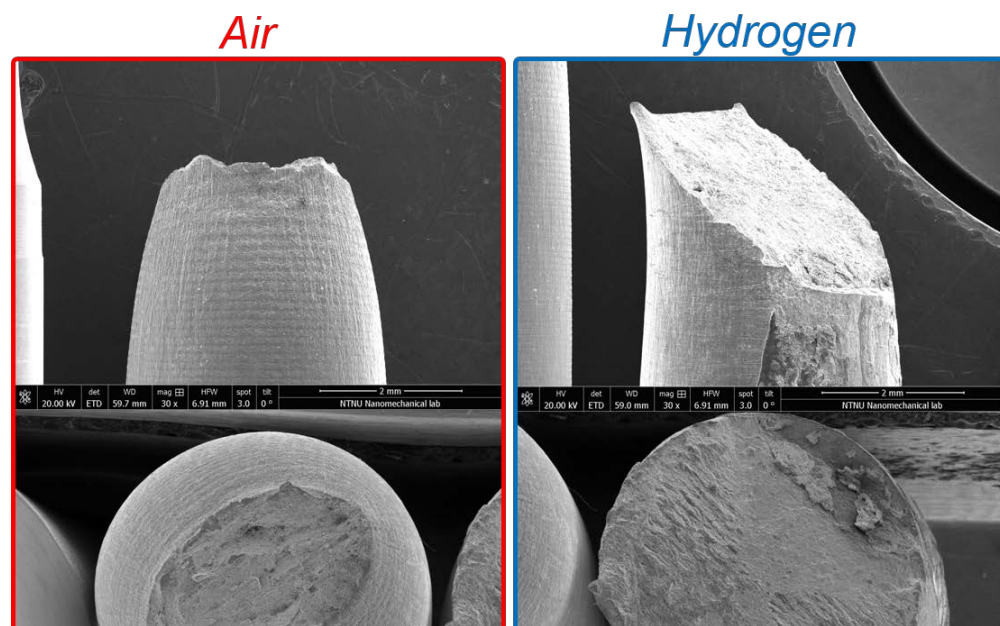
Report

Materials testing and characterization of four X60-X65 pipeline steels

Slow strain rate tensile testing of base metal and weld thermal heat affected zone material in air and in-situ H charging conditions, optical microscopy, and hardness testing (HV10).

Author(s)

Antonio Alvaro,
Anette Brocks Hagen
Malin Lervåg
Bård Nyhus
Vigdis Olden



Report

Materials testing and characterization of four X60-X65 pipeline steels

Slow strain rate tensile testing of base metal and weld thermal heat affected

KEYWORDS:

Hydrogen embrittlement
Pipeline steels
Slow strain rate tensile testing

VERSION

1.1

DATE

2021-07-02

AUTHOR(S)

Antonio Alvaro,
Anette Brocks Hagen
Malin Lervåg
Bård Nyhus
Vigdis Olden

CLIENT(S)

RCN, Gassco, Equinor, TechnipFMC, NEL, Air Liquide, Tenaris.

CLIENT'S REF.

Andreas Bratland, RCN

PROJECT NO.

102017484-5

NUMBER OF PAGES/APPENDICES:

60+ 9 Appendices


ABSTRACT

This report summarizes the main results from the slow strain rate tensile testing campaign performed within the framework of the HyLINE project. The base metals and weld simulated heat affected zones of four pipeline steels, in four different positions of the pipes, have been tested under in-situ electrochemically charged hydrogen conditions and in air as a reference. Metallurgical characterization and hardness testing has also been carried out. The two materials which showed the highest and lowest susceptibility to hydrogen embrittlement quantified through the Embrittlement Index (EI) have been the S-X65 and the T-X65 materials, respectively. The materials which revealed the highest and lowest susceptibility to hydrogen embrittlement, quantified through the Embrittlement Index (EI), were the S-X65 and the T-X65 materials, respectively. These two pipeline steels have been selected for further investigation in terms of fracture toughness and fatigue crack growth resistance both in air and in hydrogen charging conditions.

PREPARED BY

Antonio Alvaro

SIGNATURE



Antonio Alvaro (Jul 2, 2021 13:28 GMT+2)

CHECKED BY

Vigdis Olden

SIGNATURE



SINTEF Industri
SINTEF Industry

Address:
Postboks 4760 Torgarden
NO-7465 Trondheim
NORWAY
Switchboard: +47 40005100

info@sintef.no

Enterprise /VAT No:
NO 919 303 808 MVA

APPROVED BY
Ragnar Fagerberg

SIGNATURE

Ragnar Fagerberg

Ragnar Fagerberg (Jul 14, 2021 10:34 GMT+2)

REPORT NO.	ISBN	CLASSIFICATION	CLASSIFICATION THIS PAGE
2020:01325	978-82-14-06429-2	Unrestricted	Unrestricted

Document history

VERSION	DATE	VERSION DESCRIPTION
1	2020-12-03	Report of the screening testing programme
1.1	2021-07-02	Final report delivered after feedback from partners

Table of contents

1	Introduction	6
2	Materials.....	7
2.1	Metallurgical characterization	7
2.1.1	S-X65	8
2.1.1.1	Base material	8
2.1.1.2	Heat Affected Zone and Weld Metal	10
2.1.2	L – X60.....	13
2.1.2.1	Base material	13
2.1.2.2	Heat Affected Zone and weld metal	15
2.1.3	V–X65	17
2.1.3.1	Base material	17
2.1.3.2	Heat Affected zone and weld metal	19
2.1.4	T–X65	21
2.1.4.1	Base material	21
2.1.4.2	Heat Affected zone and weld metal	23
3	Slow strain rate tensile testing	26
3.1	Testing procedure	26
3.2	Base metals SSRT testing	27
3.2.1	SSRT results for base metal	28
3.2.2	Position 2 results	29
3.2.3	Position 3 results	37
3.2.4	Position 5 results	41
3.2.5	Summary of the SSRT results for base metal.....	45
3.3	Weld simulated heat affected zone.....	46
3.3.1	Weld thermal simulations	46
3.4	SSRT results for the weld thermal simulated heat affected zone materials	53
3.4.1	Summary of the SSRT results for weld thermal simulated heat affected zone material.....	60
3.5	Overall summary for the SSRT testing	60
A	As received material.....	61
A.1	S–X65	61
A.2	L–X60.....	62
A.3	V –X65.....	63

A.4	T-X65	64
B	Hardness analysis	65
B.1	S-X65	65
B.2	L-X60.....	67
B.3	V-X65.....	70
B.4	T-X65.....	72
C	TECHNIP GIRTH WELD CERTIFICATE FOR T-X65 MATERIAL	74

1 Introduction

This report summarizes the results from the materials screening test programme of the pipeline steels under investigation in the HyLINE project. The main objective of the screening programme has been, through microstructural characterization and slow strain rate tensile (SSRT) in air and under in-situ electrochemically charged hydrogen, to provide a quantitative indication of the hydrogen embrittlement susceptibility of three vintage and one modern pipeline steel of X65 and X70 type. Both the base metal and the weld simulated heat affected zone of each pipeline material have been included in the programme. The work is motivated by the need of a knowledge-based choice of steels to be further investigated in terms of toughness and fatigue crack growth rates in the next phase of the project.

The metallurgical characterization (in terms of microstructure and hardness) of the materials as received (i.e., base metals and longitudinal welds), is reported in Section 2. The as-received through-thickness microstructure, grain size and volume fraction of the identified phases in the materials are presented. The pipelines have different wall thicknesses. This should be kept in mind when considering the variations in microstructure close to the surface and in the centre of the pipe wall.

The results from the SSRT testing in terms of the hydrogen induced reduction of ductility as well as post-mortem specimen investigations are summarized in section 3. The description of the procedure used for the weld thermal simulation imposed to the different base metals as well as the resulting microstructures and hardness (HV10) are also reported..

2 Materials

Four materials have been received for investigation in the HyLINE project. The materials specifics in terms of dimension, quantity and production are reported in Table 1. The pipeline steel L-X60 have the thickest pipe wall, i.e., 41 mm and the T-X65 pipeline have the thinnest pipe wall of 15.4 mm. Images of the materials as received are shown in Appendix A.

Table 1: List of materials received in SINTEF for the initial screening study.

Material tag	Pipe OD [mm]	Pipe WT [mm]	Pipe length [mm]	Type of pipe
S - X65	770	26	1000	UOE, longitudinally welded
L- X70	1100	41	1000	UOE, longitudinally welded
T-X65 (BM)	321	15.4	6000 (2x3000)	Seamless, extruded
V- X65	810	20.7	3000	UOE, longitudinally welded
T- X65 (GW)	321	15.4	3000 (1x3000)	Girth Welded, seamless, extruded

2.1 Metallurgical characterization

A metallurgical characterization has been conducted on all materials listed in Table 1. The metallurgical characterization has been performed in both longitudinal and transverse direction of the pipes and in the longitudinal- and girth welds where these are present.

Each material has been investigated in three positions in the base metal, namely the outer-, mid-, and inner position of the pipe wall. Similar system of investigation is used for the HAZ and welds where these are present in the delivered pipes. An illustration of the investigated areas of the materials are shown in Fig. 1, whereas each position, numbered from 1 to 12, is presented with an ID name for clarity. The identification name for each material, with respect to the investigated orientation, is presented in Table 2. For example, S-X65 investigated in longitudinal and transverse direction, is identified with **S-LM** (S-X65- Longitudinal Metal) and **S-TM** (S-X65- Transverse Metal), respectively.

Optical microscopy has been performed on all materials and they have been examined in all positions at four different magnifications: 50X, 200X, 500X and 1000X. The optical micrographs presented in this memo, are taken with magnification X500. Macros have been investigated and hardness values have been measured for the welded materials.

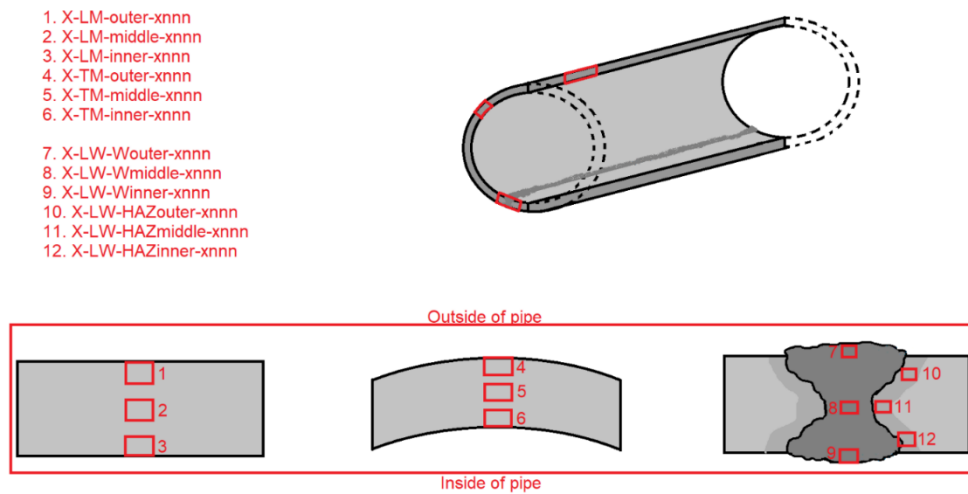


Fig. 1: Identification and markings system for the metallurgical examinations performed on the received pipes.

Table 2: Investigated pipeline steels with corresponding identification name for relevant orientations.

Material tag	Orientation and marking of microstructure test pieces		
	Longitudinal*	Transverse	Transverse (with longitudinal weld cross section)
S-X65	S-LM	S-TM	S-LW
L-X70	L-LM	L-TM	L-LW
V-X65	V-LM	V-TM	V-LW
T-X65 (BM)	TB-LM	TB-TM	n/a
T-X65 (GW)	TW-LM	n/a	n/a

*Specimens longitudinal axis relates to the pipe longitudinal axis.

2.1.1 S-X65

2.1.1.1 Base material

The S-X65 material has the grade API 5LX X65. The pipeline is produced in 1982 by the Japanese steel manufacturer Fukuyama Steel Works. The chemical composition of the material is given in Table 3. Representative micrographs of the base metal in both longitudinal and transversal direction (with respect to the longitudinal direction of the pipe), are shown in Fig. 2. Examination showed that the S-X65 base metal is mainly composed of polygonal ferrite and pearlite in a banded appearance. The pearlite distribution differs across the thickness of the pipe wall; banding is more prominent towards the outer surface. It is also observed a plate-like microstructure in a banded appearance, suggested to be bainite. The grains for all phases are coarser in the mid-section of the pipe wall. Optical micrographs from the transverse direction (**Fig. 2(d-f)**) also confirm the fine-grained appearance towards the outer surface and coarser grains in the middle.

Table 3: Chemical composition of the S-X65 material.

Element	C	Si	Mn	P	S	Cu	Cr	Ni	Mo	V	Nb	Ti	N
wt. %	0.1	<0.6	<1.6	<0.025	<0.015	<0.25	<0.25	<0.25	<0.05	<0.1	<0.05	<0.02	<0.01

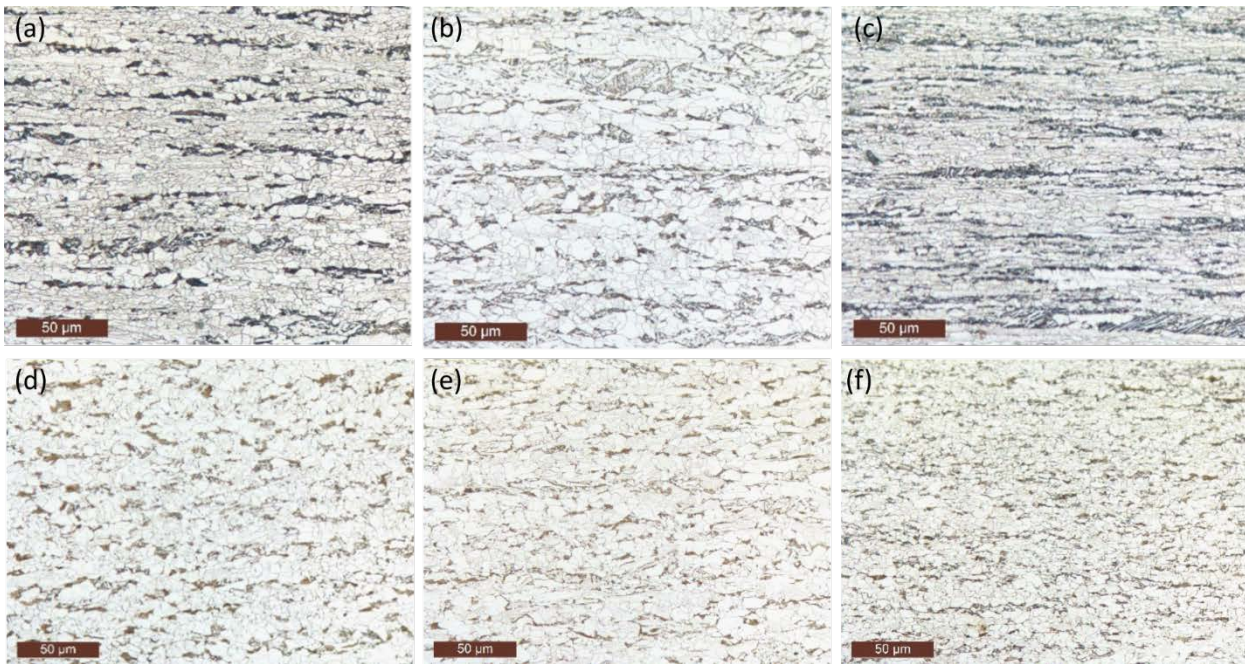


Fig. 2: Optical micrographs of S-X65 at X500 magnification, showing the representative microstructure from the (a) outer, (b) mid and (c) inner through-thickness area of the pipeline wall in the longitudinal direction (LM) and likewise in the (d-f) transversal direction (TM).

The mechanical properties of the as received material (given in the certificate) and from the slow strain rate tensile tests campaign performed in SINTEF's lab facilities, are given in Table 4. Tests are performed in air at room temperature ($\sim 20^{\circ}\text{C}$) and with a nominal strain rate of $2.5 \text{ E-}04 \text{ s}^{-1}$. The results from air and in-situ electrochemically charged hydrogen conditions, are given in the following section, *3 Slow Strain Rate Tensile Testing*.

The phase volume fraction, average grain size and the fraction of non-metallic inclusions have been estimated in several positions in the pipe-wall and presented in Table 5. The average grain size of the material is determined using the average grain intercept method (AGI), which gives an average grain size of $3.5 \mu\text{m}$, $4.2 \mu\text{m}$ and $3.7 \mu\text{m}$ in the outer, mid and inner area of the pipe wall, respectively. The phase and non-metallic inclusion volume have been estimated using the grey scale colour coding to distinguish between phases (i.e., pearlite and ferrite), as shown in Fig. 3. It should be noted that for steels mainly containing ferrite and pearlite, this method is more accurate than for steels having additional phases. For instance, the

microstructure of S-X65 contains banding of pearlite and ferrite, as well as bainite. As a result, the volume fraction estimated from the black-coloured phases is a combination of pearlite and bainite.

Table 4: Mechanical properties of S-X65 (from certificate) and obtained from mechanical tests of the mid and inner in longitudinal direction and inner transverse direction, performed at SINTEF.

Material	$\sigma_{0.2}$ [MPa]	σ_{UTS} [MPa]	EL%	HV
As received	526	627	24	-
S mid	445	584		187 (± 0.6)
S Inner	518	590		185 (± 0.2)
S mid (T)	507	598		-

(T)= Specimens oriented in the transverse direction

*X65 YS min. = 448 MPa, UTS min. = 531 MPa (API 5L specifications for Linepipe)

Table 5: Phase volume and grain size of S-X65 microstructure from the outer, mid, and the transversal mid position of the pipe wall.

Material	Ferrite [%]	Pearlite/bainite [%]	Grain size [μm]	Non-metallic inclusions [%]
Outer	84.6	15.4	3.5	0.06
Mid	83	17	4.2	0.06
Mid (T)*	87	13	3.7	0.04

*T= data from the mid area of the pipe in the transversal direction.

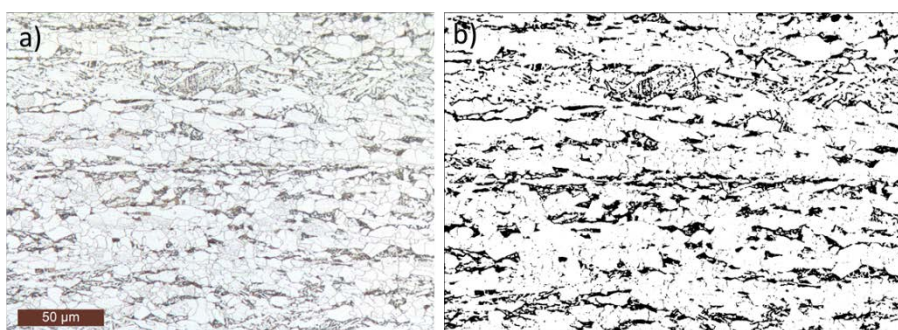


Fig. 3: a) Example of optical micrograph of S-X65 (mid position) microstructure (X500), used for estimation of phase volume fraction, as shown in b). The white areas are ferrite, and the black areas are pearlite and bainite.

2.1.1.2 Heat Affected Zone and Weld Metal

The macrograph of the longitudinal two pass submerged arc weld in S-X65 are shown in Fig. 4 and the corresponding hardness values are plotted in Fig. 5. The macro hardness profile in the transverse area of the welded joint is analysed. Indentations were performed in the base metal, HAZ, weld metal on both sides of

the joint and in the outer, mid, and inner position of the pipe-wall. Fig. 5 shows a gradual increase in hardness towards the middle of the joint, i.e. the weld metal. The representative microstructures from the HAZ and weld metal in the outer, mid, and inner position, are shown in Fig. 6 and Fig. 7, respectively.

The microstructure in the HAZ primarily consists of bainite and ferrite in a coarse-grained appearance, depending on its location relative to the weld. The bainitic microstructure is more prominent towards the outer and inner surfaces. Typical morphologies of grain boundary ferrite and small amounts of possibly acicular ferrite and Widmanstätten ferrite can be seen. The presence of ferrite is more prominent in the HAZ mid position, in terms of enlarged grains of polygonal ferrite. The inner HAZ microstructure exhibit nearly similar morphology as the HAZ outer. Non-metallic inclusions and possible carbides are observed throughout the thickness of the pipe wall.

The microstructure of the weld metal mainly consists of polygonal ferrite and bainite in a fine-grained appearance (in contrast to that observed in HAZ). The prior austenite grains with grain boundary ferrite are seen throughout the thickness, reaching a maximum in the middle. Moreover, the ferrite grains are larger in the middle than towards the outer surfaces (X200). At higher magnification, non-parallel, needle-shaped features are observed, assumed to be acicular ferrite. In addition, some features of Widmanstätten ferrite and non-metallic inclusions are observed. A detailed report of the hardness measurements is attached in APPENDIX B.

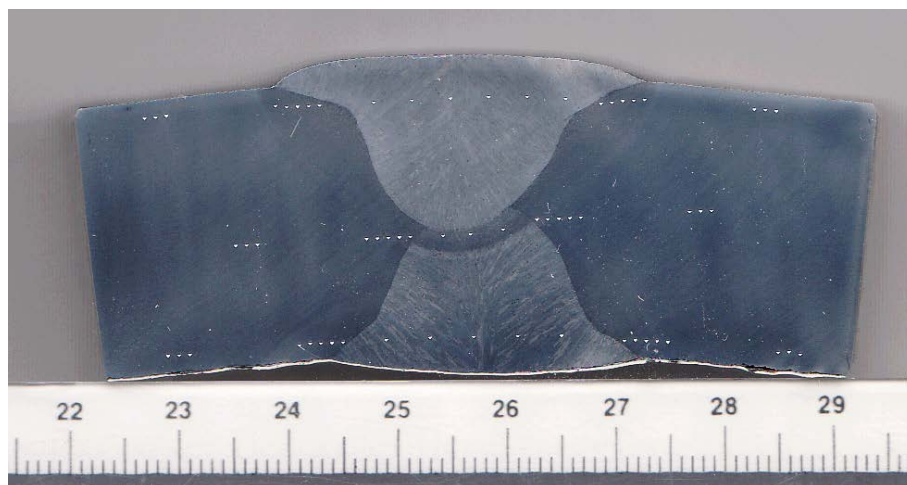


Fig. 4: Macrograph of the longitudinal weld in S-X65 with residual imprints from hardness measurements.

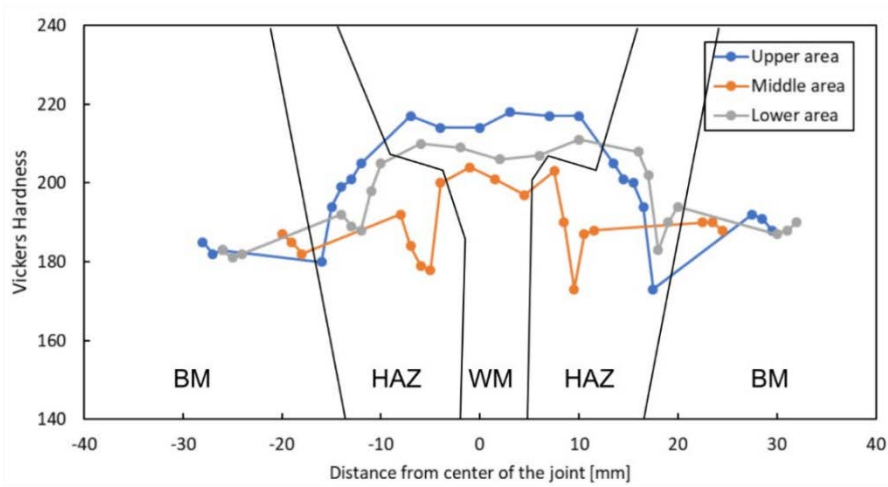


Fig. 5: Vickers hardness (HV10) in S-X65 base metal, HAZ and weld in the upper, mid, and lower area, with respect to the centre of the joint.

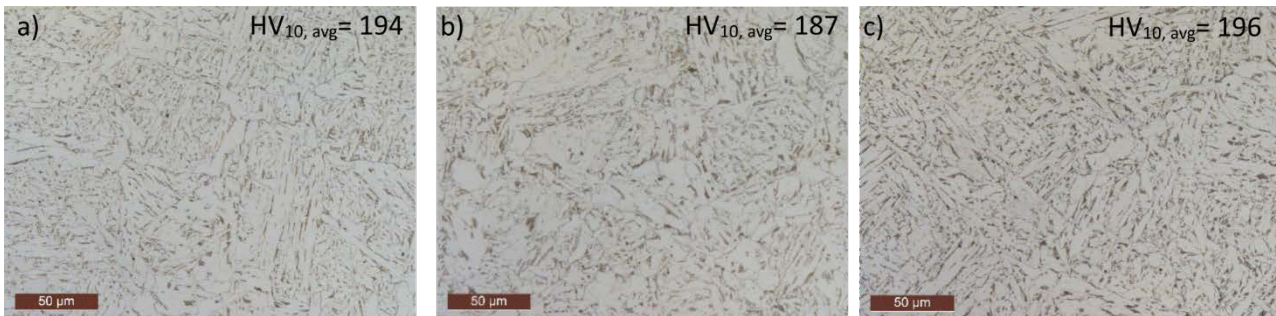


Fig. 6: Optical micrographs of HAZ from the longitudinal weld in S-X65 from the a) outer, b) mid and c) inner area of the pipe wall thickness. Average Vickers hardness values from the representative microstructures are given.

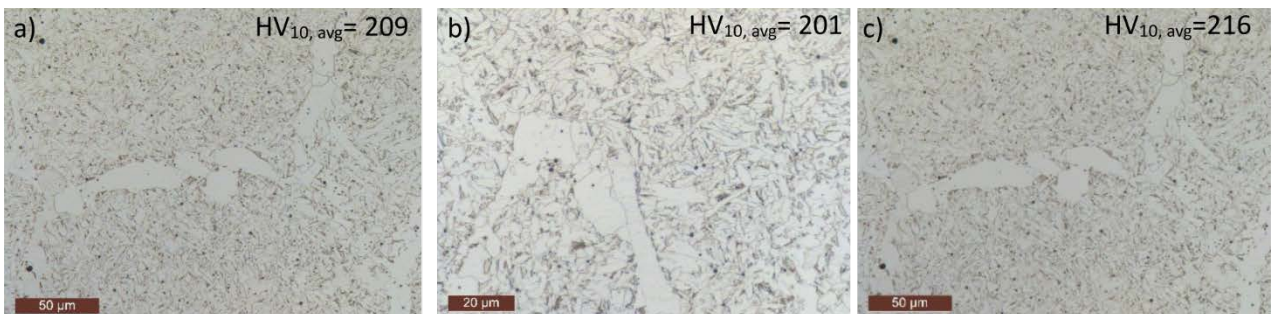


Fig. 7: Optical micrographs of the weld metal from the longitudinal weld in S-X65 from the a) outer, b) mid and c) inner area of the pipe wall thickness. Average Vickers hardness values from the representative microstructures are given.

2.1.2 L – X60

2.1.2.1 Base material

The L-X60 material has the grade API 5LX X60 and is produced in 2004 by Kashima Steel Works. Chemical composition of the material is given in Table 6. Representative micrographs of the base metal in the longitudinal and transversal direction (with respect to the longitudinal direction of the pipe), are given in Fig. 8. The metallurgical features and distribution of phases are comparable with that observed for S-X65. The microstructure mainly consists of polygonal ferrite and banded pearlite. The pearlite distribution differs across the thickness of the pipe wall; banding is more prominent towards the outer surface. In addition, bands of probably bainite are observed in the microstructure throughout the pipe wall thickness. The grains of all phases are coarser in the mid-section of the pipe wall. Optical micrographs from the transverse direction (Fig. 8 d-f) also confirm the fine-grained appearance towards the outer surface and coarser grains in the middle.

Table 6: Chemical composition of L-X60 material measured from both inner and mid position of the pipe wall.

Element	C	Si	Mn	P	S	Cu	Cr	Ni	Mo	V	Nb	Ti	N
wt. % Inner	0.068	0.28	1.58	0.006	<0.001	0.26	0.18	0.42	<0.01	0.047	0.046	0.016	0.002
wt. % middle	0.066	0.28	1.57	0.006	<0.001	0.26	0.18	0.41	<0.01	0.047	0.045	0.016	0.002

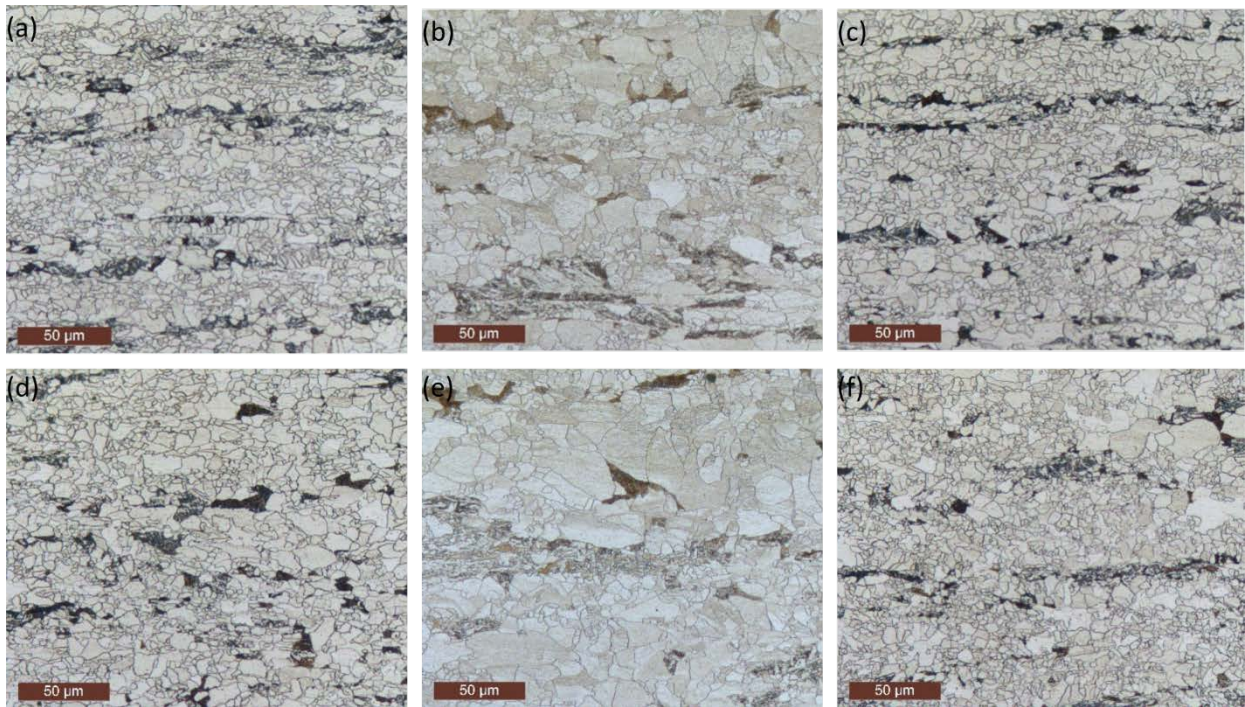


Fig. 8: Optical micrographs of the L-X60 material at X500 magnification, showing the representative microstructure from the (a) outer, (b) mid and (c) inner through-thickness area of the pipeline wall in the longitudinal direction (LM) and likewise in the (d-f) transversal direction (TM).

The mechanical properties of the as received material (given in the certificate) and from slow strain rate tensile tests performed in SINTEF's lab facilities, are given in Table 7. Tests are performed in air at room temperature ($\sim 20^{\circ}\text{C}$) and with a nominal strain rate of $2.5 \cdot 10^{-4} \text{ s}^{-1}$. The phase volume fraction, average grain size and the fraction of non-metallic inclusions have been estimated from several locations throughout the pipe wall thickness and are presented in Table 8.

Table 7: Mechanical properties of L-X60 as received (from certificate) and obtained from mechanical tests performed at SINTEF. Data from the mid, inner and mid transverse direction are given.

Material	$\sigma_{0.2}$ [MPa]	σ_{UTS} [MPa]	EL%	HV
As received	544*	604	44	-
L mid	413	530		185 ± 2.1
L Inner	481	555		197 ± 7.9
L mid (T)	388	546		-

*The yield strength given in the certificate is from $\sigma_{0.5}$.

Table 8: Phase volume and grain size of L-X60 microstructure from the outer, mid, and the transversal mid position of the pipe wall.

Material	Ferrite [%]	Pearlite/bainite [%]	Grain size [μm]	Non-metallic inclusions [%]
Outer	93	7	4.6	0.018
Middle	92	8	6.8	0.017
Middle (T)*	93	8	8.7	0.039

*T= data from the middle area of the pipe in the transversal direction.

2.1.2.2 Heat Affected Zone and weld metal

The macrograph of the longitudinal two pass submerged arc weld in L-X60 are shown in Fig. 9 and the corresponding macro hardness profile in the transverse area of the welded joint are given in Fig. 10. Indentations were performed in the base metal, HAZ, weld metal on both sides of the joint and in the outer, mid -and inner position of the pipe wall. The representative microstructures from the HAZ and weld metal in the outer, mid, and inner position, are shown in Fig. 11 and Fig. 12, respectively. Average hardness (HV_{10}) values are given for each microstructure.

The microstructure in the HAZ in the outer and inner region of the pipe wall, differ significantly from that observed in the HAZ middle. A coarse-grained structure with bainite and ferrite is typically observed at the outer and inner HAZ. The bainite is seen within the interior of prior austenite grain boundaries. Small amounts of acicular ferrite are possibly present. In contrast, the HAZ mid position exhibits a fine-grained structure of ferrite and possibly bainite. Several dark spots in the HAZ middle can be seen, which is a result of the segregation of alloying elements, seen as dark longitudinal lines at lower magnifications.

The weld metal contains mainly acicular ferrite, together with some grain boundary ferrite and Widmanstatten ferrite. The microstructure of the mid area differs from that seen on the outer surfaces, in terms of a more fine-grained structure, with the presence of some polygonal ferrite, acicular ferrite and non-metallic inclusions. Non-metallic inclusions and possible carbides are observed throughout the thickness of the pipe wall. A detailed report for the hardness measurements is attached in APPENDIX B.

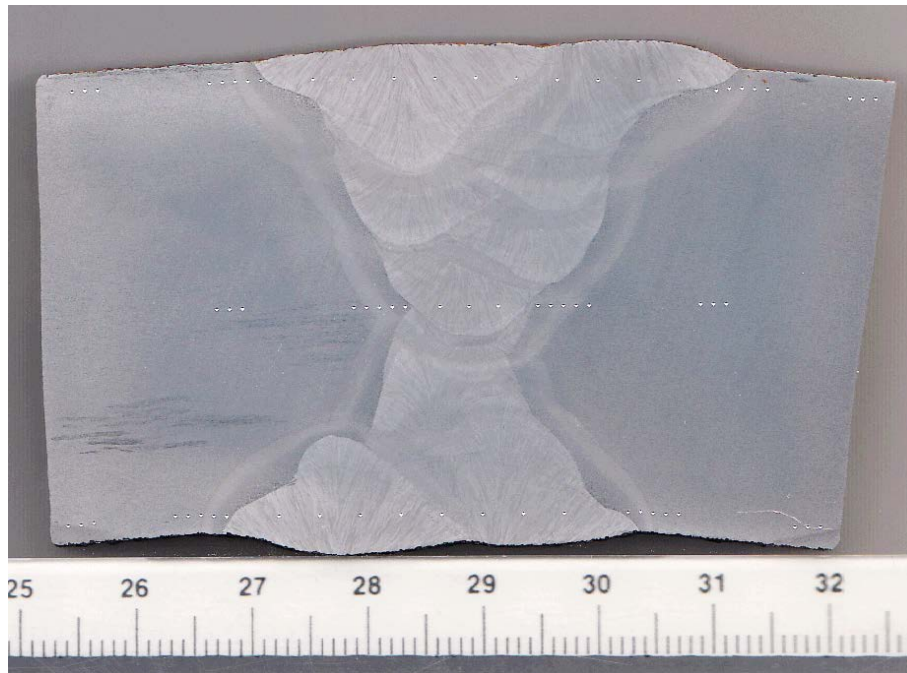


Fig. 9: Macrograph of the longitudinal weld in L-X60 with residual imprints from hardness measurements.

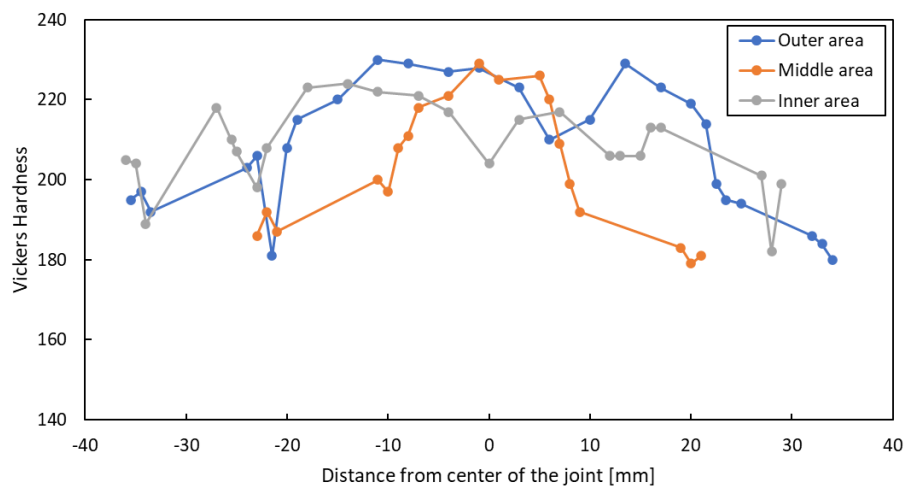


Fig. 10: Vickers hardness (HV₁₀) results for L-X60 base metal, HAZ and weld in the outer, mid, and inner position of the pipe.

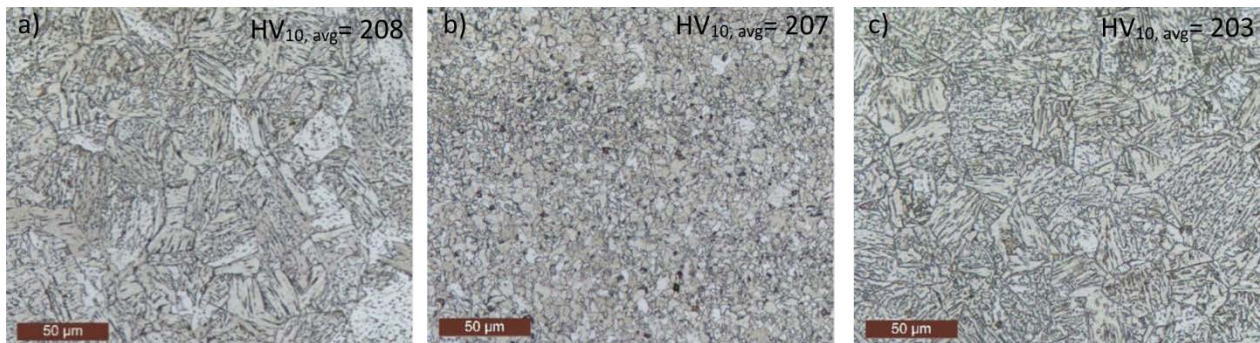


Fig. 11: Optical micrographs of HAZ from the longitudinal weld in L-X60 from the a) outer, b) mid and c) inner position of the pipe wall thickness. Average Vickers hardness values from the representative microstructures are presented below each image.

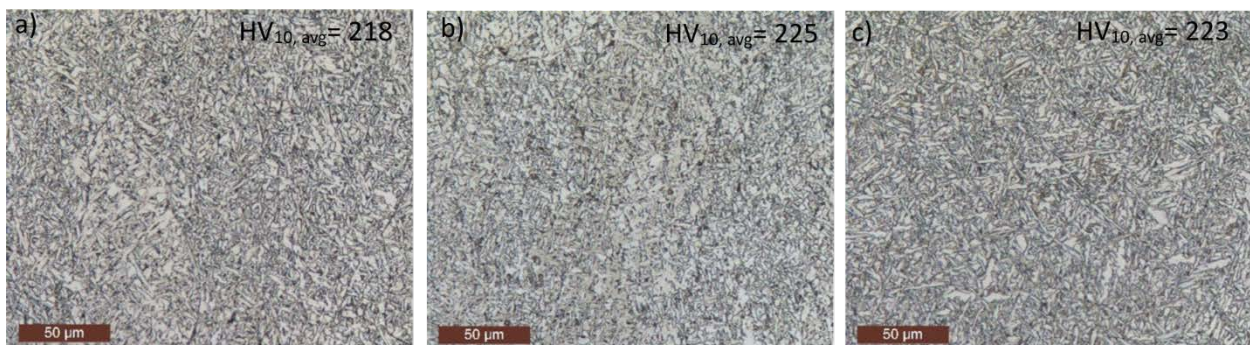


Fig. 12: Optical micrographs of the weld metal from the longitudinal weld in L-X60 from the a) outer, b) mid and c) inner position of the pipe wall thickness. Average Vickers hardness values from the representative microstructures are presented below each image.

2.1.3 V-X65

2.1.3.1 Base material

The V-X65 material has the grade API 5LX X65 and its chemical composition is given in Table 9. The certificate for this steel is not available, therefore, as received mechanical properties are not given. Representative micrographs of the base metal in both longitudinal and transversal direction (with respect to the longitudinal direction of the pipe), are given in Fig. 13. The microstructure consists of polygonal ferrite and pearlite in alternating layers. The microstructure is more fine-grained towards the outer surfaces of the pipe wall, leading to smaller distance between the pearlite bands. Also, the bands are more continuous than that observed for S-X65 and L-X60, where the pearlite is more scattered in some areas of the pipe. Optical micrographs from the transverse direction (Fig. 13 (d-f)) also confirm the fine-grained appearance towards the outer surface and coarser grains in the middle.

Table 9: Chemical composition of V-X65 material.

Element	C	Si	Mn	P	S	Cu	Cr	Ni	Mo	V	Nb	Ti	N
wt. %	0.12	0.26	1.36	0.020	0.003	0.010	0.022	0.25	0.002	0.065	0.041	0.002	0.032

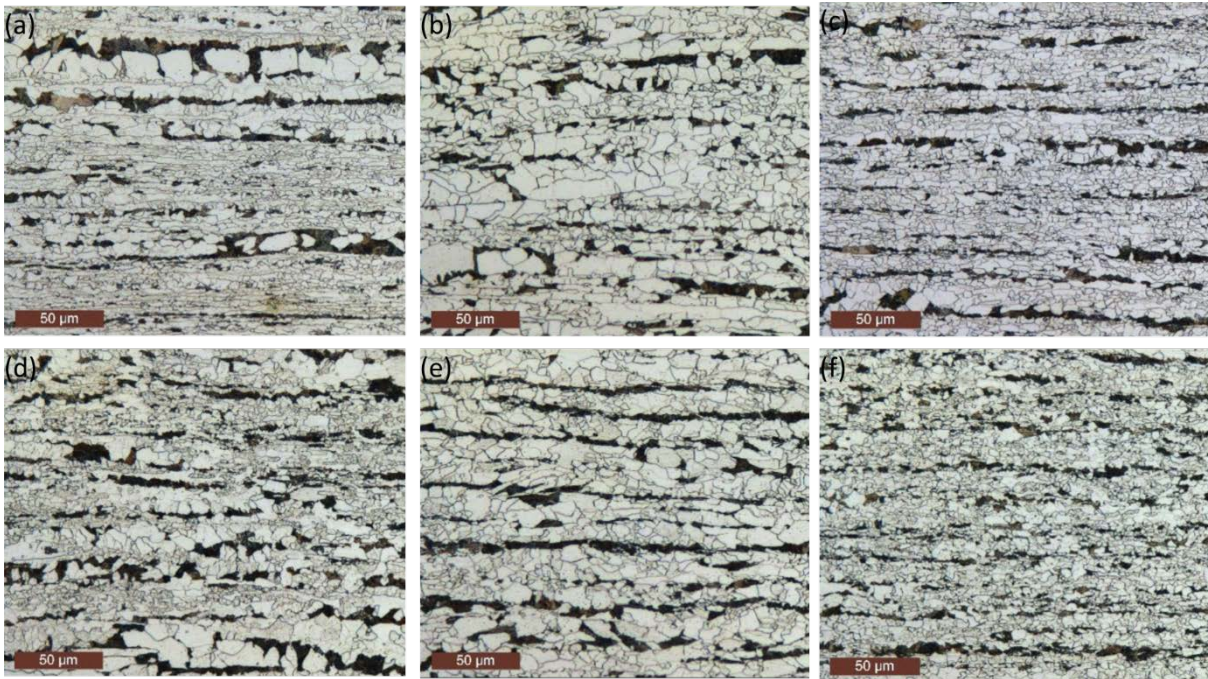


Fig. 13: Optical micrographs of the V-X65 material at X500 magnification, showing the representative microstructure from the (a) outer, (b) middle and (c) inner through-thickness area of the pipeline wall in the longitudinal direction (LM) and likewise in the (d-f) transversal direction (TM).

The tensile properties from slow strain rate testing, are given in Table 10. Testing have been performed in air at room temperature ($\sim 20^{\circ}\text{C}$) and with a nominal strain rate of $2.5\text{E}10^{-4} \text{ s}^{-1}$. The phase volume fraction, average grain size and the fraction of non-metallic inclusions have been estimated from several locations throughout the pipe wall thickness and are presented in Table 11.

Table 10: Mechanical properties of V-X65 obtained from mechanical tests performed at SINTEF. Data from the mid, inner and mid transverse (T) direction are given.

Material	$\sigma_{0.2}$ [MPa]	σ_{UTS} [MPa]	HV
As received	-	-	-
V mid	440	594	194 \pm 1.4
V Inner	474	604	200 \pm 0.8
V mid (T)*	500	629	-

Table 11: Phase volume and grain size of V-X65 microstructure from the outer, mid, and the transversal (T) mid position of the pipe wall.

Material	Ferrite [%]	Pearlite [%]	Grain size [μm]	Non-metallic inclusions [%]
Outer	86	14	3.7	0.034
Mid	87	13	5.2	0.035
Mid (T)*	83	17	5	0.047

2.1.3.2 Heat Affected zone and weld metal

The macrograph of the longitudinal two pass submerged arc weld in V-X65 is shown in Fig. 14 and the corresponding macro hardness profile in the transverse area of the welded joint are given in Fig. 15. Indentations were performed in the base metal, HAZ and weld metal on both sides of the joint and in the outer, mid, and inner position of the pipe wall. The representative microstructures from the HAZ and weld metal in the outer, mid, and inner position, are shown in Fig. 16 and Fig. 17, respectively. Average hardness (HV_{10}) values are given for each microstructure in Fig. 16 and Fig. 17.

Optical microscopy of the HAZ of the longitudinal weld in the V-X65 pipe reveal a coarse-grained microstructure consisting of bainite plates in the interior of prior austenite grains. Moreover, grain boundary (allotriomorphic) ferrite is present at prior austenite grain boundaries. This microstructure is typically observed at the outer and inner area of the pipe. In contrast, the HAZ in the mid-position of the pipe, contain a rather fine-grained structure, consisting of polygonal ferrite and bainite embedded within the ferrite grains. There is also observed several black spots in the mid-section (Fig. 16 (b)) that possibly occur as a result of the etching.

The weld metal (Fig. 17) has a refined microstructure on the outer and inner part of the pipe. The microstructure mainly consists of acicular ferrite and allotriomorphic ferrite. The mid-section is composed of larger polygonal ferritic grains and acicular ferrite. Non-metallic inclusions are observed throughout the pipe wall thickness in the weld metal. A detailed report for the hardness measurements is attached in APPENDIX B.

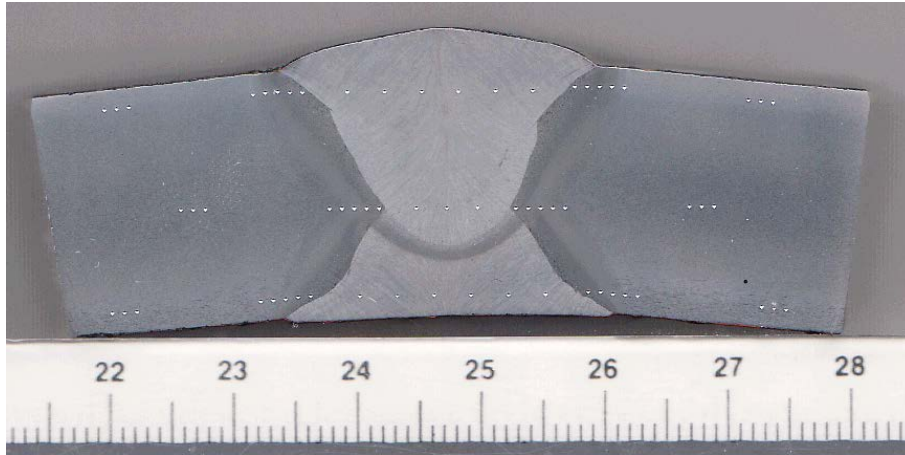


Fig. 14: Macrograph of the longitudinal weld in V-X65 with residual imprints from hardness measurements.

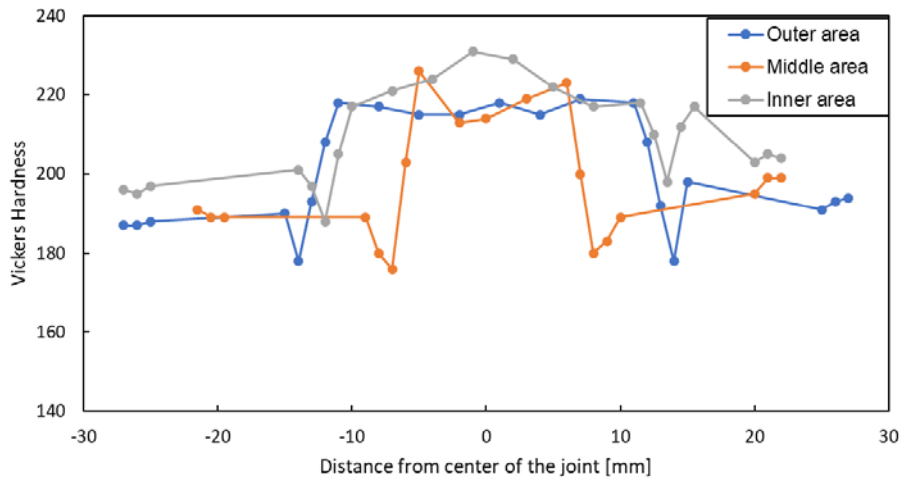


Fig. 15: Vickers hardness (HV₁₀) in V-X65 base metal, HAZ and weld in the upper, mid and lower area in the pipe wall.

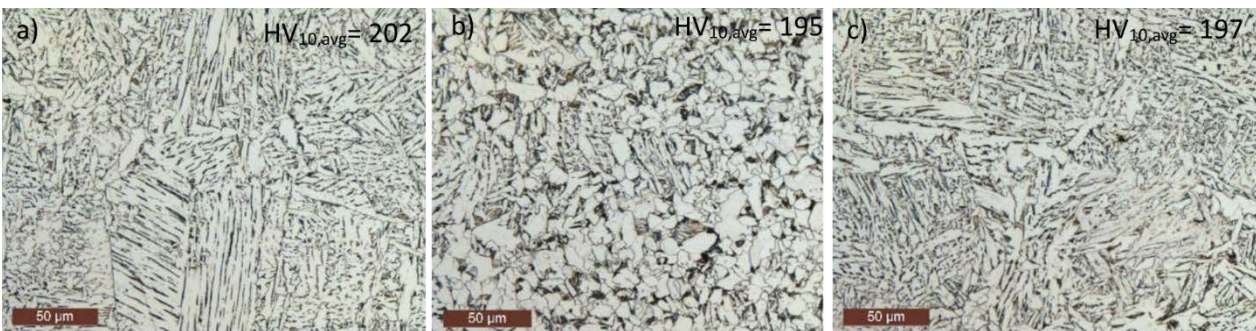


Fig. 16: Optical micrographs of HAZ from the longitudinal weld in V-X65 from the a) outer, b) mid and c) inner area of the pipe wall thickness. Average Vickers hardness values from the representative microstructures are presented below each image.

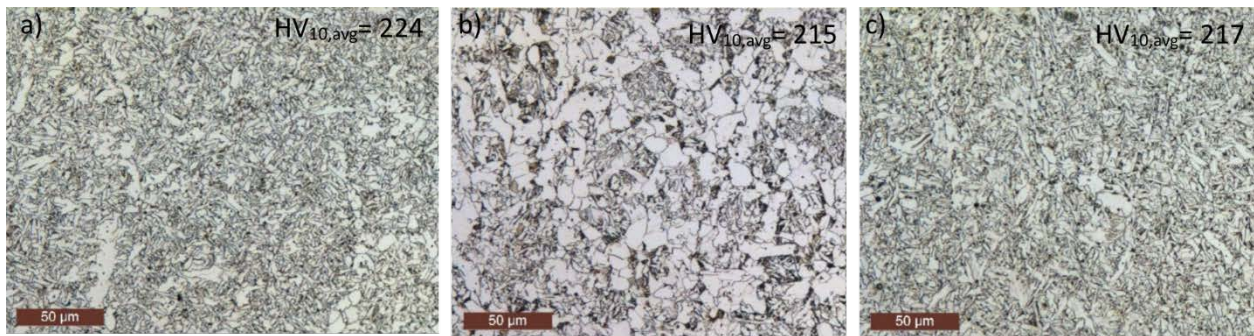


Fig. 17: Optical micrographs of the weld metal from the longitudinal weld in V-X65 from the a) outer, b) mid and c) inner area of the pipe wall thickness. Average Vickers hardness values from the representative microstructures are presented below each image.

2.1.4 T-X65

2.1.4.1 Base material

The T-X65 material with the API 5L grade X65 is a seamless pipe produced in 2019. It is the newest steel investigated in the HyLINE project and contains a different microstructure compared to that seen in the highly anisotropic pipeline steels. The chemical composition is given in Table 12. Representative micrographs of the microstructure in both longitudinal and transversal direction (with respect to the longitudinal direction of the pipe), are given in Fig. 18. The metallurgical features and distribution of phases differ from the typical banded appearance of ferrite/pearlite observed in the others investigated pipeline steels. The microstructure in T-X65 is fine-grained and consist of ferrite and bainite homogeneously distributed, obtained from quenching and tempering. Fig. 18 (c) and (f) reveal a larger amount of bainite in the inner area of the pipe and a more fine-grained appearance towards the outer surface is observed Fig. 18 (a) and (d).

Table 12: Chemical composition of T-X65 material.

Element	C	Si	Mn	P	S	Cu	Cr	Ni	Mo	V	Nb	Ti	N
wt. %	0.07	0.22	1.19	0.011	0.003	0.14	0.15	0.15	0.12	0.02	0.019	0.001	0.01

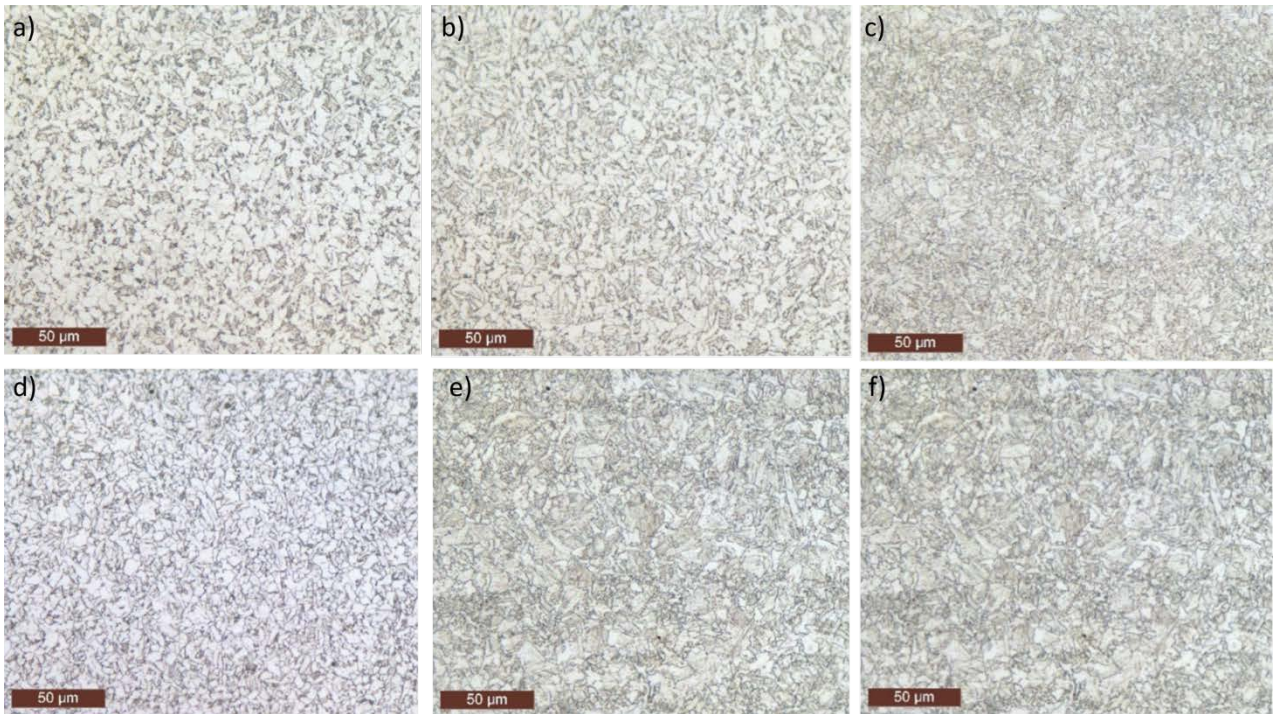


Fig. 18: Optical micrographs of the T-X65 material at X500 magnification, showing the representative microstructure from the (a) outer, (b) mid and (c) inner through-thickness area of the pipeline wall in the longitudinal direction (LM) and likewise in the (d-f) transversal direction (TM).

The mechanical properties of the as received material (given in the certificate) and from slow strain rate tensile tests performed in SINTEF's lab facilities, are given in Table 13. Tests are performed in air at room temperature ($\sim 20^{\circ}\text{C}$) and with a nominal strain rate of $2.5 \text{ E-}04 \text{ s}^{-1}$. The phase volume fraction, average grain size and the fraction of non-metallic inclusions have been estimated from several locations throughout the pipe wall thickness and are presented in Table 14.

Table 13: Mechanical properties of T-X65 as received (from certificate) and obtained from mechanical tests performed at SINTEF. Data from the mid, inner and mid transverse direction are given.

Material	$\sigma_{0.2}$ [MPa]	σ_{UTS} [MPa]	HV
As received	498*	583	-
T mid	495	576	190 \pm 1.8
T Inner	564	633	203 \pm 1.1
T mid (T)	543	610	-

*The yield strength given in the certificate is from $\sigma_{0.5}$.

Table 14: Phase volume and grain size of T-X65 microstructure from the outer, mid, and the transversal mid position of the pipe wall.

Material	Ferrite [%]	Bainite [%]	Grain size [μm]	Non-metallic inclusions [%]
Outer	76	24		0.04
Inner	89	11	~ 7	0.04
Mid (T)*	87	13		0.06

*T= data from the mid area of the pipe in the transversal direction.

2.1.4.2 Heat Affected zone and weld metal

T-X65 pipeline steel does not contain a longitudinal weld as the other steels presented in this report. Thus, a circumferential girth weldment was carried out by Technip (procedure and the welding parameters are summarized in the certificate in APPENDIX C).

The macrograph of the girth weld is shown in Fig. 19 and the corresponding macro hardness profile in the transverse area of the welded joint are given in Fig. 20. Indentations were performed in the base metal, HAZ, weld metal on both sides of the joint and in the outer, mid, and inner position of the pipe wall. The representative microstructures from the HAZ and weld metal in the outer, mid, and inner position, are shown in Fig. 21 and Fig. 22, respectively. Average hardness (HV_{10}) values are given for each microstructure in the figures. The detailed report for the hardness measurements is attached in APPENDIX B.

Optical microscopy of the HAZ microstructure of the girth weld, reveal a gradually change towards the inner area of the pipe. The outer area shows a refined microstructure (compared to the other areas in this weld) with ferrite and bainite. The bainitic microstructure is coarser and larger in the mic section of the pipe and appear on prior austenite grains. The prior austenite grains are more prominent in the microstructure towards the inner surface of the pipe. Also, the interior of the prior austenite grains, are composed of bainite and possibly martensite plates and some grain boundary ferrite are observed at the prior austenite grains. The weld metal consists of bainite and ferrite. The microstructure obtains different characteristics throughout the pipe wall thickness, whereas a larger amount of bainite is seen in the outer area, a more fine-grained microstructure is observed in the middle consisting of ferrite and bainite, and a combination of the two former descriptions are observed in the inner area of the pipe wall thickness.

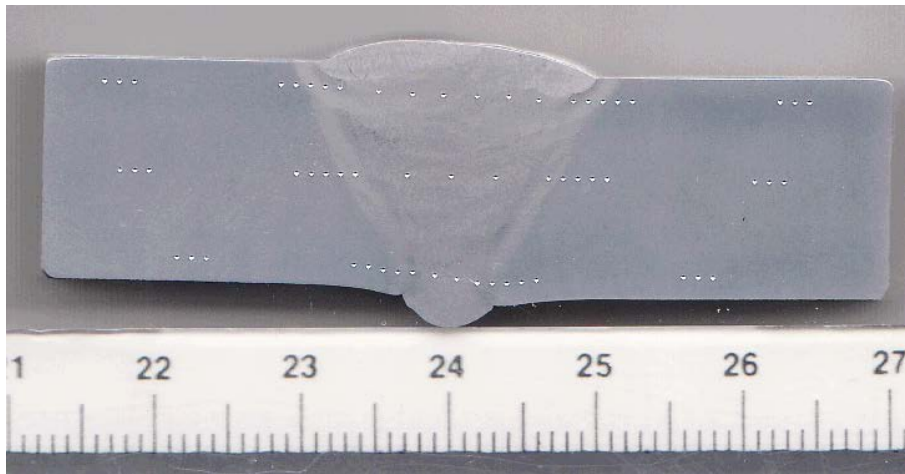


Fig. 19: Macrograph for the girth weld in the T-X65 material with hardness indentations marks.

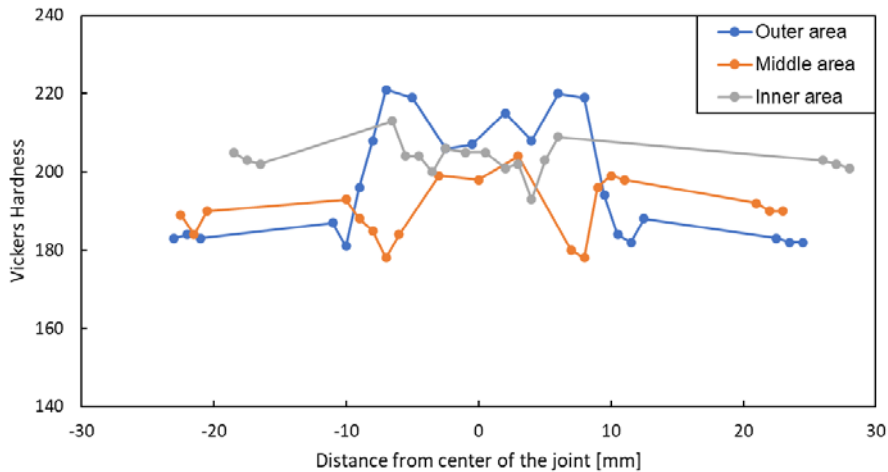


Fig. 20: Vickers hardness (HV10) in T-X65 base metal, HAZ and weld in the upper, mid, and lower area of the pipe wall.

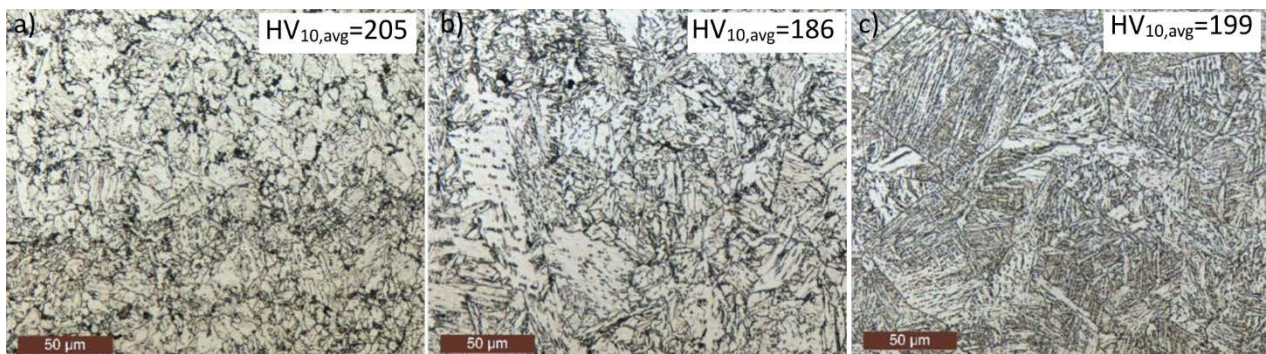


Fig. 21: Optical micrographs of HAZ from the girth weld in T-X65 from the a) outer, b) mid and c) inner area of the pipe wall thickness. Average Vickers hardness values from the representative microstructures are presented below each image.

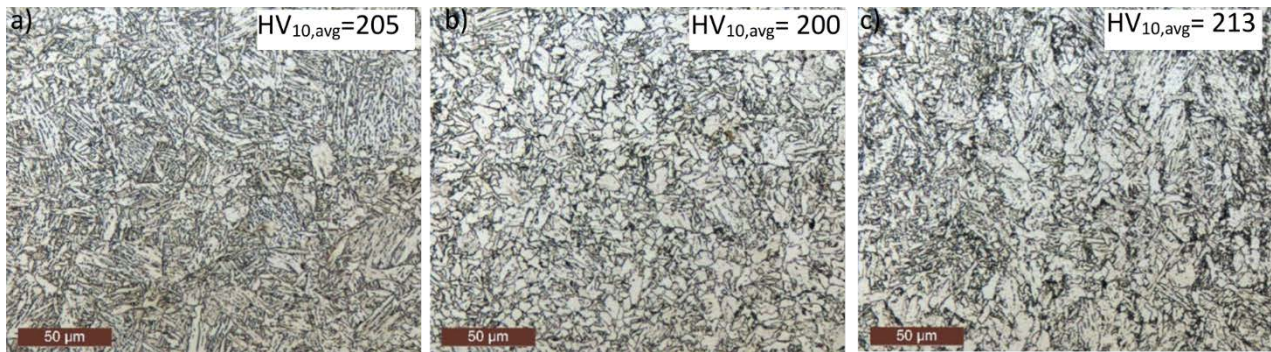


Fig. 22: Optical micrographs of the weld metal from the girth weld in T-X65 from the a) outer, b) mid and c) inner area of the pipe wall thickness. Average Vickers hardness values from the representative microstructures are presented below each image.

3 Slow strain rate tensile testing

Slow strain rate tensile testing in air and under in-situ electrochemically charged hydrogen conditions has been performed for all the pipe materials. Testing have been performed on samples from base metal and weld simulated heat affected zone, as described in Sections 3.2 and 3.3, respectively.

3.1 Testing procedure

Each material and condition have been tested in air and under electrochemically charged hydrogen conditions. Two nominal strain rates have been applied: $2.5E-04 \text{ sec}^{-1}$ and $1E-06 \text{ sec}^{-1}$. All tests were carried out at room temperature ($\sim 20 \text{ }^\circ\text{C}$). For the tests in hydrogen, the test specimens were in-situ cathodically charged in a $0.1 \text{ M Na}_2\text{SO}_4$ electrolyte under a constant potential of $-1050 \text{ mV}_{\text{SCE}}$. Multimeters were used during the whole test in order to check the values and to keep the electrochemical circuit running as designed. The test specimen geometry and the test set-up are presented in Fig. 23:

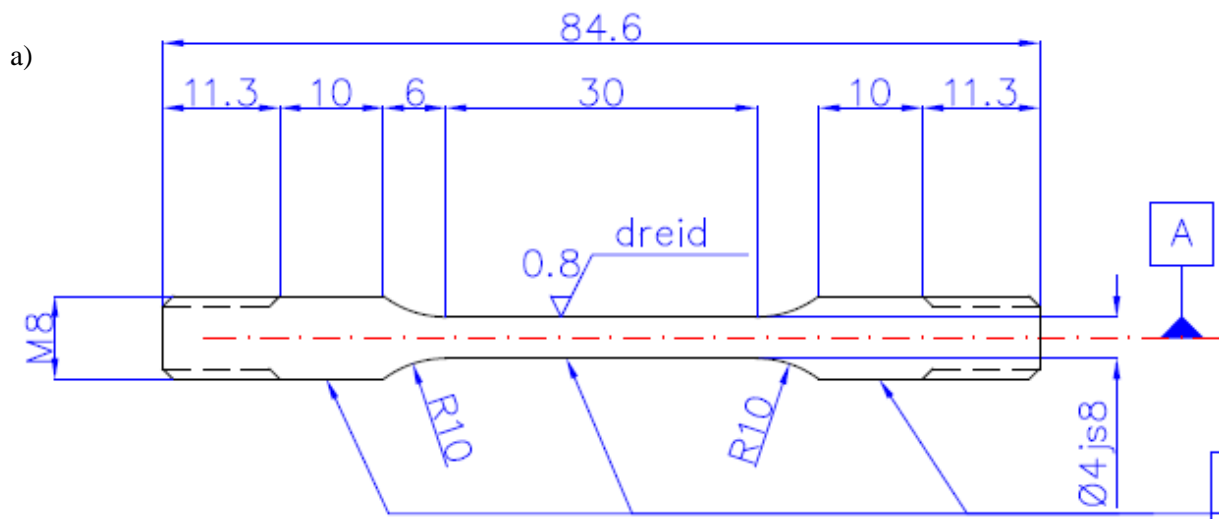




Fig. 23: a) Specimen geometry used for SSRT; b) Test set-up with mounted specimens and c) in-situ electrochemical hydrogen charging ongoing.

3.2 Base metals SSRT testing

SSRT testing has been performed on the base metal of all the pipes. The position and the direction of the specimens tested, as well as their identification is reported in Fig. 24:

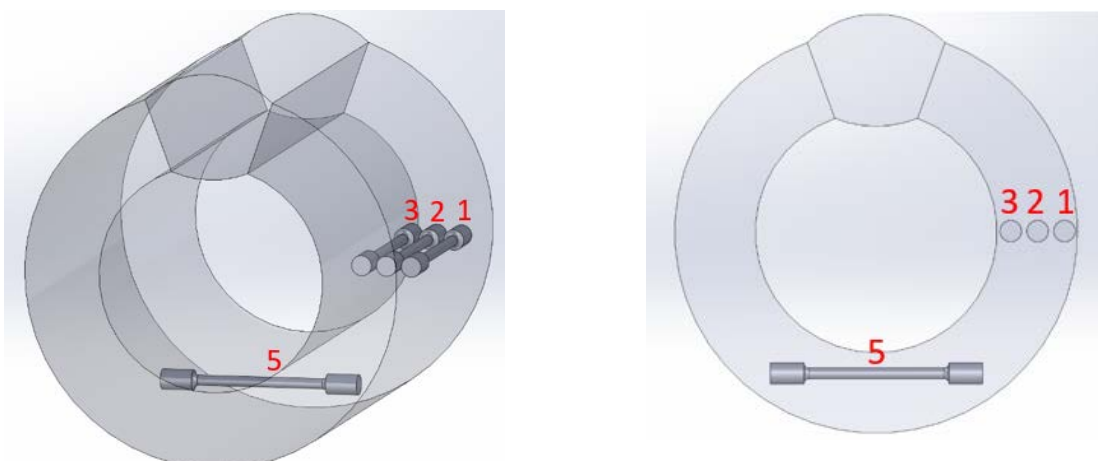


Fig. 24: Schematic sketch of the positioning of the specimens with respect to the pipe with identification number reported.

3.2.1 SSRT results for base metal

For each of the materials and their position, the comparison of the curves when tested in air and in hydrogen conditions is reported together with the picture of their fractured surfaces at two magnifications. Most of the test in air has been run at a strain rate of $2.5E-04 \text{ s}^{-1}$. For the samples from position 2 of S-X65 and T-X65, the test in air have been run also at the same nominal strain rate as for the testing in hydrogen, i.e. and $1E-06 \text{ s}^{-1}$. These are indicated with the letters "SS" in the tables and figures below. For each material and position, two embrittlement indicators have been calculated and reported. These are:

the hydrogen Embrittlement Index (EI), defined as:

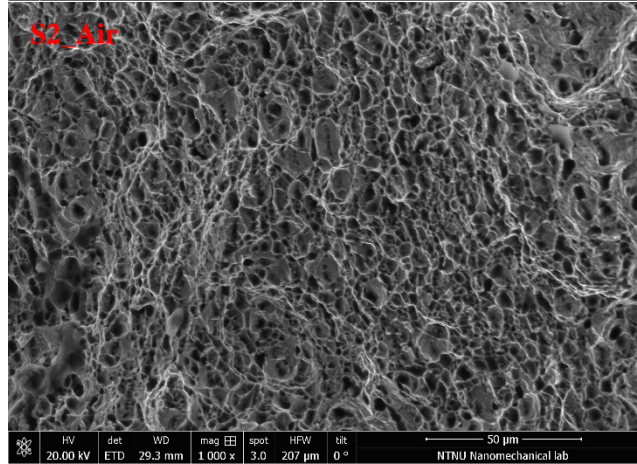
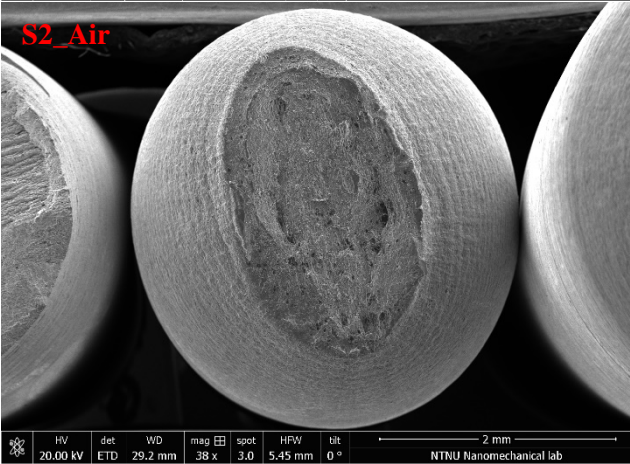
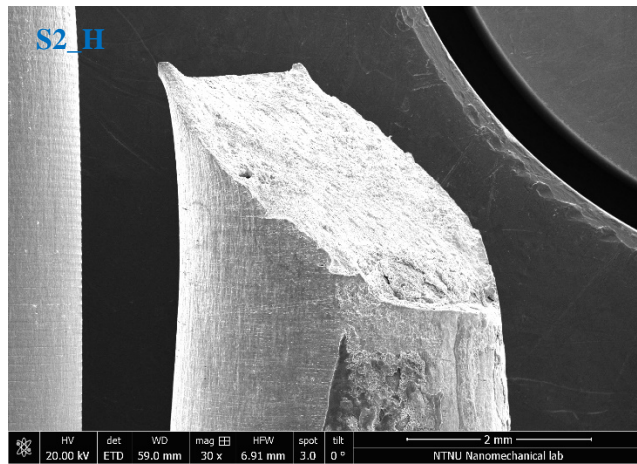
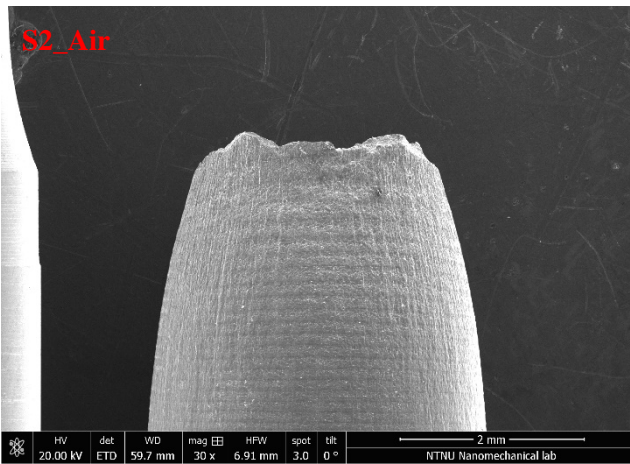
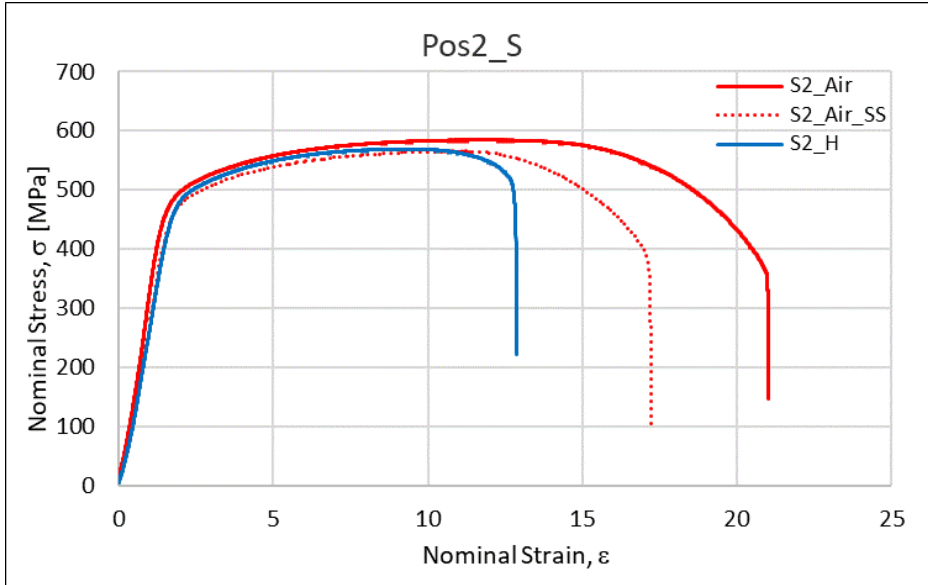
$$EI[\%] = \frac{R_{A,air} - R_{A,H}}{R_{A,air}} \cdot 100 \quad \text{Eq. 1}$$

where R_A indicates the reduction of area; and *the ductility reduction* defined as:

$$\varepsilon_{f,red} = \frac{\varepsilon_{f,H}}{\varepsilon_{f,air}} \cdot 100 \quad \text{Eq. 2}$$

3.2.2 Position 2 results

S-X65 – Pos2



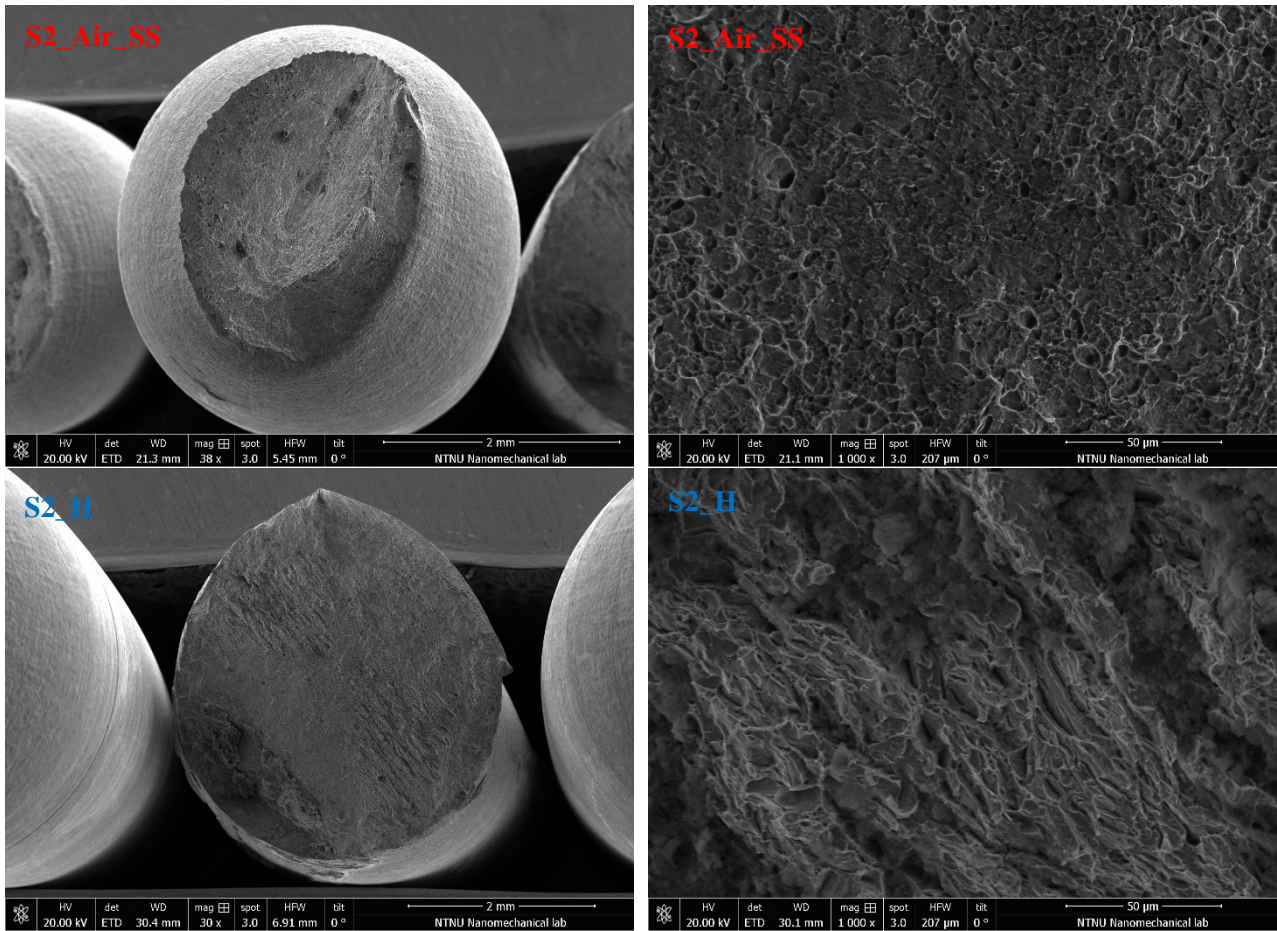
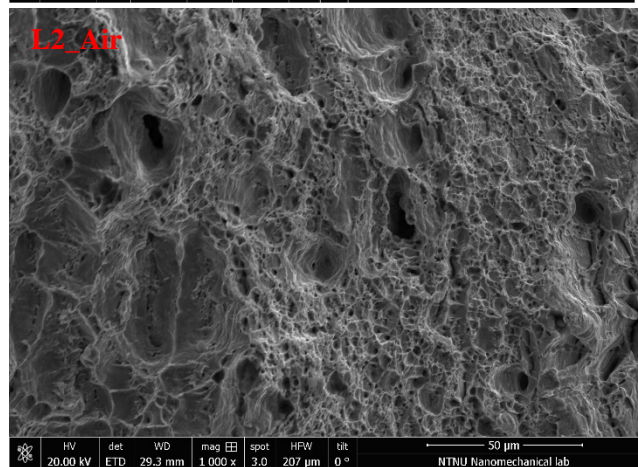
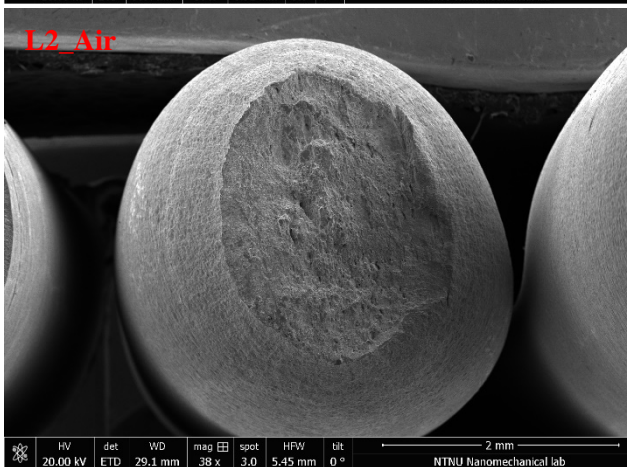
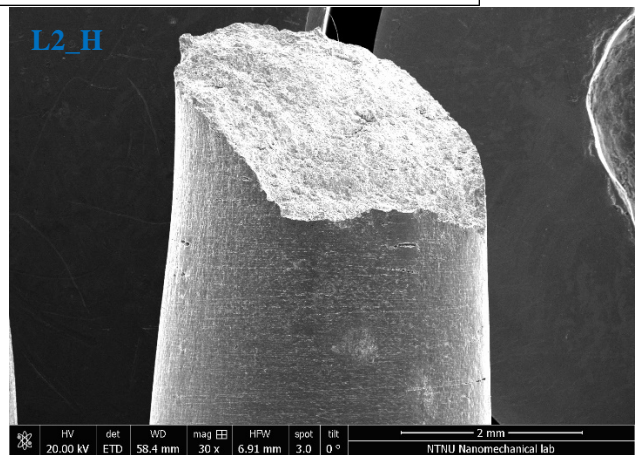
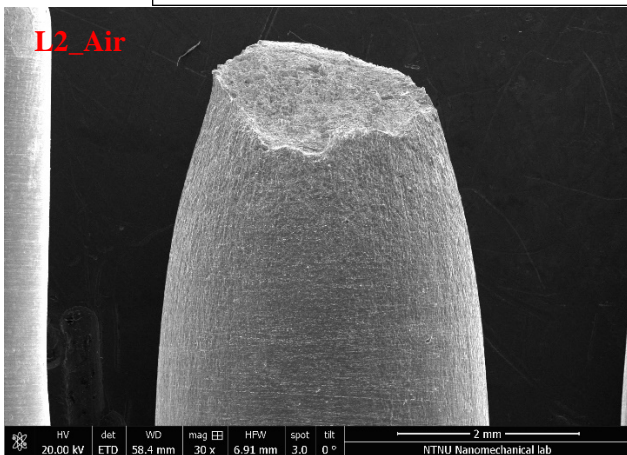
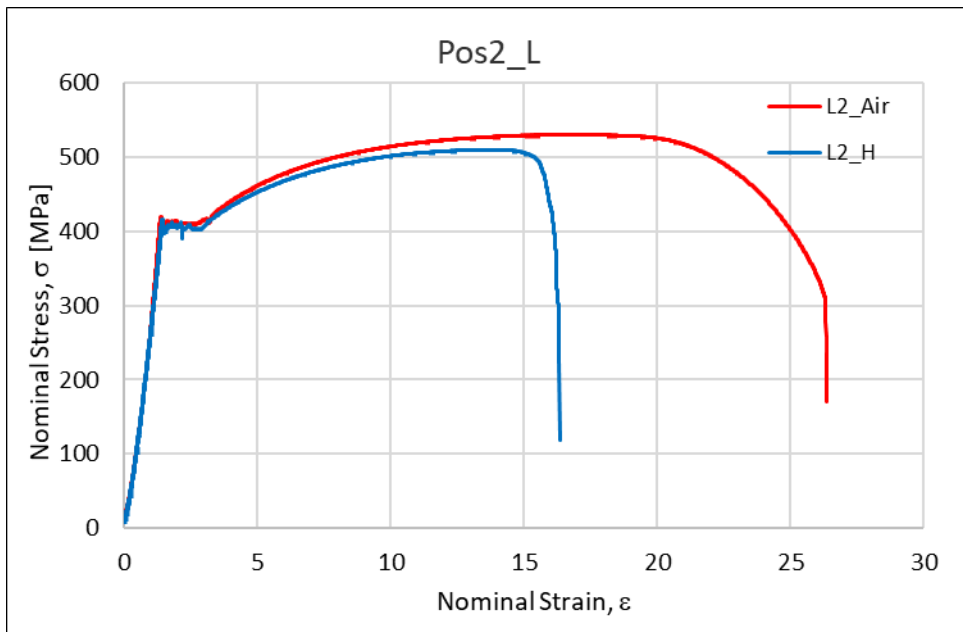


Fig. 25: SSRT results and post-mortem analysis for the S-X65 material from position 2.

L-X60 – Pos2



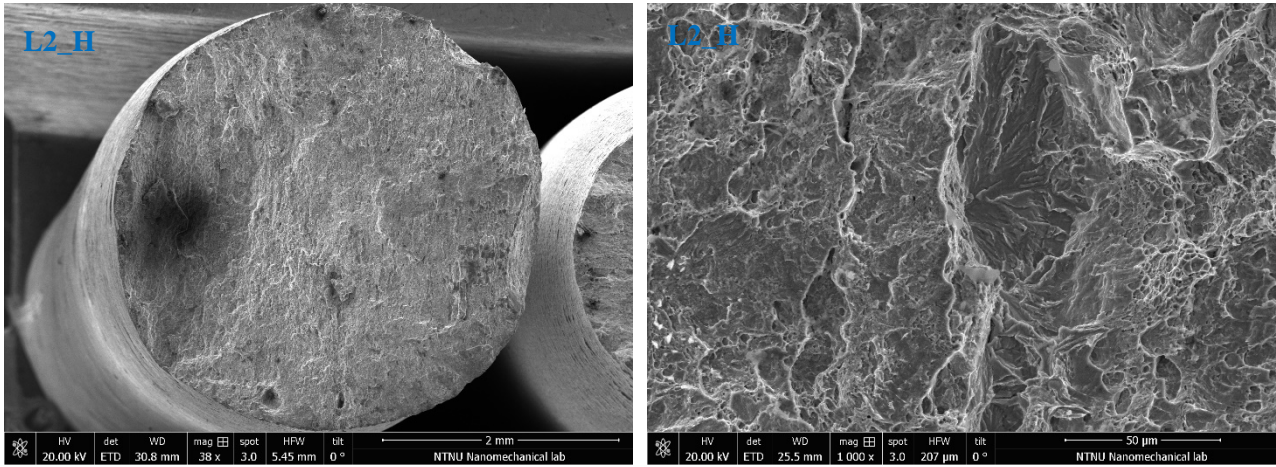
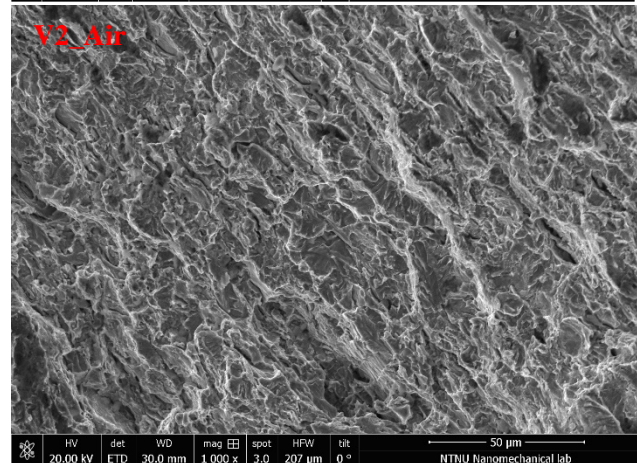
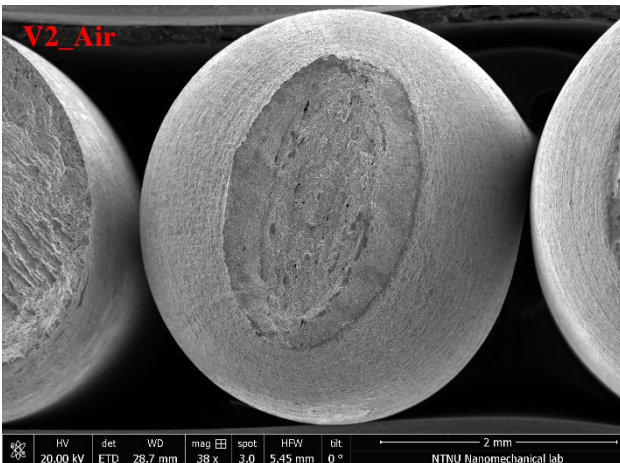
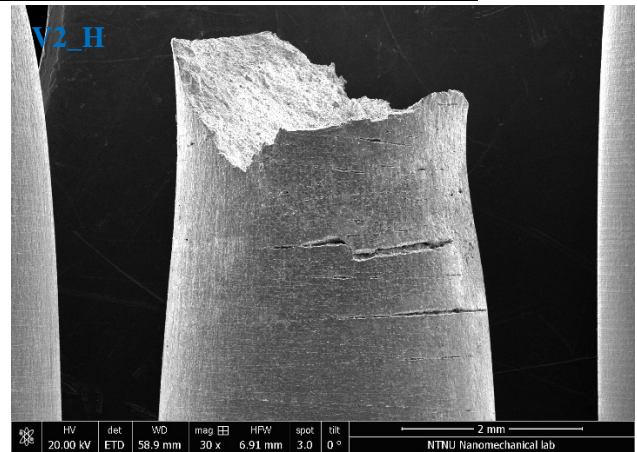
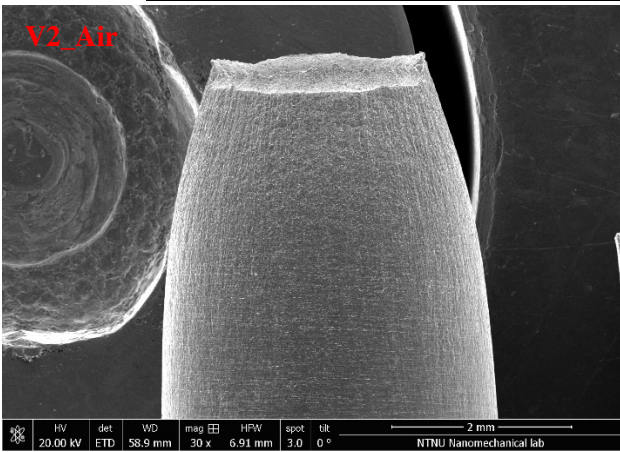
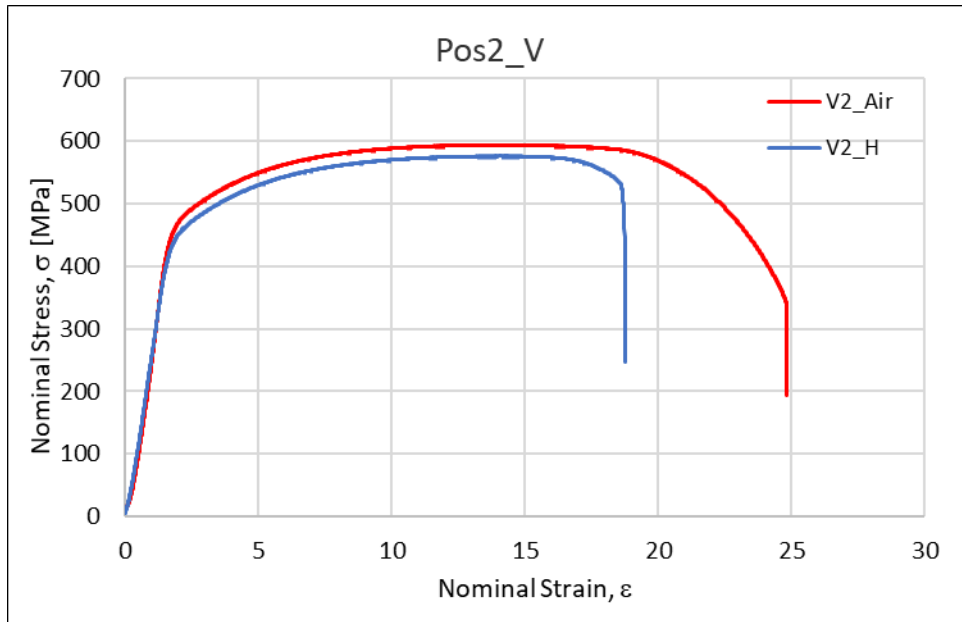


Fig. 26: SSRT results and post-mortem analysis for the L-X60 material from position 2.

V-X65 – Pos2



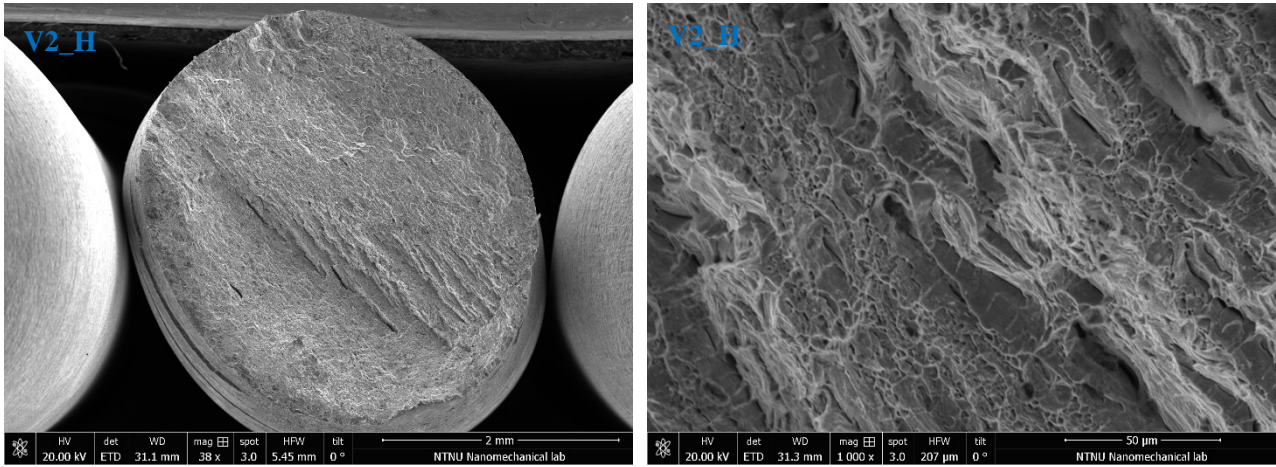
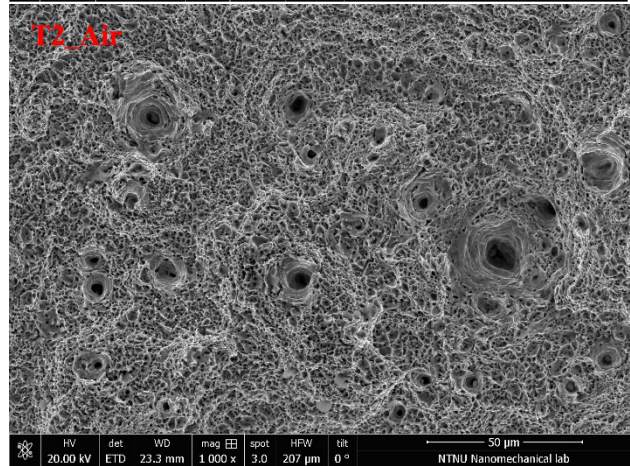
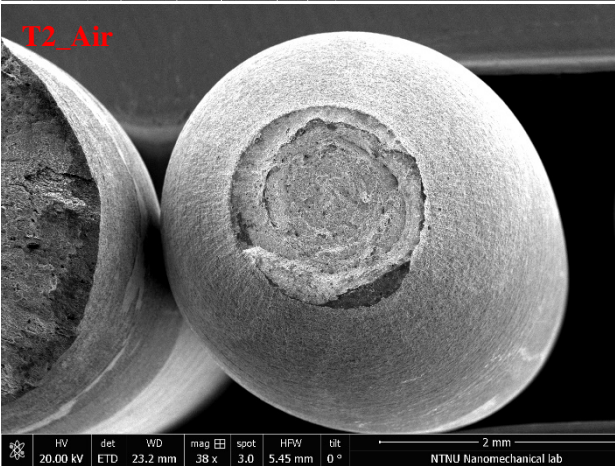
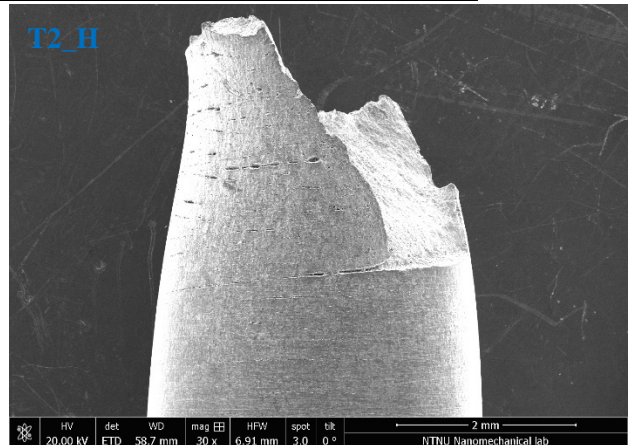
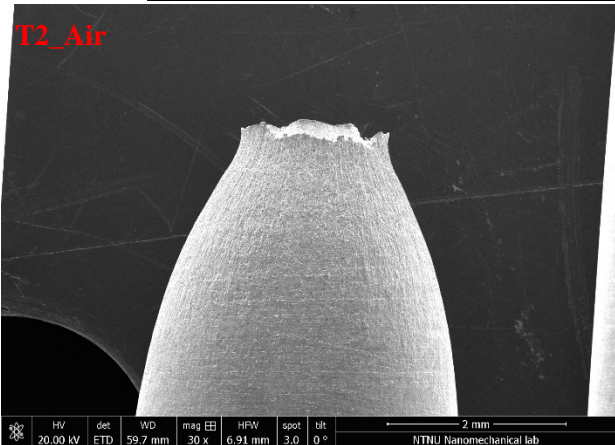
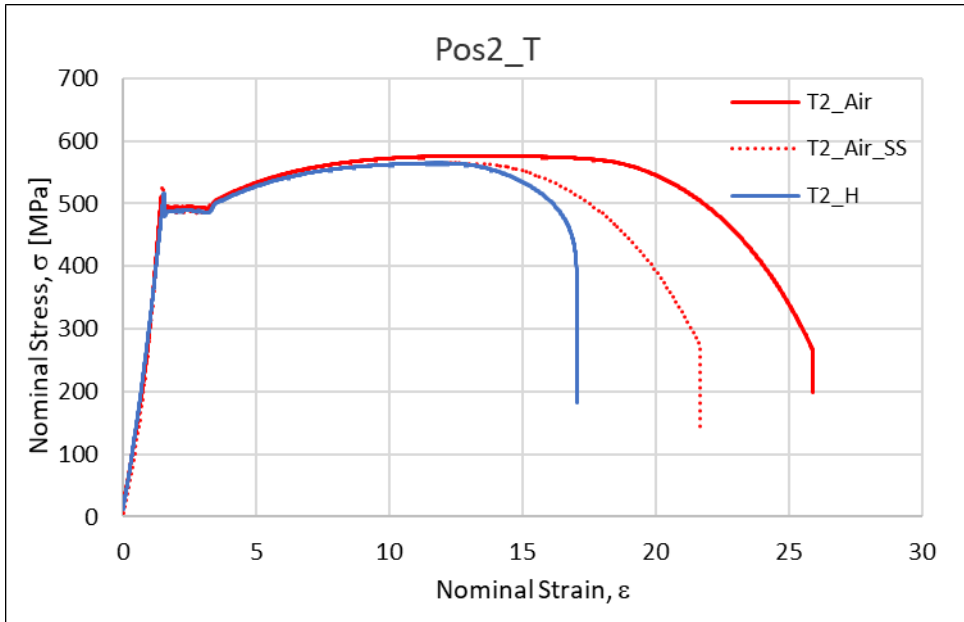


Fig. 27: SSRT results and post-mortem analysis for the V-X65 material from position 2.

T-X65 – Pos2



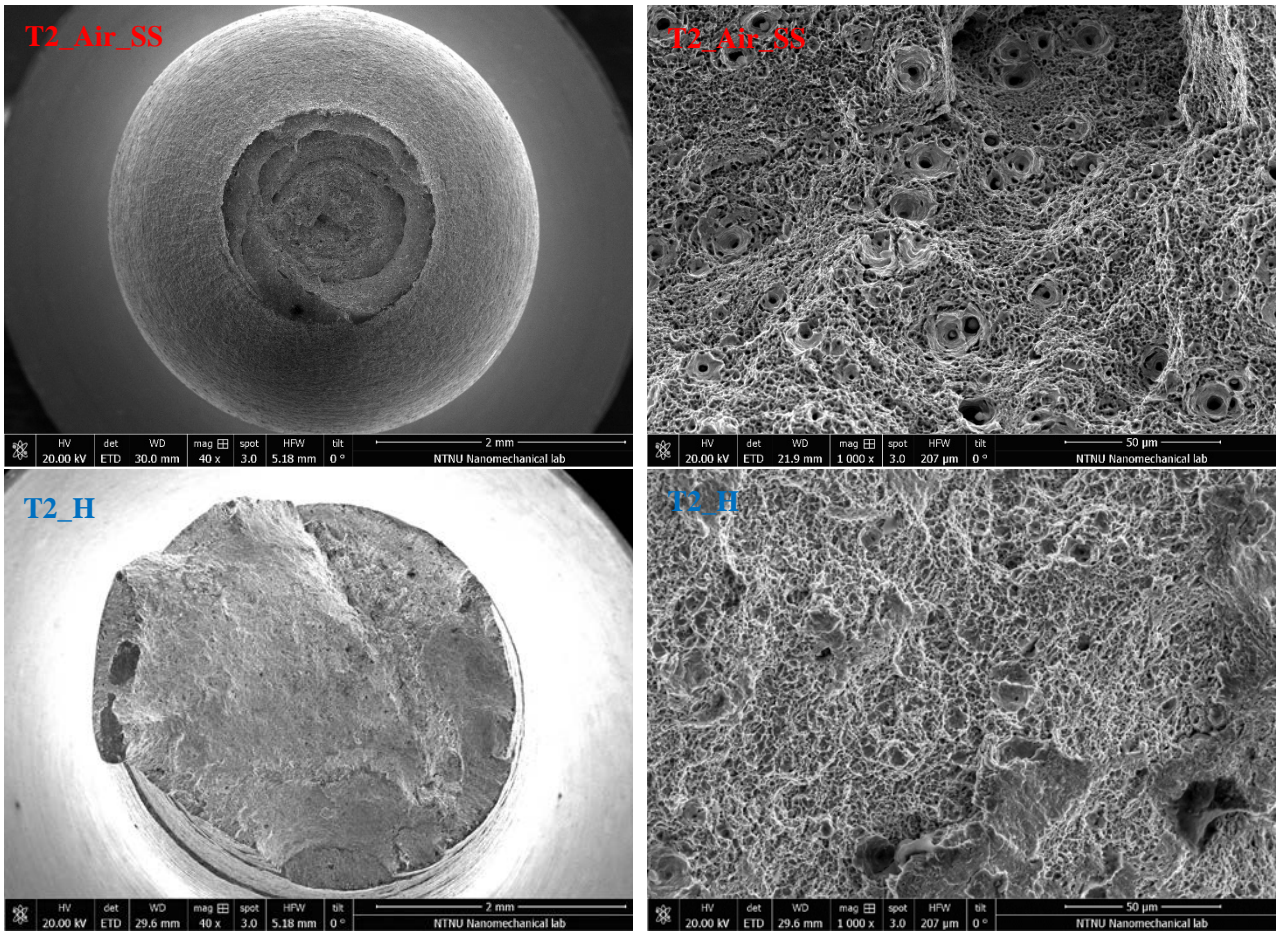


Fig. 28: SSRT results and post-mortem specimen analysis for the T-X65 material from position 2.

3.2.3 Position 3 results

S-X65 – Pos3

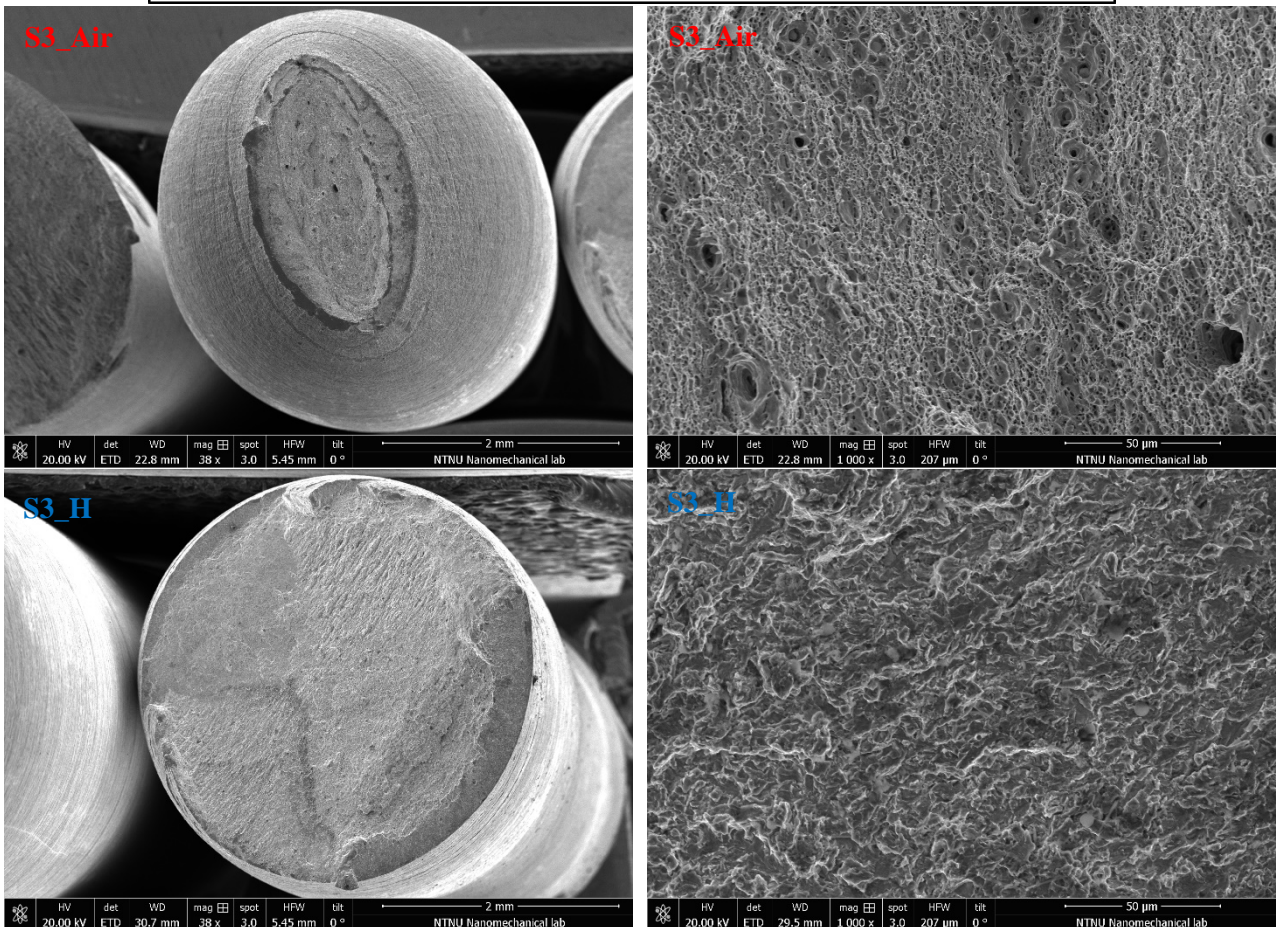
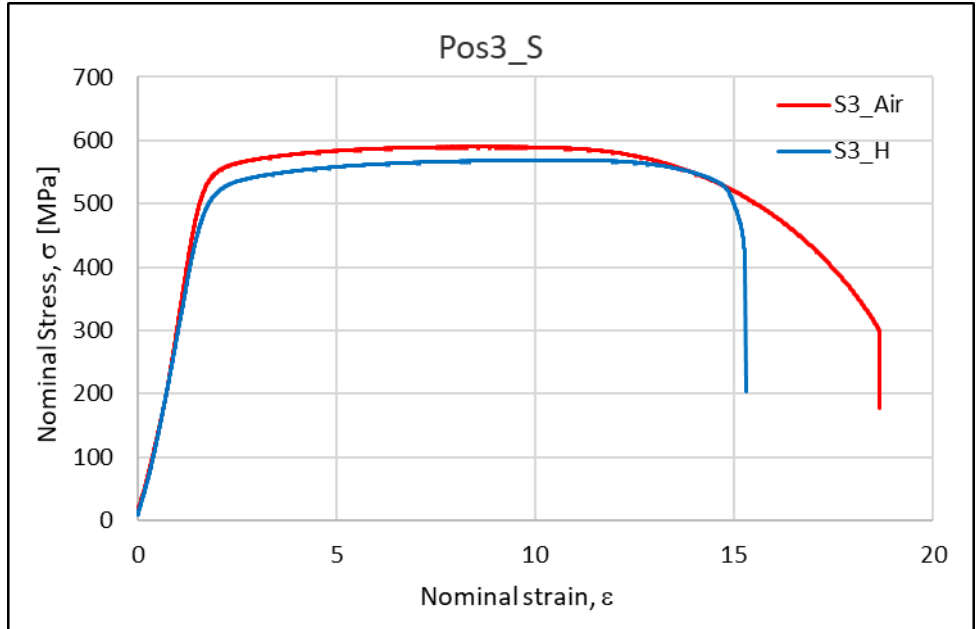


Fig. 29: SSRT results and post-mortem analysis for the S-X65 material from position 3.

L-X60 – Pos3

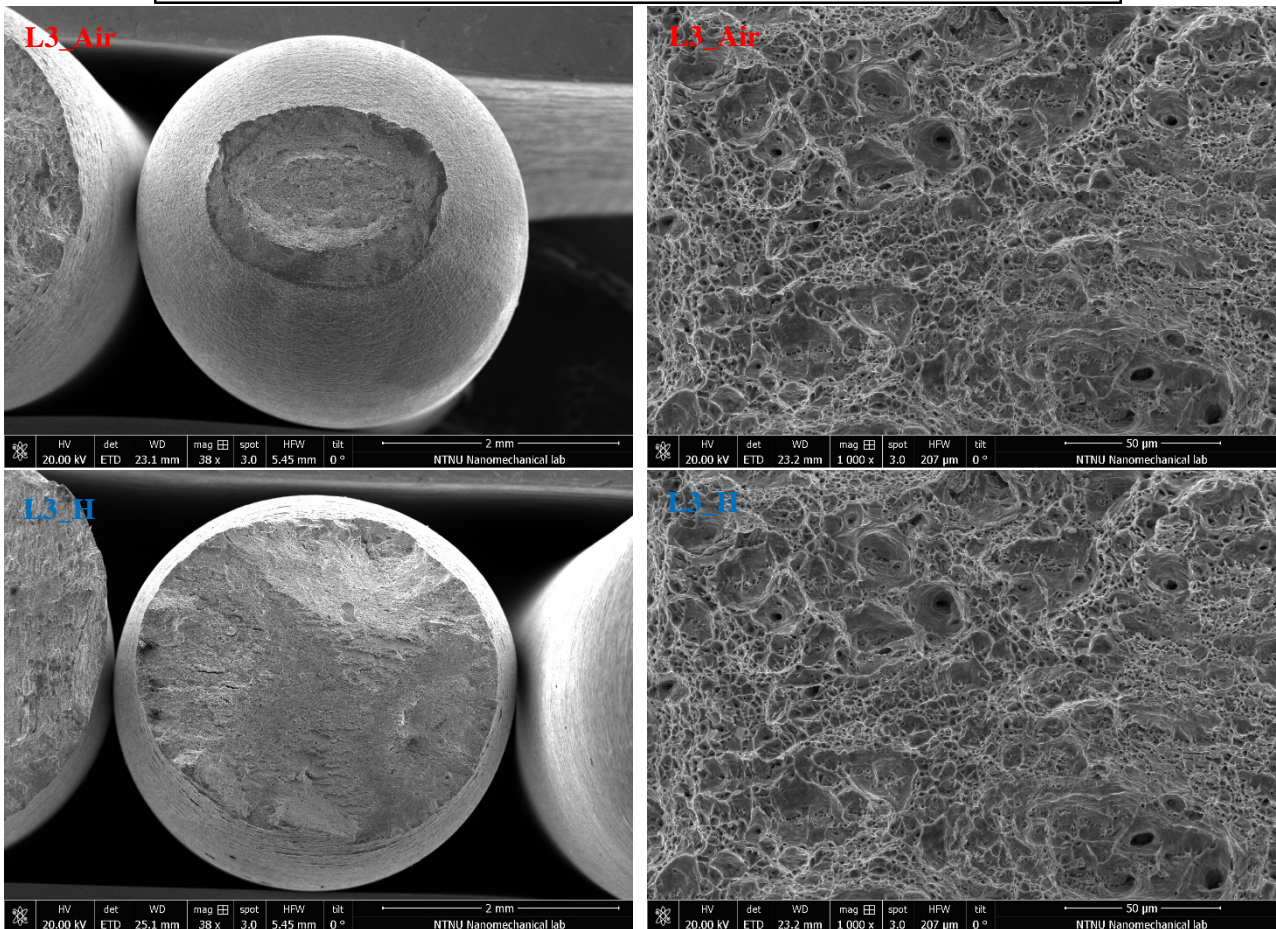
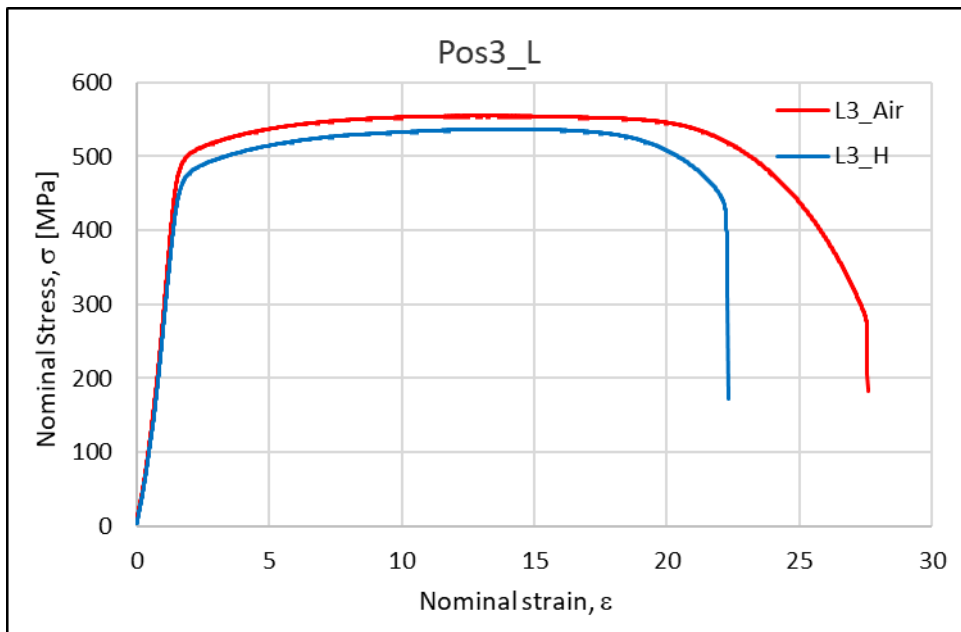


Fig. 30: SSRT results and post-mortem analysis for the L-X60 material from position 3.

V-X65 – Pos3

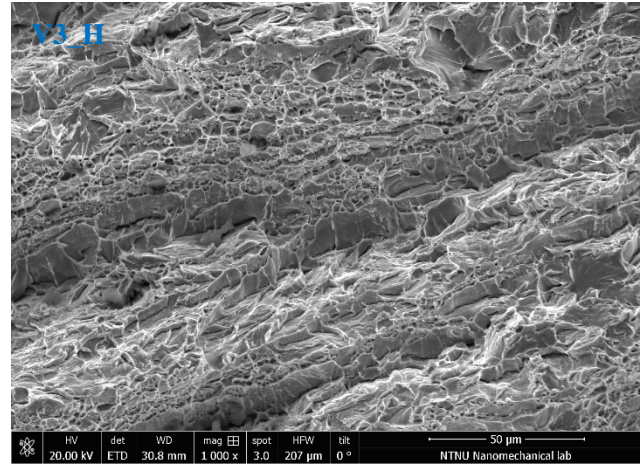
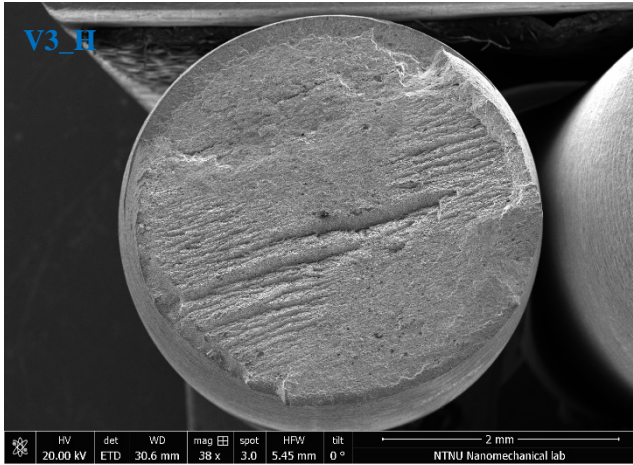
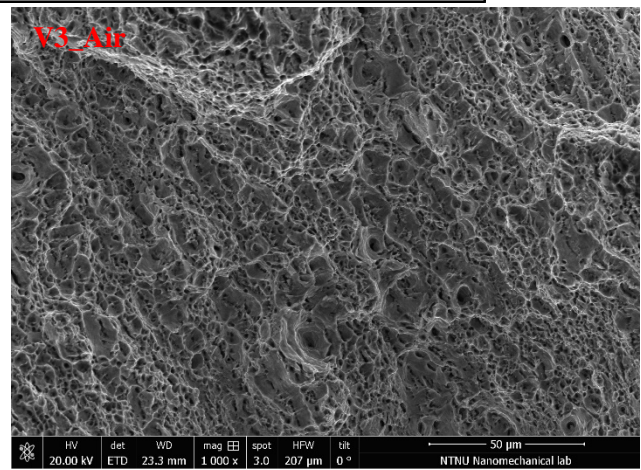
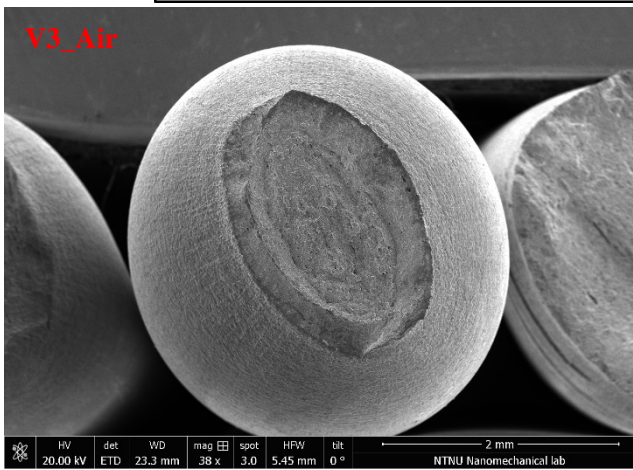
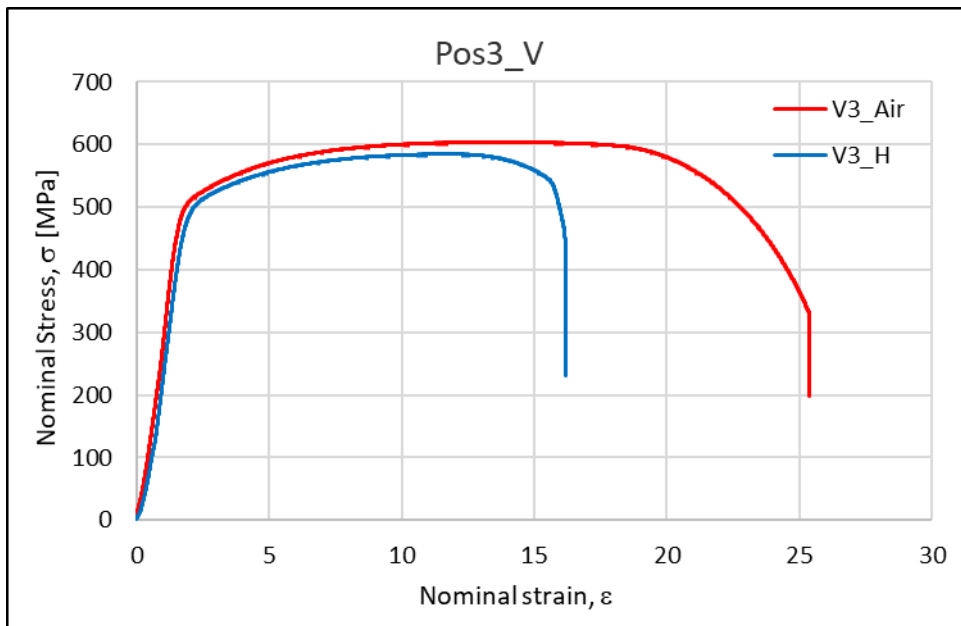


Fig. 31: SSRT results and post-mortem for V-X65 material from position 3.

T-X65 – Pos3

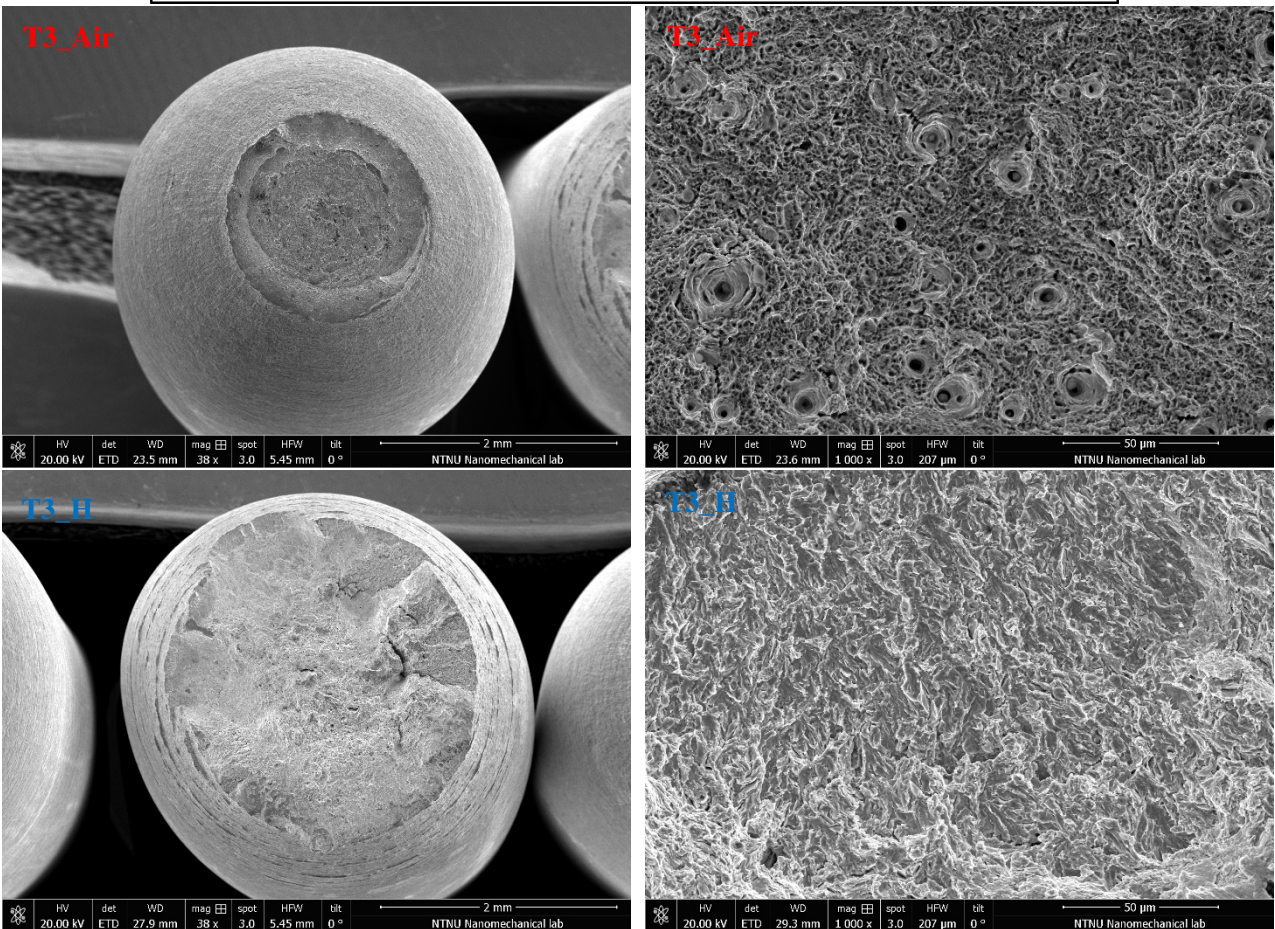
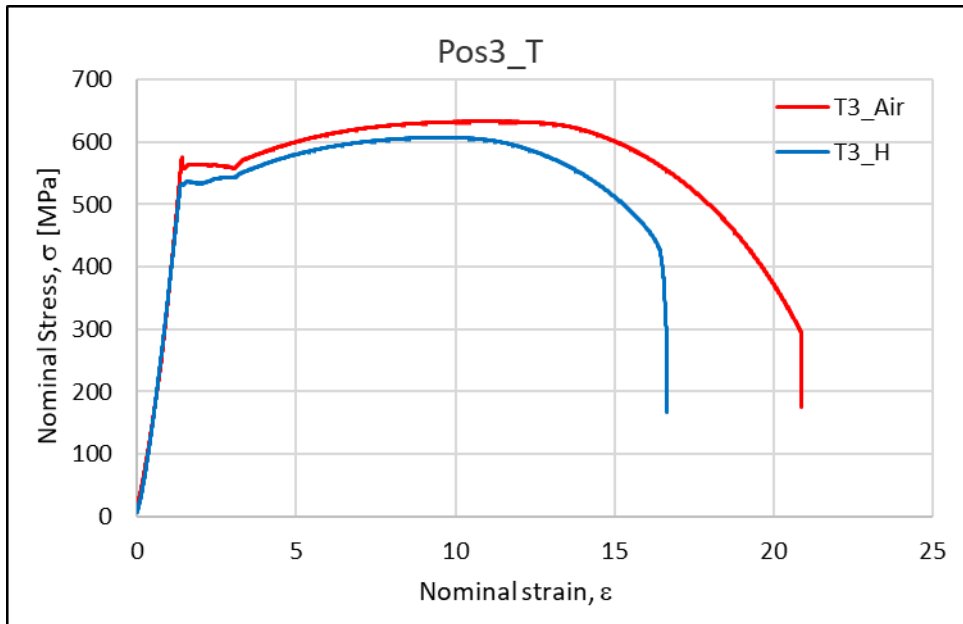


Fig. 32: SSRT results and post-mortem analysis for T-X65 material from position 3.

3.2.4 Position 5 results

S-X65 – Pos5

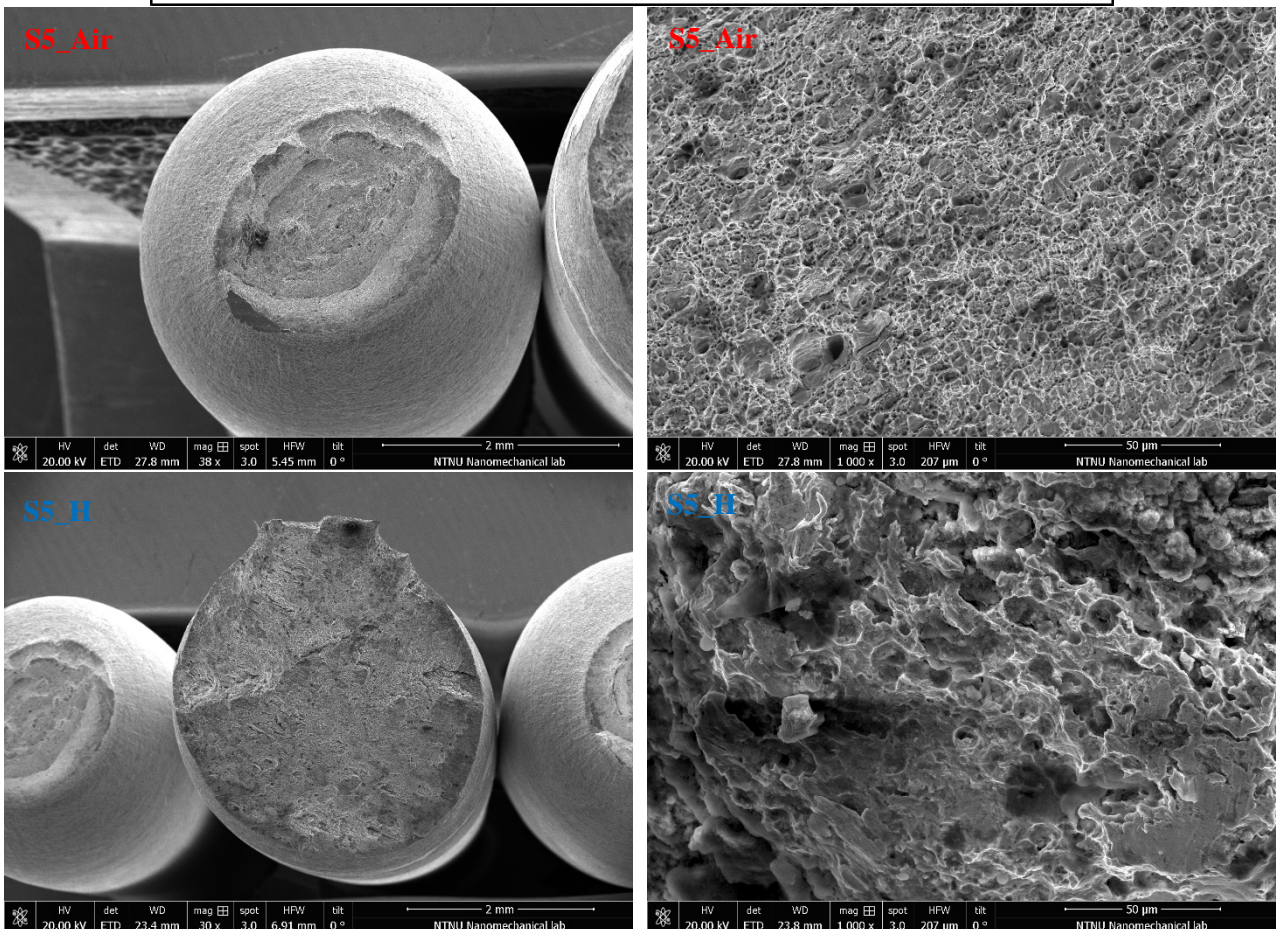
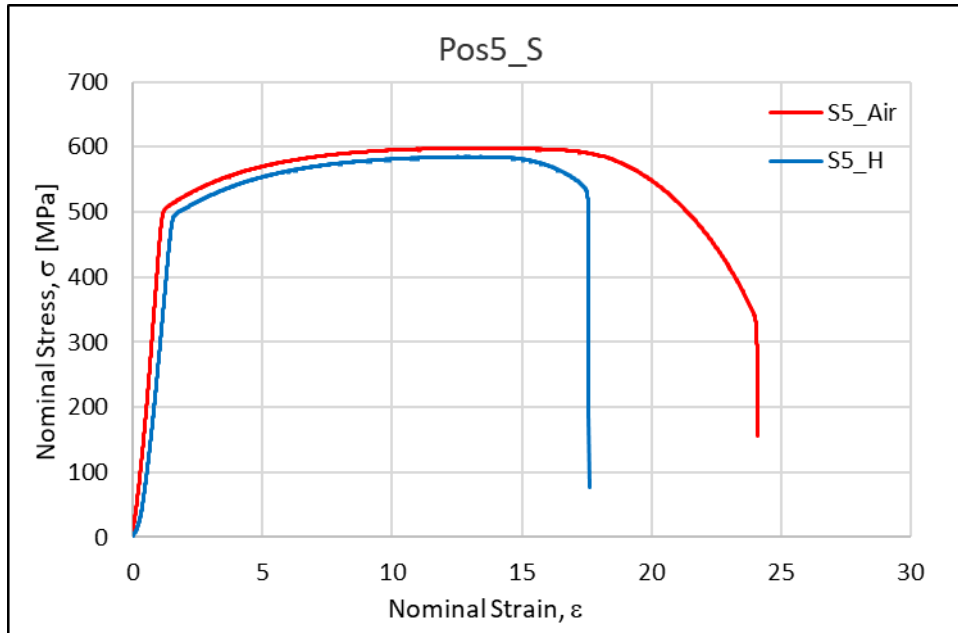


Fig. 33: SSRT results and post-mortem analysis for the S-X65 material from position 5.

L-X60 – Pos5

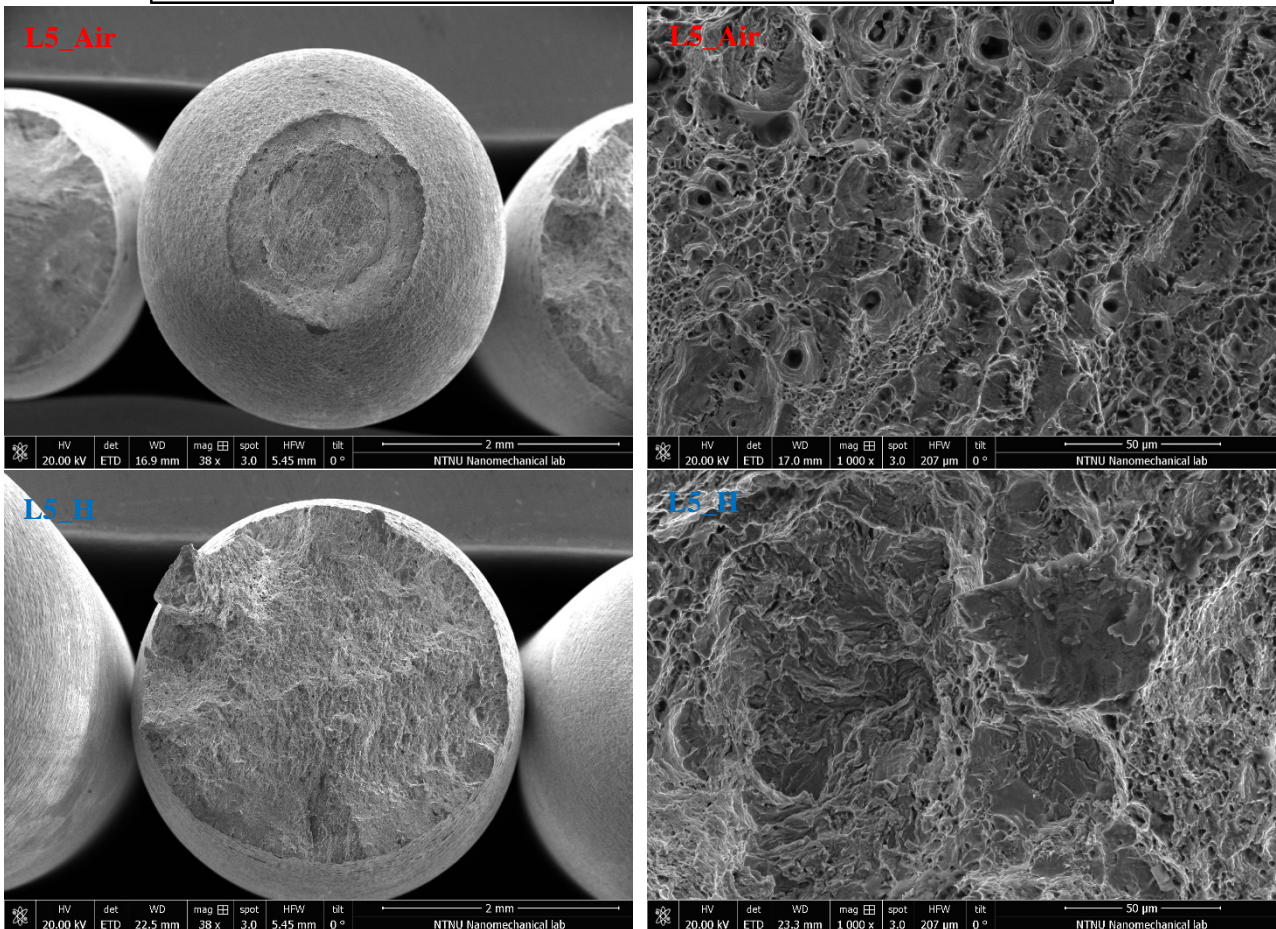
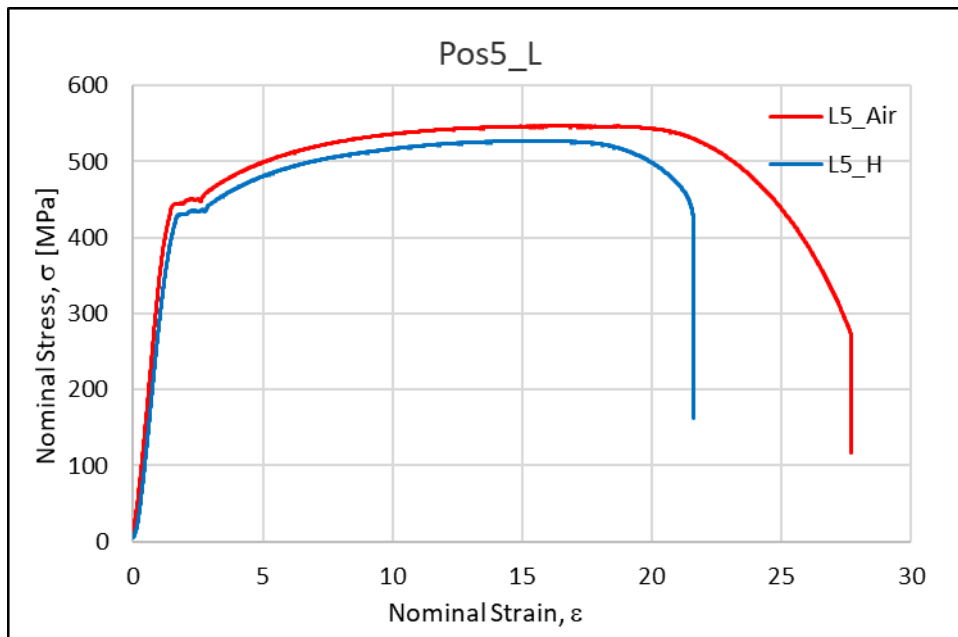


Fig. 34: SSRT results and post-mortem analysis for L-X60 material in position 3.

V-X65 – Pos5

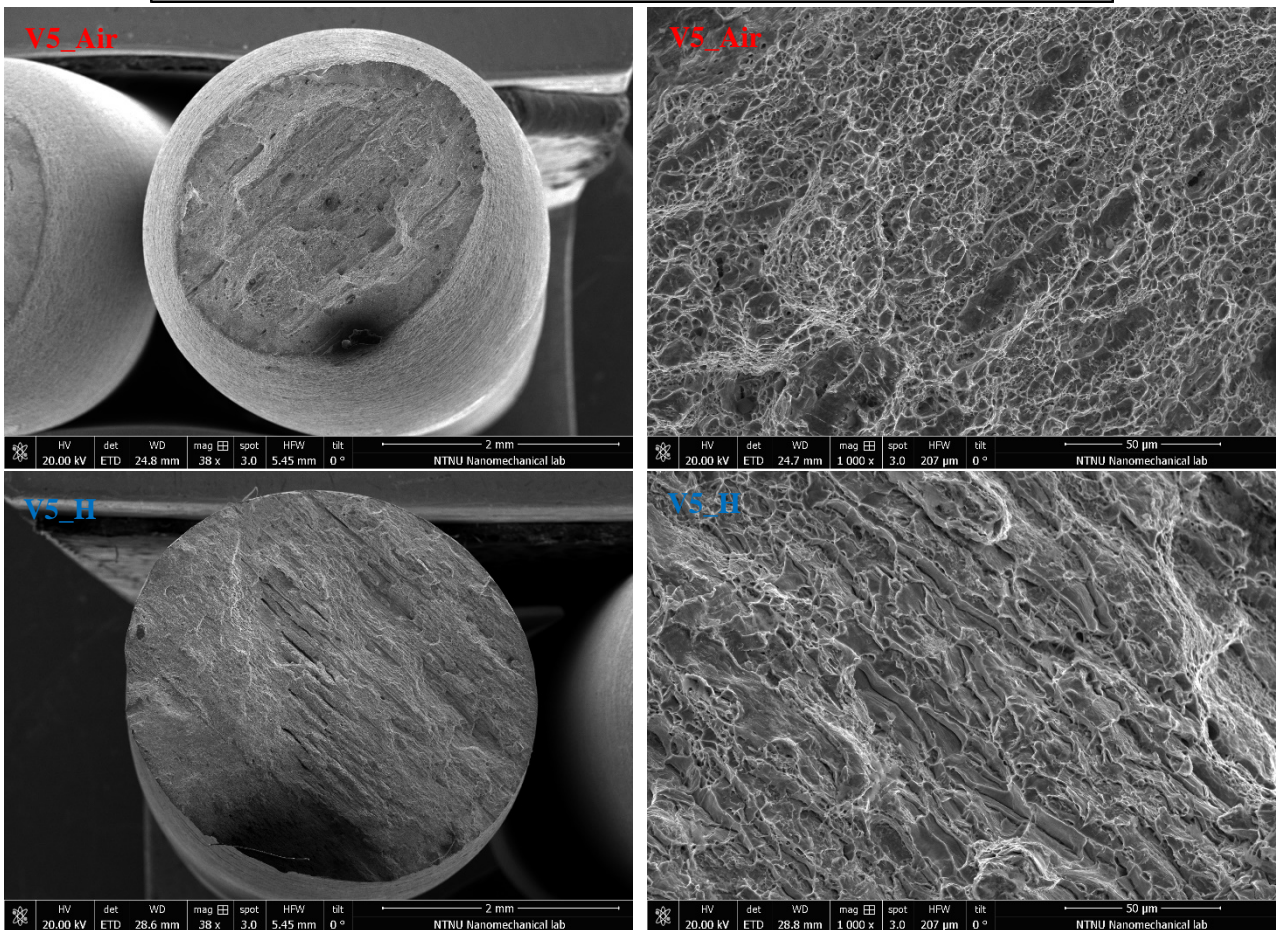
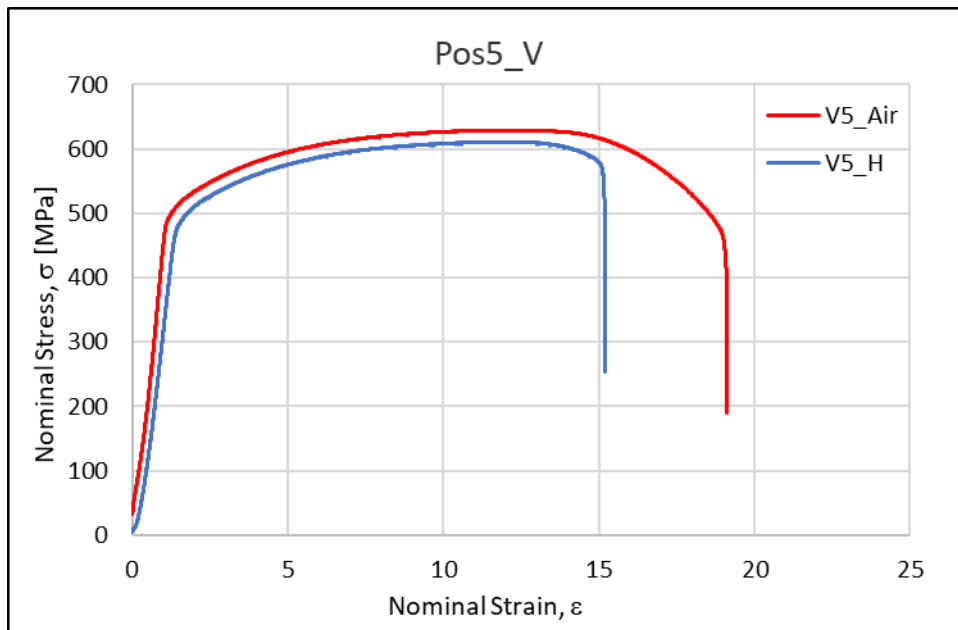


Fig. 35: SSRT results and post-mortem analysis for V-X65 material in position 5.

T-X65 – Pos5

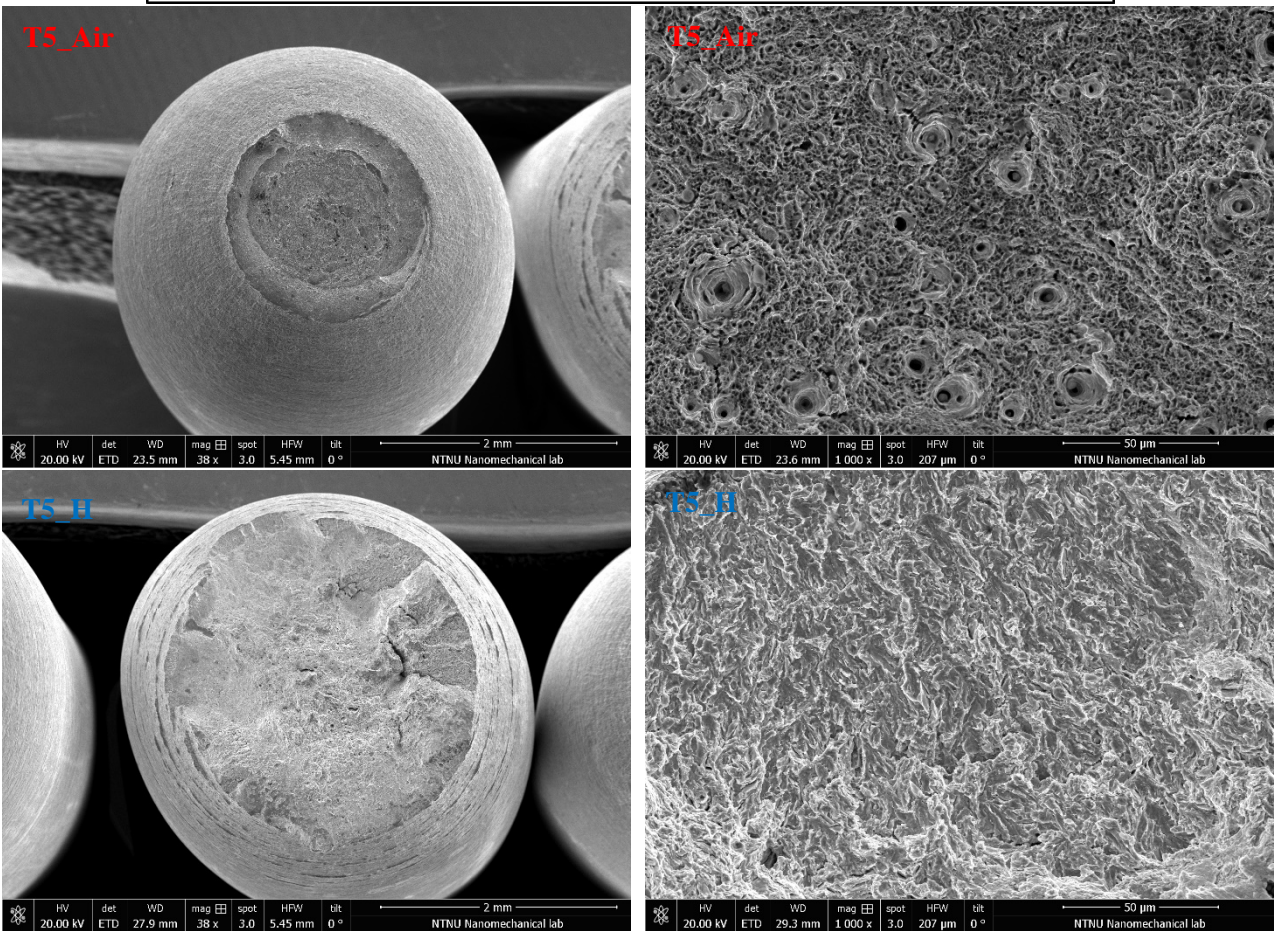
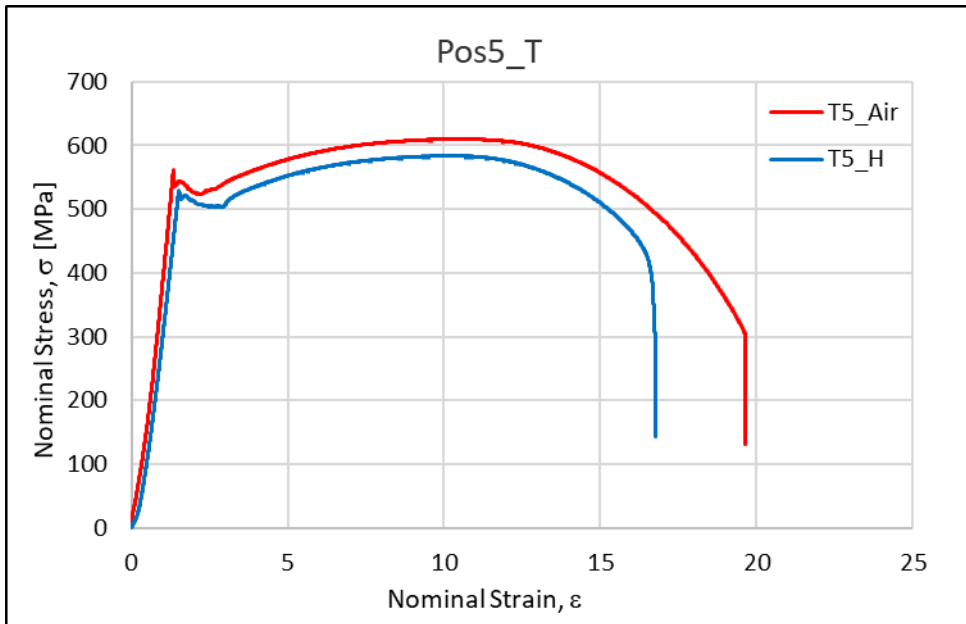


Fig. 36: SSRT results and post-mortem analysis for T-X65 material in position 5.

3.2.5 Summary of the SSRT results for base metal.

All the result presented in the previous sections are summarized in Table 15, in terms of Embrittlement Index and reduction of ductility, as defined in Eq. 1 and Eq. 2.:

Table 15: Summary of the SSRT test results for the base materials. The values in blue represent are obtained by referring to the tests in air performed at the slowest strain rate of 1E-06 s⁻¹.

Material	Condition	σ_{\max} [MPa]	$\sigma_{\max,H}/\sigma_{\max,a}$	ϵ_f	z [%]	ϵ_{red} [%]	EI [%]
L2	Air	530	0,96	26,3	74,0	61,4	56,8
	CP	510		16,1	32,0		
S2	Air	584	0,97	21,0	77,0	61,0	62,3
	Air-SS	565		17,1	67,0		
	CP	569	1,01	12,8	29,0	74,9	56,7
V2	Air	594	0,97	24,9	76,0	74,7	51,3
	CP	576		18,6	37,0		
T2	Air	576	0,98	25,9	85,0	65,3	42,4
	Air-SS	565		21,7	84,0		
	CP	565	1,00	16,9	49,0	78,0	41,7
L3	Air	555	0,97	27,5	83,0	80,7	31,3
	CP	536		22,2	57,0		
S3	Air	590	0,96	18,7	82,0	80,7	54,9
	CP	569		15,1	37,0		
V3	Air	604	0,94	25,3	79,0	63,2	51,9
	CP	569		16,0	38,0		
T3	Air	633	0,96	20,9	84,0	77,5	29,8
	CP	607		16,2	59,0		
L5	Air	546	0,97	27,7	83,0	78,0	44,6
	CP	527		21,6	46,0		
S5	Air	598	0,98	24,0	78,0	73,3	47,4
	CP	585		17,6	41,0		
V5	Air	629	0,97	19,1	62,0	79,1	50,0
	CP	611		15,1	31,0		
T5	Air	610	0,96	19,5	80,0	89,2	26,3
	CP	584		17,4	59,0		

The plots in Fig. 37 provide a visual comparison of the hydrogen embrittlement susceptibility quantified through both EI and $\epsilon_{f,\text{red}}$:

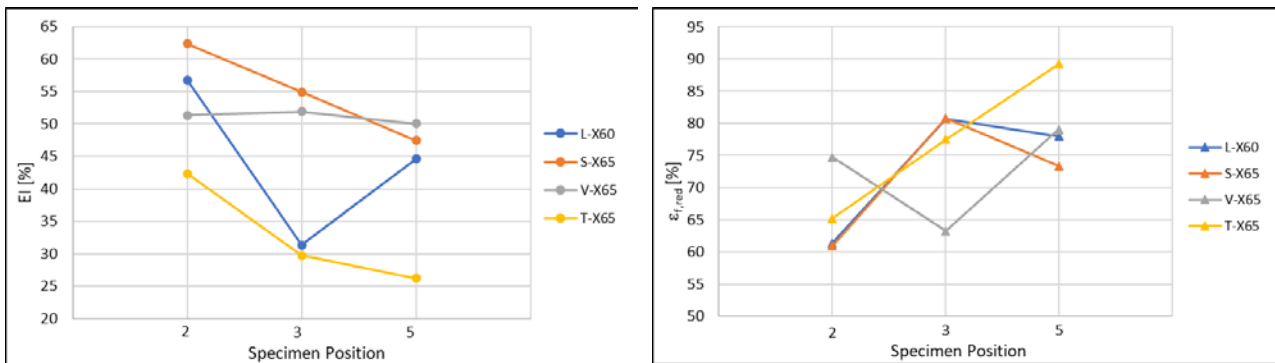


Fig. 37: Plots reporting the embrittlement index EI and the ductility reduction vs. the specimen position for the material tested.

3.3 Weld simulated heat affected zone

Slow strain rate tensile testing was also performed on weld simulated heat affected zones. The base materials used for the weld thermal simulations have been extracted from position 2 as indicated in Fig. 24. The testing procedure is identical to the one presented in section 3.2. Due to limitations with respect to the Gleeble thermal-simulator, the diameter of the cross section for the tensile specimen was reduced from 6 mm to 4 mm. The new tensile specimen design used for the SSRT testing on weld simulated HAZ is reported in Fig. 38.

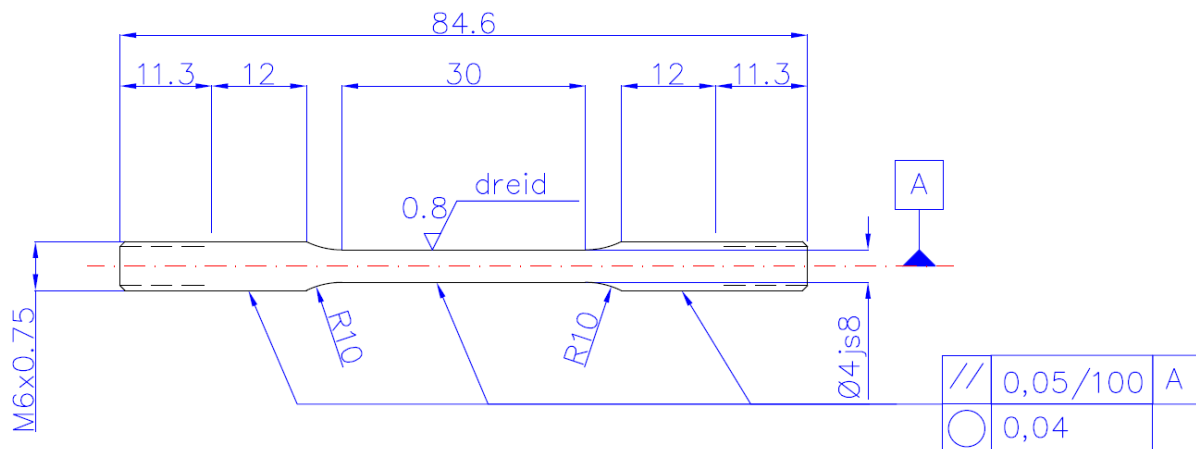


Fig. 38: Specimen design used for SSRT testing on weld simulated HAZ.

3.3.1 Weld thermal simulations

The rationale used to define the thermal simulations was to obtain the "worst" acceptable HAZ, based on acceptance criteria dictated by DNVGL OSF101 standard, i.e. HV10 values as close as possible to 300. In this sense, metallurgical characterization and hardness values have been measured after the simulations and are reported below. The specimens were mounted in the thermo mechanical simulator (Gleeble) by using so called 'hot grips': stainless steel grips which provide the lowest contact area on the specimen, and the best temperature distribution along the axis of the specimen. The specimens were heated to 1350 °C and let to cool through the grips and jaws down to 1250 °C. At 1250 °C a first air quenching was imposed until the specimen reached 850 °C: at this temperature a second more powerful air quenching was activated. The

target cooling rate was obtained through balancing air quenching and resistance heating through the grips. Each thermal simulation was instrumented by three thermocouples spotwelded to the specimen (a bar of the material with a 6 mm diameter), as indicated in Fig. 39:

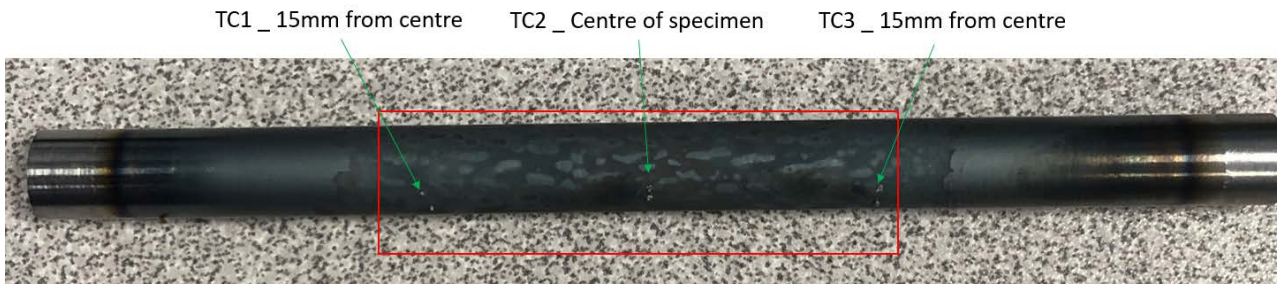


Fig. 39: specimen used for the thermal simulation in the Gleeble machine with indication of the thermocouples positioning.

The thermocouple placed in the centre of the specimen and indicated as TC2, is the one giving the feedback to the whole system while TC1 And TC3, place 15 mm on each side from TC2 are used to obtain the temperature outputs. After several attempts followed by metallographic characterization, the following thermal treatment cycle was found to be the most suitable to obtain microstructural homogeneity and the target HV₁₀ values for the materials extracted from position 2:

Heating rate= 150 °C/sec;

Peak temperature 1350 °C

$\Delta T_{800-500}$ = 5 sec

The relevant plots describing the applied thermal cycles are reported in the following sections.

S-X65

The applied thermal cycles are reported in Fig. 40 in form of temperature vs. time readings from the thermocouples:

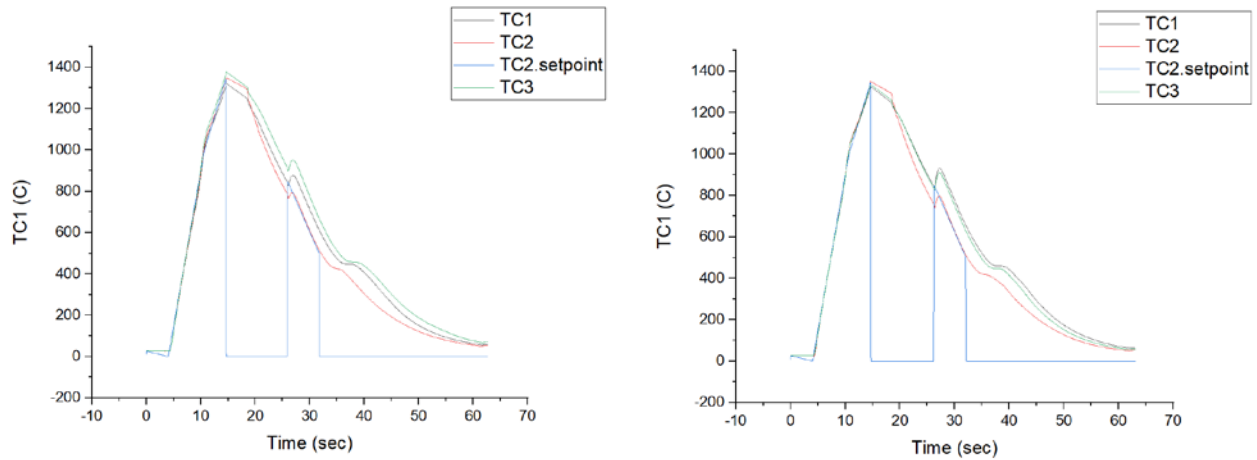


Fig. 40: Temperature vs. time plots obtained from the three thermocouples mounted on the S-X65 material extracted from position 2. These two specimens were tested to obtain the hydrogen susceptibility of the material heat affected zone.

The metallurgical characterization of the thermal simulated specimens is presented in Fig. 41.

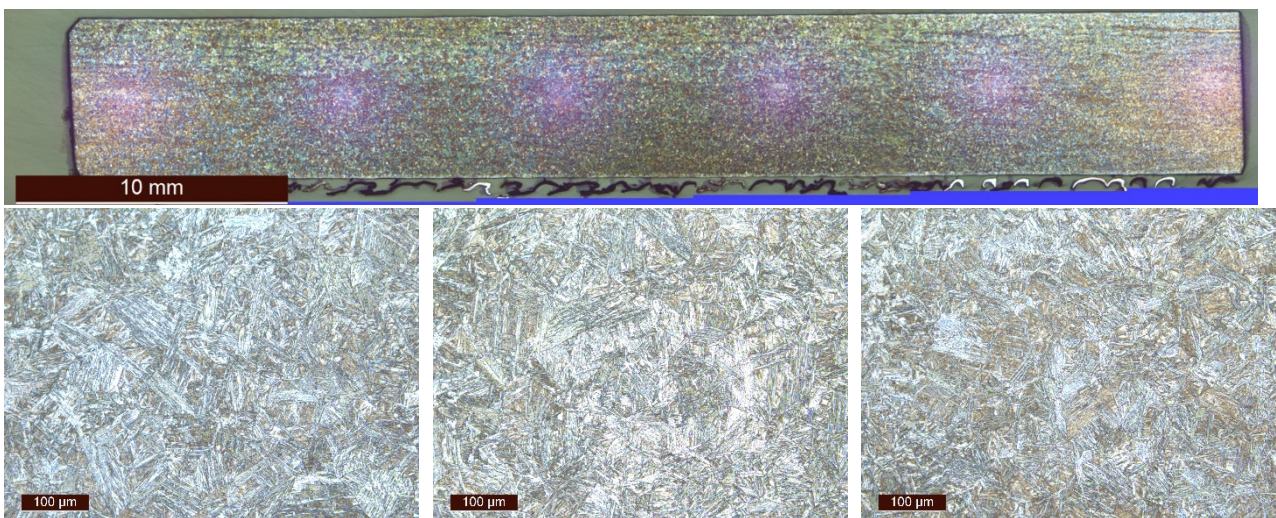


Fig. 41: Metallurgical characterization of heat treated on S-X65 material. The magnified pictures on the bottom row are taken to the position in correspondence of the thermocouples, i.e. TC1, TC2 and TC3, respectively.

The microstructure consists of prior austenitic grains, bainite (white) and martensite (brown). There is observed a higher concentration of bainite than martensite. The prior austenitic grains are much smaller than the ones observed in T-X65, and a little smaller than the ones observed in L-X60.

The representative hardness values and their positioning are reported in Fig. 42.

Vickers Hardness measurements				
Indentation no.	Hardness section no. (see figure above)			
	1	2	3	4
1	290	291	280	276
2	288	296	288	269
3	286	291	285	269
4	295	286	285	268
5	301	292	289	268
6	304	283	286	275
7	306	306	288	277
8	305	291	290	279
9	299	304	298	284
10	310	305	295	276
11	304	301	294	295
12	303	298	292	286
13	299	303	312	283
14	300	316	298	284
15	300	306	306	271
16	397	298	302	271
17	295	298	311	273
18	286	292	293	267
19	290	298	289	264
20	291	287	296	267

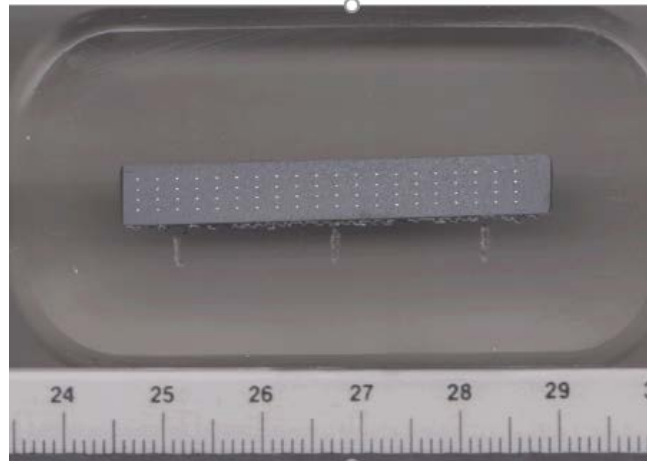
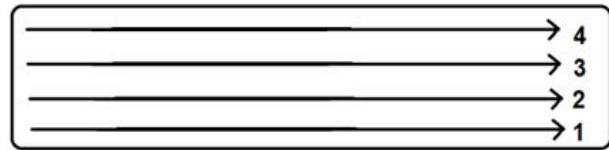


Fig. 42: Hardness values measured on the heat-treated specimen of S-X65 material extracted from position 2. Indentation ID numbers are taken going from the left to the right of each relevant reference line.

Overall maximum, minimum and average HV10 values are 316, 264 and 291 (s.d. 12).

L-X60

The applied thermal cycles are reported in Fig. 43 in form of temperature vs. time readings from the thermocouples:

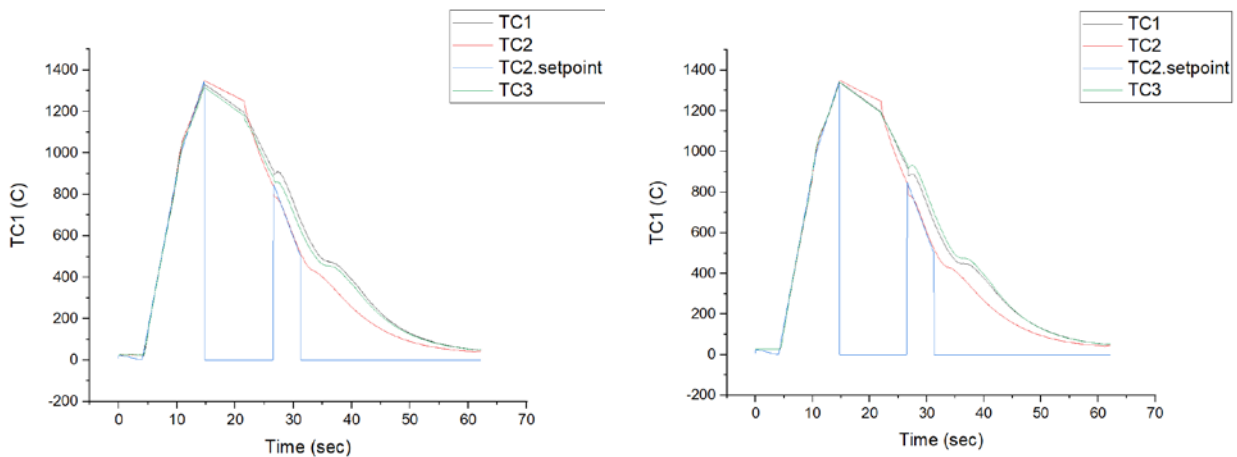


Fig. 43: Temperature vs. time plots obtained from the three thermocouples spot welded on the L-X60 material extracted from position 2. These two specimens were tested to obtain the hydrogen susceptibility of the material heat affected zone.

The metallurgical characterization of the thermal simulated specimens is presented in Fig. 44:

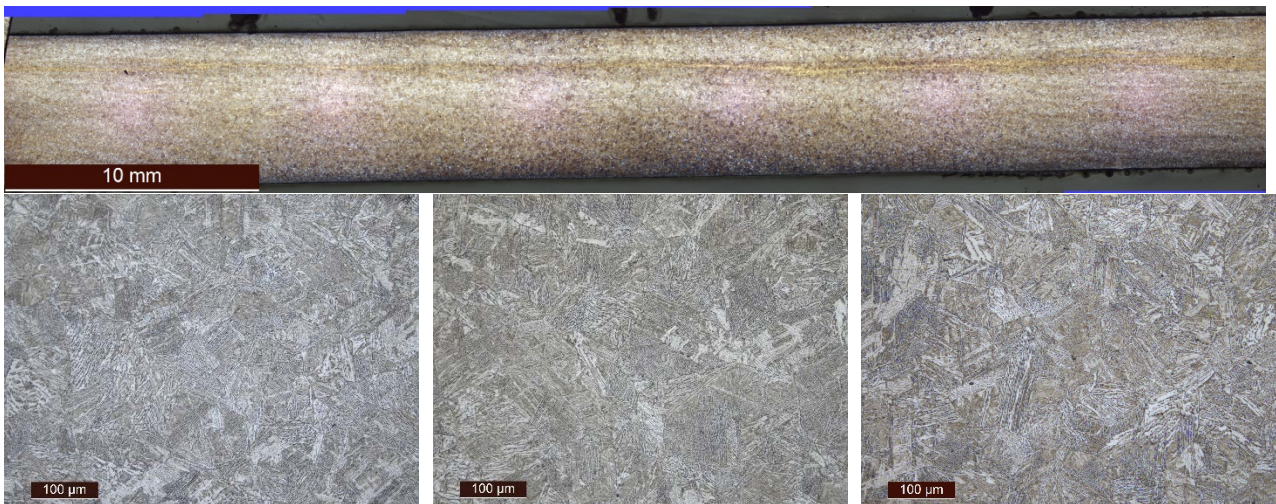


Fig. 44: Metallurgical characterization of heat treated L-X60 material. The magnified pictures on the bottom row are taken to the position in correspondence of the thermocouples, i.e. TC1, TC2 and TC3, respectively.

The microstructure consists of prior austenitic grains, bainite (white) and martensite (brown). There is observed a higher concentration of bainite than martensite. The prior austenitic grains are much smaller than the ones observed in T-X65, and a little bigger than the ones observed in S-X65. This the “band” that’s observed has a higher concentration of martensite than bainite. The representative hardness values and their positioning are reported in Fig. 45.

Vickers Hardness measurements			
Indentation no.	Hardness section no. (see figure above)		
	1	2	3
1	286	277	274
2	281	270	294
3	288	271	298
4	275	267	295
5	272	265	290
6	277	268	294
7	277	271	308
8	295	264	309
9	288	273	283
10	284	276	292
11	287	273	305
12	286	268	314
13	293	278	312
14	293	275	315
15	298	282	286
16	288	270	295
17	292	263	271
18	274	275	286
19	279	281	282
20	289	283	268
21	272	290	265
22	298	279	270
23	287	270	273
24	277	271	267

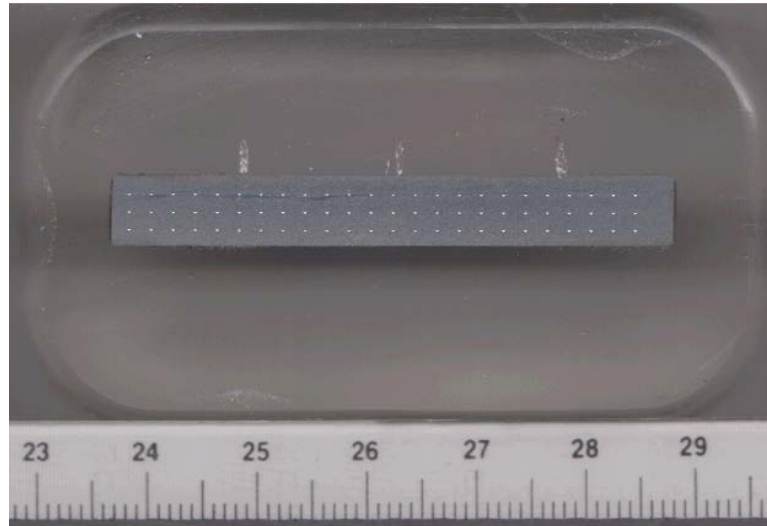
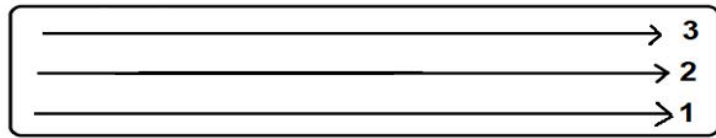


Fig. 45: Hardness values measured on the heat-treated specimen of L-X60 material extracted from position 2. Indentation ID numbers are taken going from the left to the right of each relevant reference line.

Overall maximum, minimum and average HV10 values are 315, 263 and 283 (s.d. 13). The highest hardness values are found in the banding in hardness line 3.

T-X65

The applied thermal cycles are reported in Fig. 46 by temperature vs. time readings from the thermocouples:

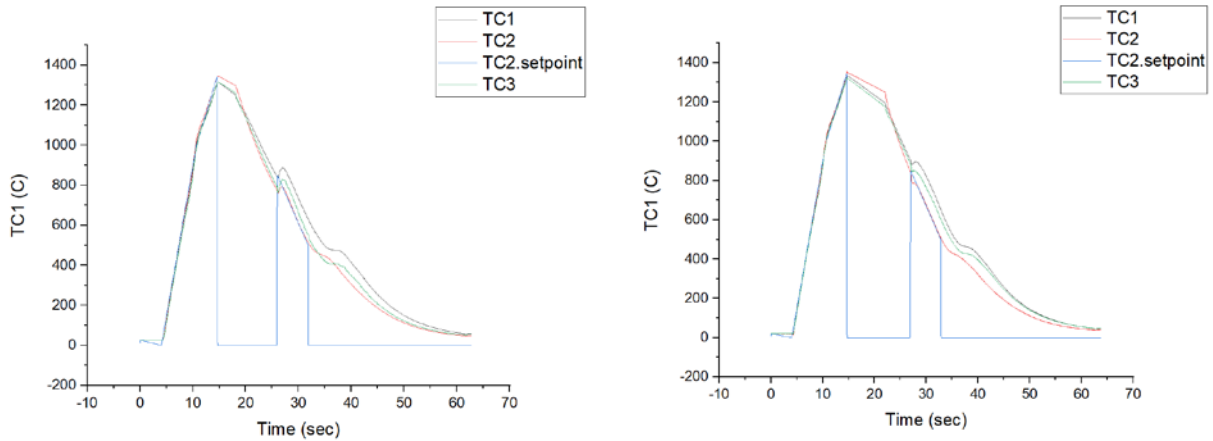


Fig. 46: Temperature vs. time plots obtained from the three thermocouples mounted on the T-X65 material extracted from position 2. These two specimens were tested to obtain the hydrogen susceptibility of the material heat affected zone.

The metallurgical characterization of the thermal simulated specimens is presented in Fig. 47.

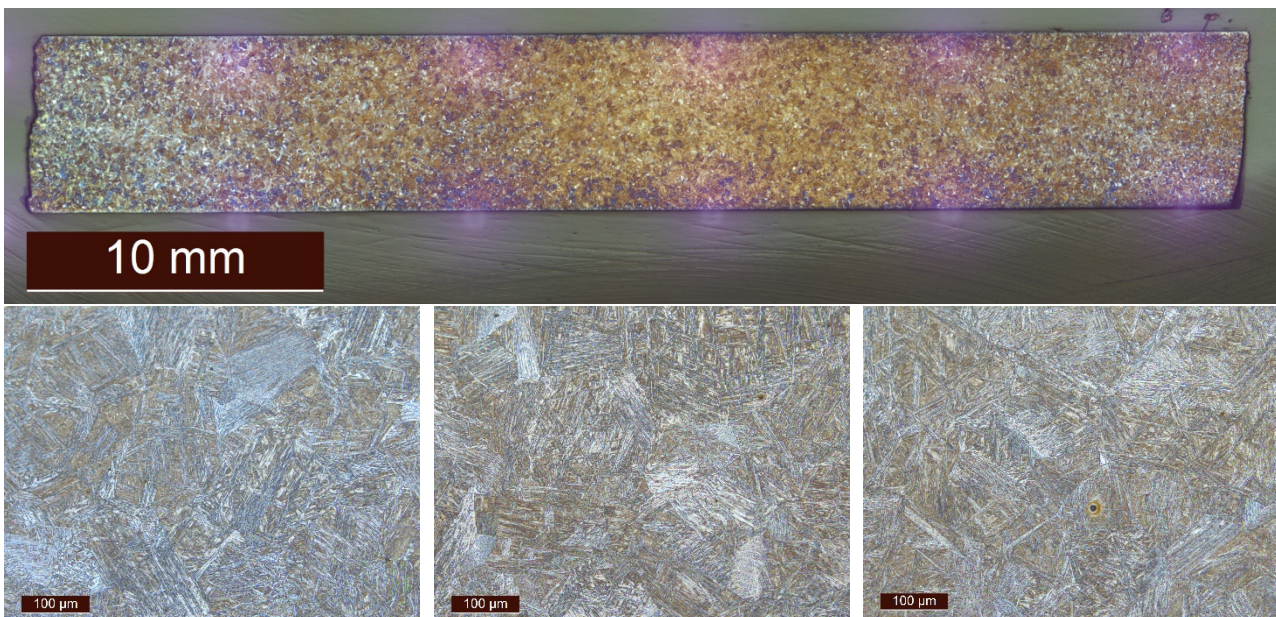


Fig. 47: Metallurgical characterization of heat treated on T-X65 material. The magnified pictures on the bottom row are taken to the position in correspondence of the thermocouples, i.e. TC1, TC2 and TC3, respectively.

The microstructure consists of prior austenitic grains, bainite (white) and martensite (brown). The prior austenitic grains are larger than the ones observed in S-X65 and L-X60.

The representative hardness values and their positioning are reported in Fig. 48:

Vickers Hardness measurements					
Indentation no.	Hardness section no. (see figure above)				
	1 Length	2	3	4	5
1	297	286	285	309	298
2	285	289	289	309	294
3	295	296	286	308	292
4	282	291	292	301	296
5	296	304	301	284	290
6	300	308	308	290	288
7	314	314	302	291	291
8	322	310	311	283	279
9	324	306	314	286	277
10	308	310	300	273	276
11	315	315	315		
12	310				
13	286				
14	303				
15	283				
16	294				
17	284				
18	275				
19	264				

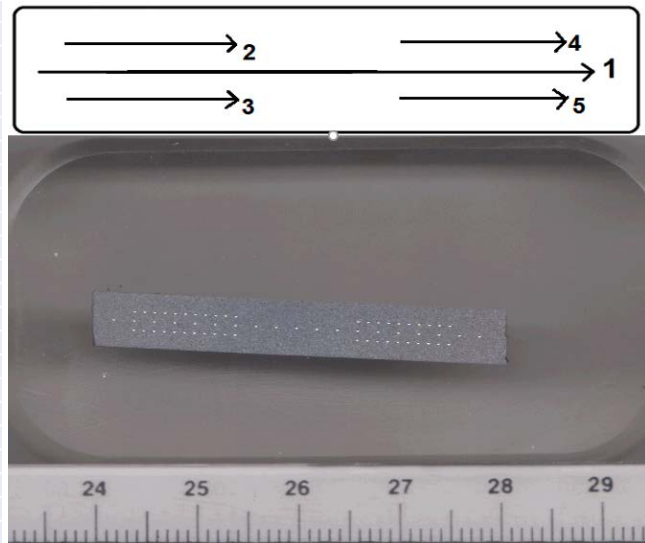


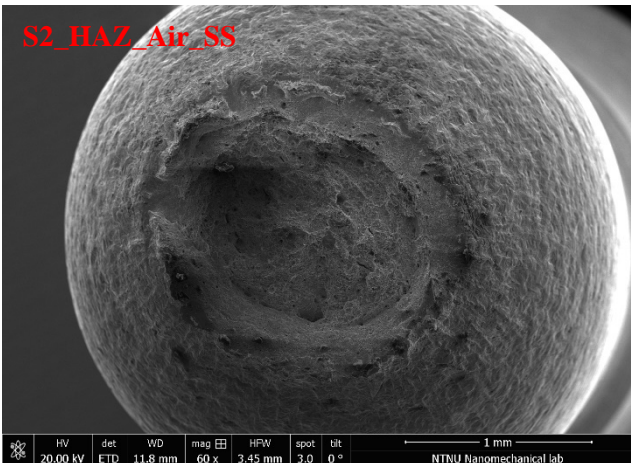
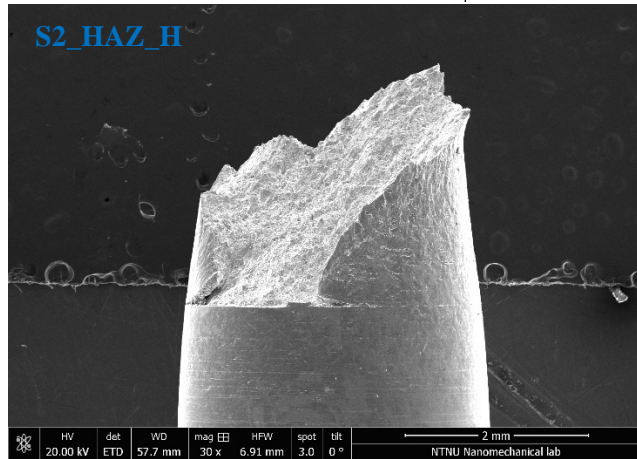
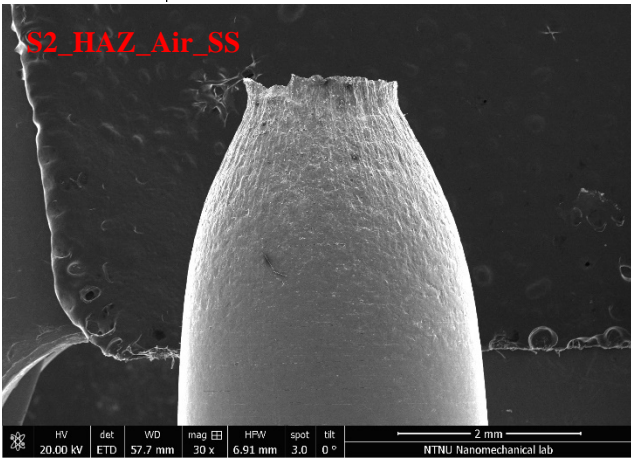
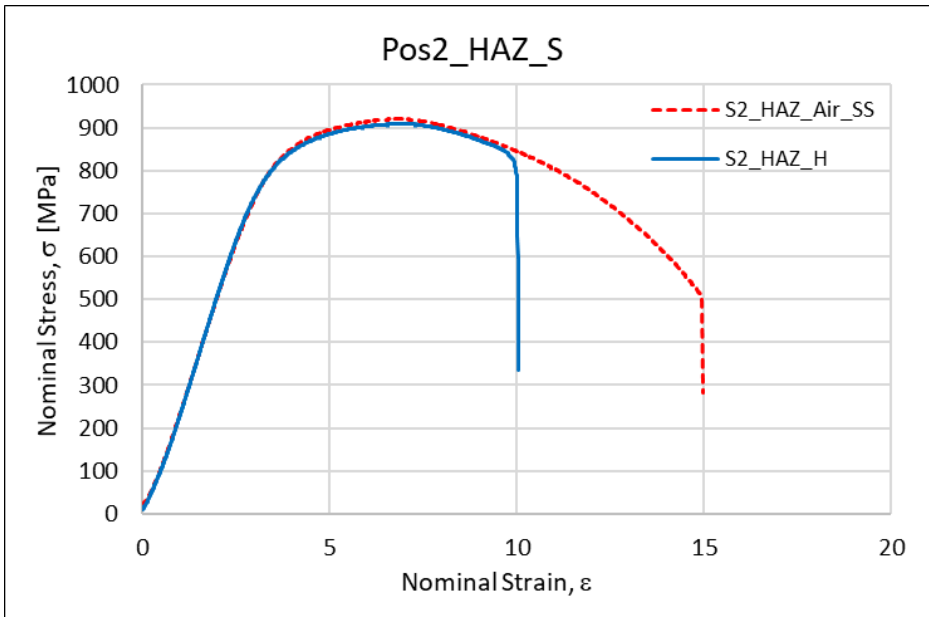
Fig. 48: Hardness values measured on the heat-treated specimen of T-X65 material extracted from position 2. Indentation ID numbers are taken going from the left to the right of each relevant reference line.

Overall maximum, minimum and average HV10 values are 324, 273 and 296 (s.d. 13).

3.4 SSRT results for the weld thermal simulated heat affected zone materials

For each of the materials, the comparison of the curves when tested in air and in electrochemically charged conditions is reported together with the picture of their fractured surfaces at two magnifications is reported. For the HAZ zones both the testing in air and in electrochemically charged hydrogen has been performed at a nominal strain rate of $1E-06 \text{ s}^{-1}$. For this reason, the test in air are identified with "SS" in the tables and figures below.

S-X65 position 2 – weld simulated heat affected zone.



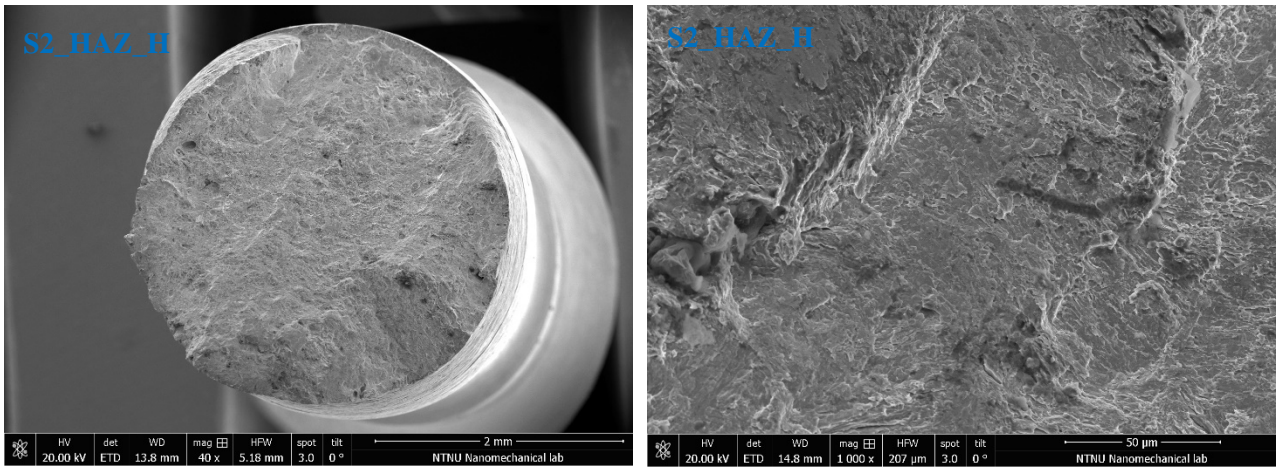
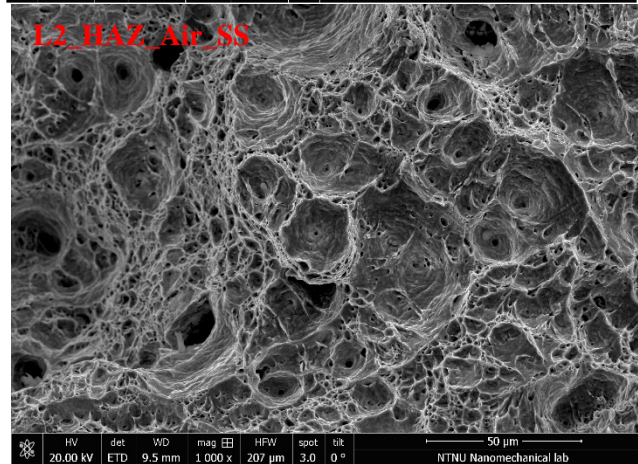
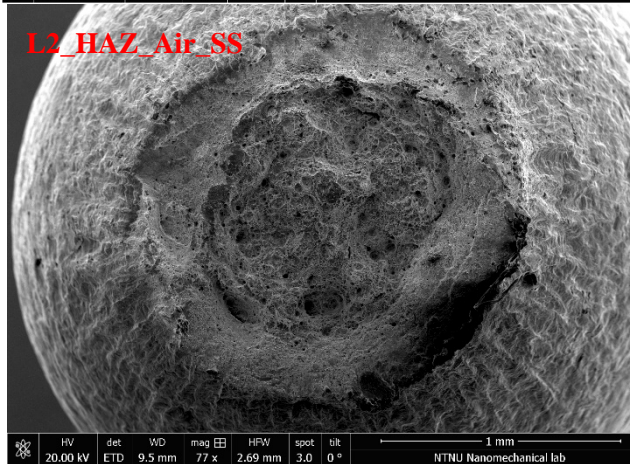
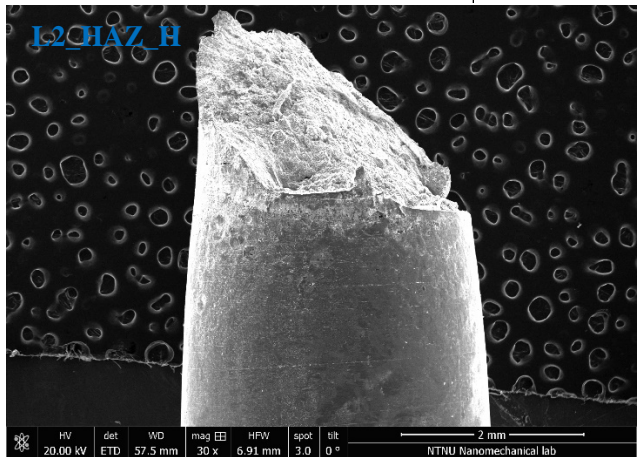
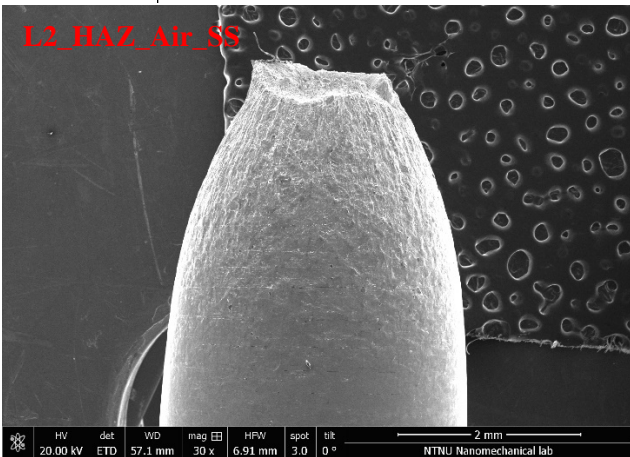
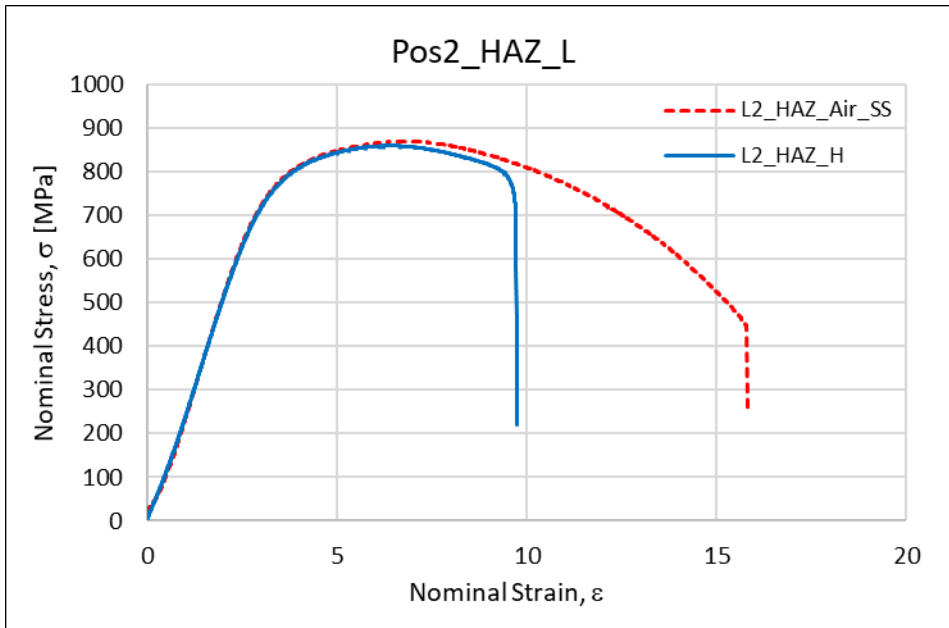
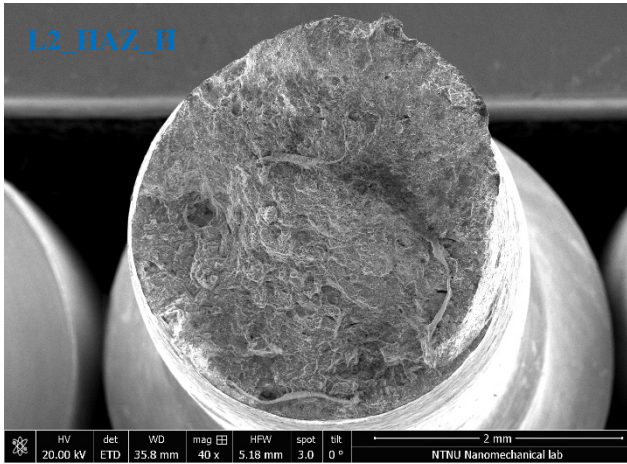


Fig. 49: Results and post-mortem specimen analysis from SSRT performed on weld simulated HAZ from position 2 from the S-X65 material.

L-X60 position 2 – weld thermal simulated heat affected zone



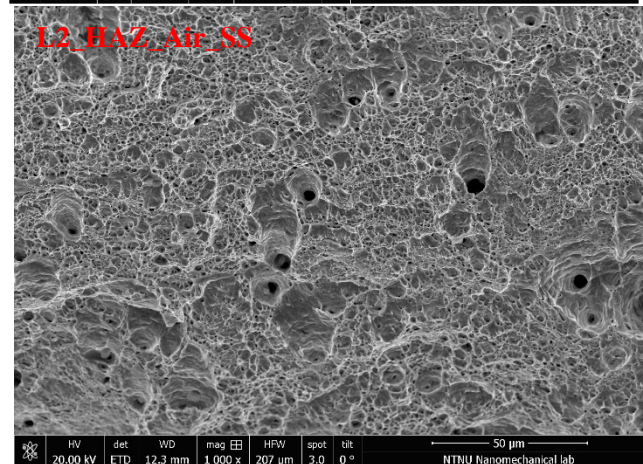
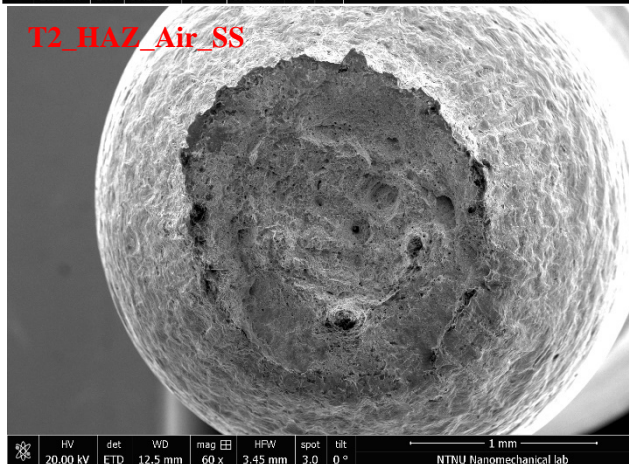
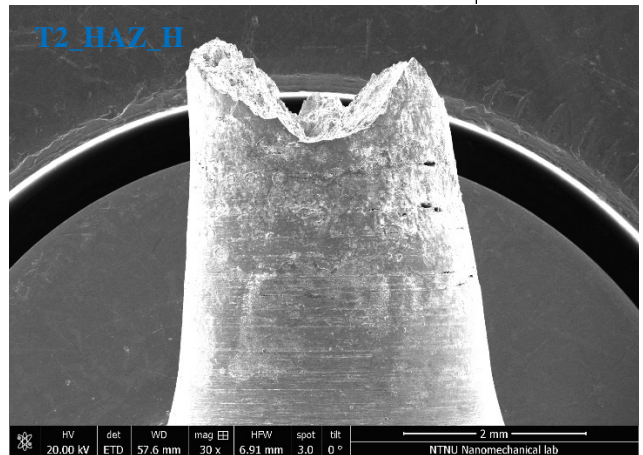
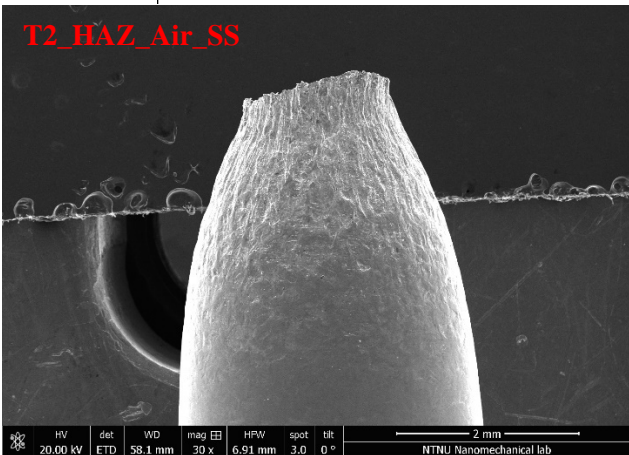
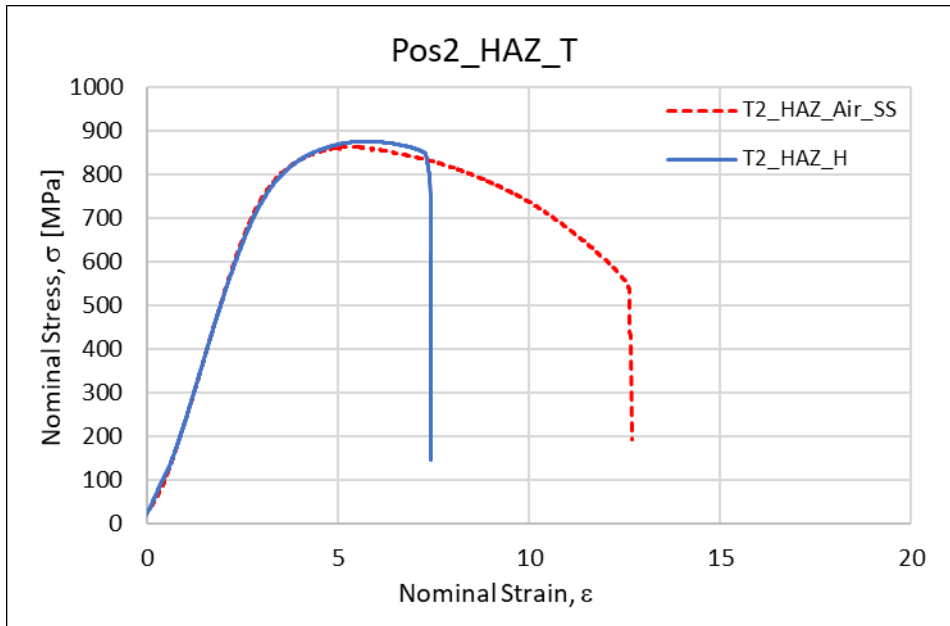


L2_HAZ_H

Surface not available due to corrosion

Fig. 50: Results and post-mortem specimen analysis from SSRT performed on weld simulated HAZ from position 2 of the L-X60 material.

T-X65 position 2 – weld thermal simulated heat affected zone.



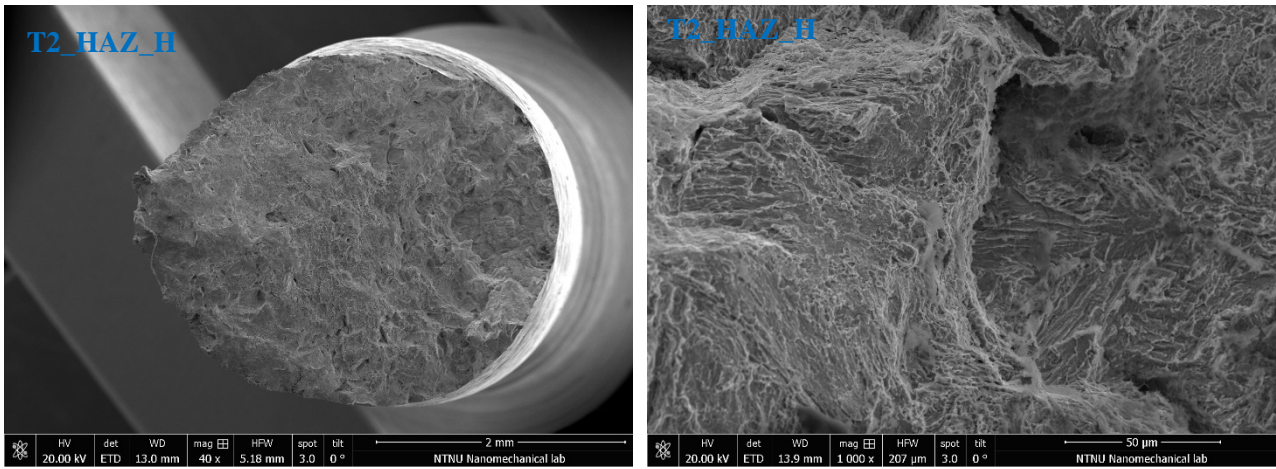


Fig. 51: Results and post-mortem specimen analysis from SSRT performed on weld simulated HAZ from position 2 from the T-X65 material.

3.4.1 Summary of the SSRT results for weld thermal simulated heat affected zone material

All the SSRT results for the weld simulated specimens are summarized in Table 16, in terms of the Embrittlement Index and reduction of ductility, as defined in Eq. 1 and Eq. 2.

Table 16: Summary of the SSRT testing performed on the different weld simulated heat affected zones.

Material	Condition	σ_{\max} [MPa]	$\sigma_{\max,H}/\sigma_{\max,a}$	ϵ_f	z [%]	ϵ_{red} [%]	EI [%]
S2_HAZ	Air_SS	921	0,99	15,8	76,0	63,6	67,1
	CP	910		10,0	25,0		
L2_HAZ	Air-SS	896	0,96	15,8	79,0	61,6	69,6
	CP	862		9,7	24,0		
T2_HAZ	Air-SS	862	1,03	12,6	72,0	58,7	64,0
	CP	887		7,4	25,9		

3.5 Overall summary for the SSRT testing

As a summary, the SSRT test results for the base metals and the weld simulated HAZ indicate that:

- Negligible or no degradation in strength is observed for the materials tested in electrochemically hydrogen charging condition as compared to air while they all to a different extent show loss in ductility. The trends depicted by the relative reduction of area and hydrogen embrittlement index are consistent.
- Surface cracks are observed on all the specimens tested in hydrogen after testing, both at the necked and the uniformly strained section of the specimens.
- Based on the ductility loss of the base metal specimens the L-X60 and S-X65 materials from position 2 of the pipe are the most susceptible to hydrogen, with S-X65 being the overall worst. On the other hand, the T-X65 material is the overall least susceptible.
- All weld simulated heat affected zones (obtained from position 2 of the different materials) revealed similar embrittlement index values. This is consistent with their similar metallurgy and HV_{10} values.
- Fracture surface investigation of BM and weld simulated HAZ in hydrogen consistently shows lateral surface cracks both in the necked and uniaxially stressed material zones. Quasi-cleavage and secondary cracks are typical fracture morphologies. The centre of the specimens, however, shows ductile features (dimples). In proportion, the portion of fracture surfaces which present typical hydrogen affected features (QC facets or secondary cracking) for HAZ is more predominant for HAZ rather than BM.
- The T-X65 material (both in for BM and HAZ) showed more presence of secondary cracks as compared to the others.

A As received material

A.1 S-X65

 SINTEF		PRØVEREGISTRERING	
SINTEF Materialer og kjemi Laboratorium for materialprøving		PROSJEKTNUMMER <div style="text-align: center; font-size: 1.2em;">102017484</div>	
ANKOMST DATO <div style="text-align: center; font-size: 1.2em;">2019.07.09</div>		SIGNATUR VED MOTTAK 	EMBALLASJE <div style="text-align: center; font-size: 1.2em;">Palle</div>
TYPE PRØVE(R)/PRØVEMATERIALE (ANTALL, DIMENSJONER OG MERKING) 2 Stk. Halvdeler Stålrør Merket: 05-A-00040X65 Dimensjoner: L = 1000mm Ø = 770mm Wt = 26mm			
			

Ett eksemplar av skjemaet skal i perm hos verksmester og ett eksemplar i prosjektmappen hos prosjektleder

Vedlegg 7 til KS 24-10 / revisjon 01 / side 1 av 1

A.2 L-X60

 SINTEF		PRØVEREGISTRERING	
SINTEF Materialer og kjemi Laboratorium for materialprøving		PROSJEKTNUMMER 102017484	
ANKOMST DATO 2019.07.09	SIGNATUR VED MOTTAKE 	EMBALLASJE Palle	
TYPE PRØVE(R)/PRØVEMATERIALE (ANTALL, DIMENSJONER OG MERKING) 2 Stk. Halvdeler Stålrør Merket: G13052 Dimensjoner: L = 1000mm Ø = 1100mm Wt = 41mm			
			

Ett eksemplar av skjemaet skal i perm hos verksmester og ett eksemplar i prosjektmappen hos prosjektleder

Vedlegg 7 til KS 24-10 / revisjon 01 / side 1 av 1

A.3 V-X65

 SINTEF		PRØVEREGISTRERING	
SINTEF Materialer og kjemi Laboratorium for materialprøving		PROSJEKTNUMMER <p style="text-align: center; font-size: 1.2em;">102017484</p>	
ANKOMST DATO <p style="text-align: center; font-size: 1.2em;">2019.07.01</p>	SIGNATUR VED MOTTAK 	EMBALLASJE <p style="text-align: center; font-size: 1.2em;">Paller</p>	
TYPE PRØVE(R)/PRØVEMATERIALE (ANTALL, DIMENSJONER OG MERKING) 1 Stk. Stålrør m/langsøm Bitumen Pipe			
Dimensjoner: L = 3000mm Ø = 810mm Wt = 20,7mm			
			

Ett eksemplar av skjemaet skal i perm hos verksmester og ett eksemplar i prosjektmappen hos prosjektleder

Vedlegg 7 til KS 24-10 / revisjon 01 / side 1 av 1

A.4 T-X65

 SINTEF		PRØVEREGISTRERING	
SINTEF Materialer og kjemi Laboratorium for materialprøving		PROSJEKTNUMMER <div style="text-align: center; font-size: 1.2em;">102017484</div>	
ANKOMST DATO <div style="text-align: center; font-size: 1.2em;">2019.07.09</div>		SIGNATUR VED MOTTÅK 	EMBALLASJE <div style="text-align: center; font-size: 1.2em;">Palle</div>
TYPE PRØVE(R)/PRØVEMATERIALE (ANTALL, DIMENSJONER OG MERKING) 3 Stk. Stålrør X-65 1 Stk. Levert Technip Dimensjoner: L = 3000mm Ø = 321mm Wt = 15,4mm			
			

Ett eksemplar av skjemaet skal i perm hos verksmester og ett eksemplar i prosjektmappen hos prosjektleder

Vedlegg 7 til KS 24-10 / revisjon 01 / side 1 av 1

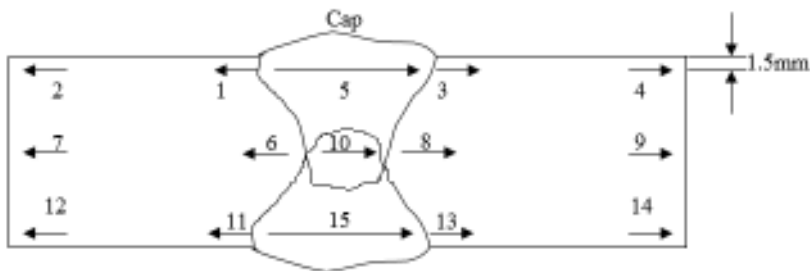
B Hardness analysis

B.1 S-X65

 SINTEF SINTEF Industri Materials Testing Laboratory	VICKERS HARDNESS ON MACRO SECTION OF WELD			
	Id. TEST MACHINE Zwick/Roell ZHV	PERFORMED BY Malin Alette Lervåg	DATE 20.08.2019	PROJECT NO. 102017484

MACRO AND HARDNESS TESTING

Test force: 10 kg



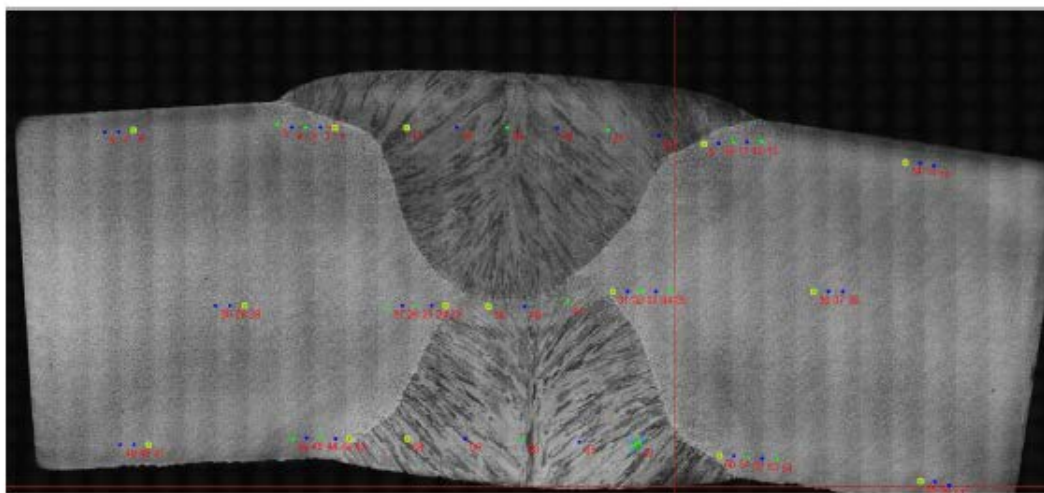
Sketch of the hardness sections.

Vickers Hardness measurements										
Indentation no.	Hardness section no. (see figure above)									
	1	2	3	4	5	6	7	8	9	10
	HAZ	BM	HAZ	BM	WM	HAZ	BM	HAZ	BM	WM
1	205	183	205	192	217	200	182	203	190	204
2	201	182	201	191	214	178	185	190	190	201
3	199	185	200	188	214	179	187	173	188	197
4	194		194		218	184		187		
5	180		173		217	192		188		
6					217					
7										
8										
9										
10										
Max.	205	185	205	192	218	200	187	203	190	204

Vickers Hardness measurements					
Indentation no.	Hardness section no. (see figure above)				
	11	12	13	14	15
	HAZ	BM	HAZ	BM	WM
1	205	182	208	187	210
2	198	181	202	188	209
3	188	183	183	190	206
4	189		190		207
5	192		194		211
6					
7					
8					
9					
10					
Max.	205	183	208	190	211

 SINTEF SINTEF Industri Materials Testing Laboratory	VICKERS HARDNESS ON MACRO SECTION OF WELD		
	Id. TEST MACHINE Zwick/Roell ZHV	PERFORMED BY Malin Alette Lervåg	DATE 20.08.2019

Corresponding macrograph with indentations. (The ruler pitch is 1 mm)

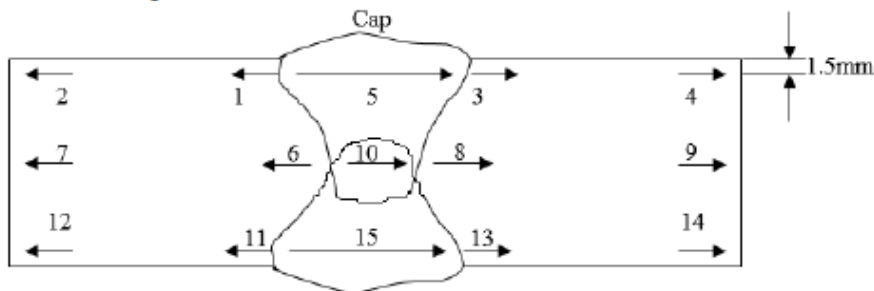


B.2 L-X60

 SINTEF SINTEF Industri Materials Testing Laboratory	VICKERS HARDNESS ON MACRO SECTION OF WELD		
	Id. TEST MACHINE Zwick/Roell ZHV	PERFORMED BY Malin Alette Lervåg	DATE 22.08.2019

MACRO AND HARDNESS TESTING

Test force: 10 kg



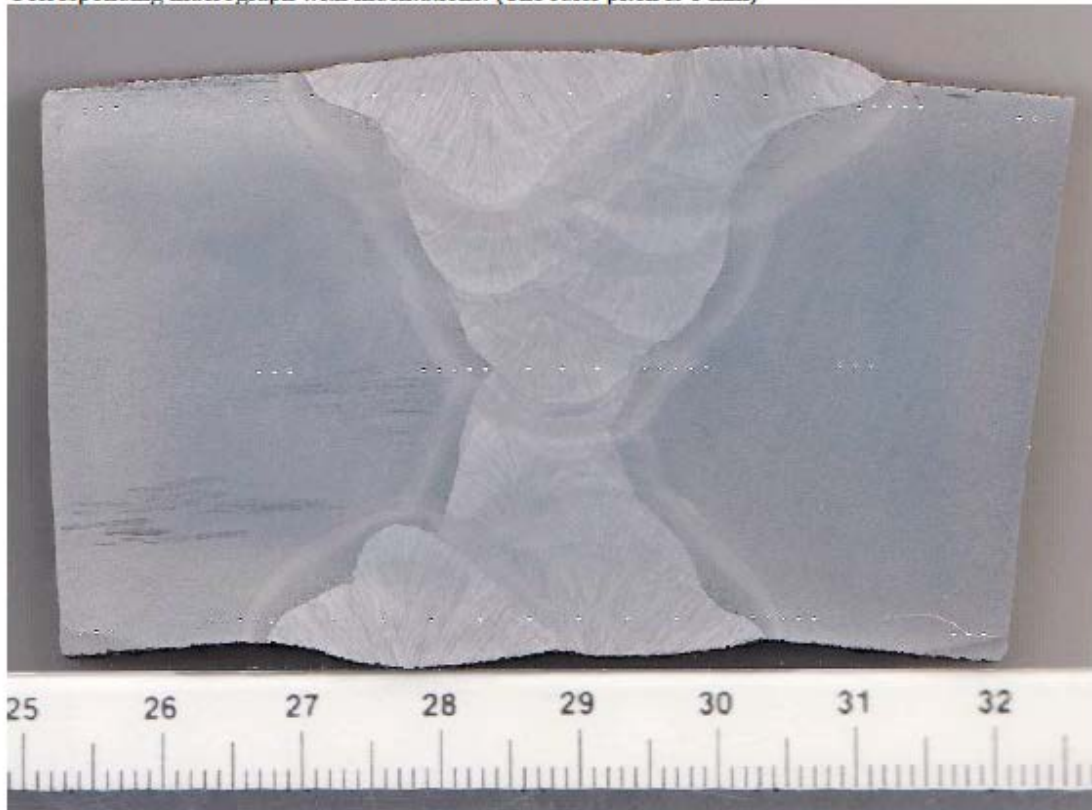
Sketch of the hardness sections.

Vickers Hardness measurements										
Indentation no.	Hardness section no. (see figure above)									
	1 HAZ	2 BM	3 HAZ	4 BM	5 WM	6 HAZ	7 BM	8 HAZ	9 BM	10 WM
1	215	192	219	186	220	218	187	226	183	221
2	208	197	214	184	230	211	192	220	179	229
3	181	195	199	180	229	208	186	209	181	225
4	206		195		227	197		199		
5	203		194		228	200		192		
6					223					
7					210					
8					215					
9					229					
10					223					
Max.	215	197	219	186	230	218	192	226	183	229

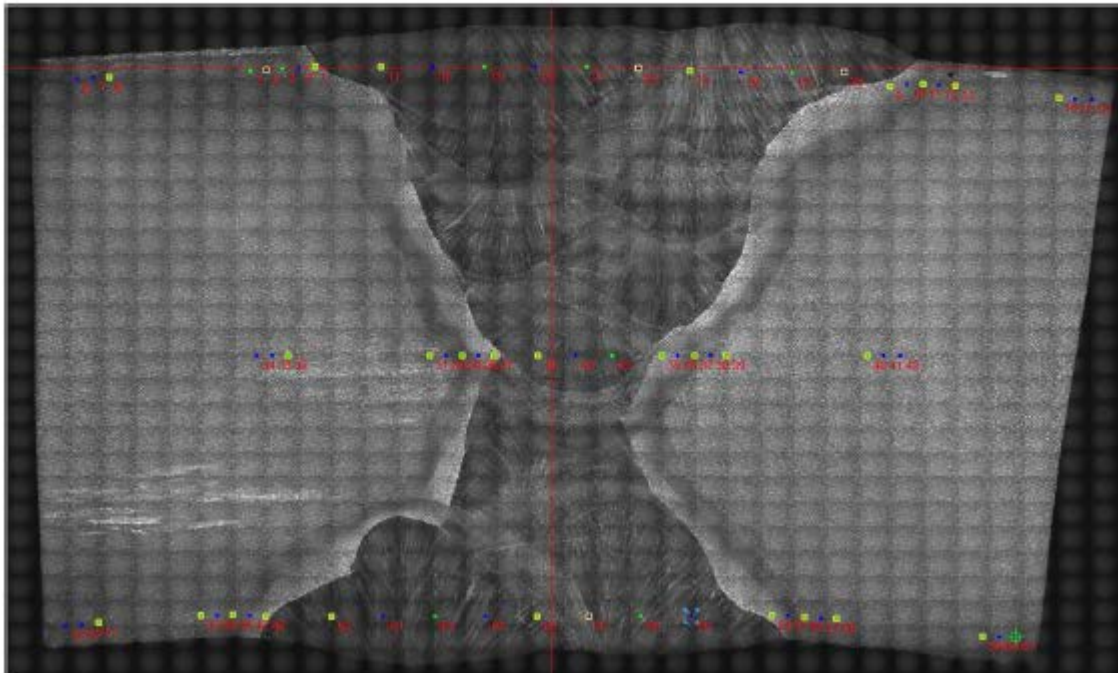
Vickers Hardness measurements					
Indentation no.	Hardness section no. (see figure above)				
	11 HAZ	12 BM	13 HAZ	14 BM	15 WM
1	218	189	206	201	223
2	210	204	206	182	224
3	207	205	206	199	222
4	198		213		221
5	208		213		217
6					204
7					215
8					217
9					
10					
Max.	218	205	213	201	224

 SINTEF SINTEF Industri Materials Testing Laboratory	VICKERS HARDNESS ON MACRO SECTION OF WELD		
	Id. TEST MACHINE Zwick/Roell ZHV	PERFORMED BY Malin Alette Lervåg	DATE 22.08.2019

Corresponding macrograph with indentations. (The ruler pitch is 1 mm)



 SINTEF SINTEF Industri Materials Testing Laboratory	VICKERS HARDNESS ON MACRO SECTION OF WELD		
	Id. TEST MACHINE Zwick/Roell ZHV	PERFORMED BY Malin Alette Lervåg	DATE 22.08.2019

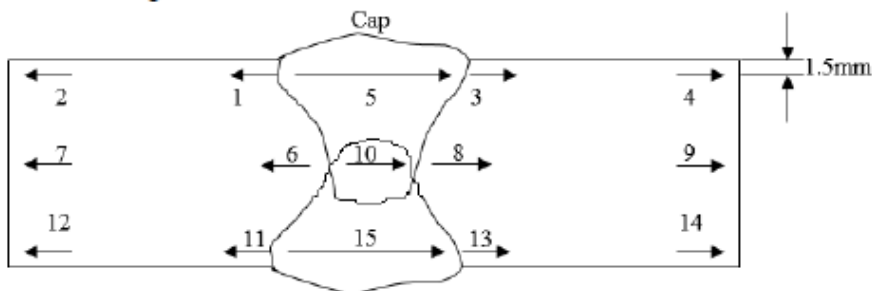


B.3 V-X65

 SINTEF SINTEF Industry Materials Testing Laboratory	VICKERS HARDNESS ON MACRO SECTION OF WELD			
	Id. TEST MACHINE Zwick/Roell ZHV	PERFORMED BY Malin Alette Lervåg	DATE 04.09.2019	PROJECT NO. 102017484-5

MACRO AND HARDNESS TESTING


Test force: 10 kg



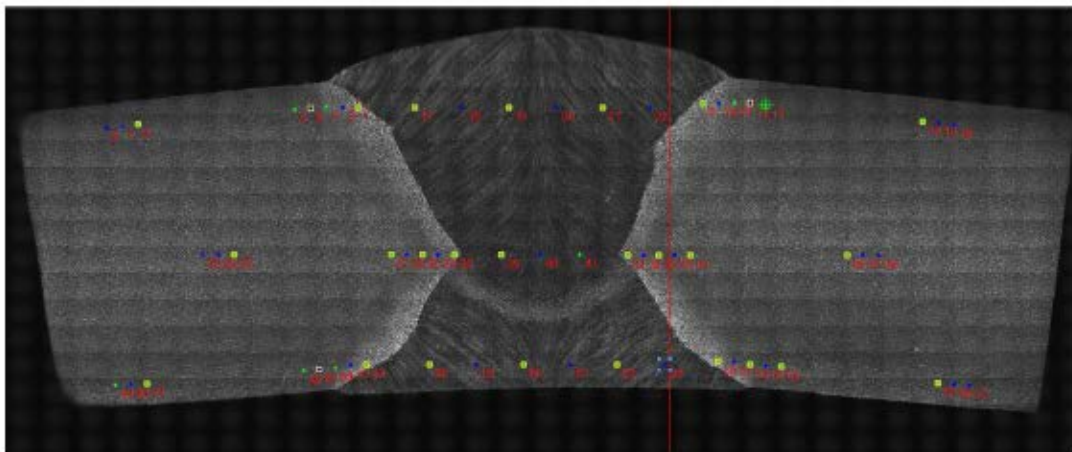
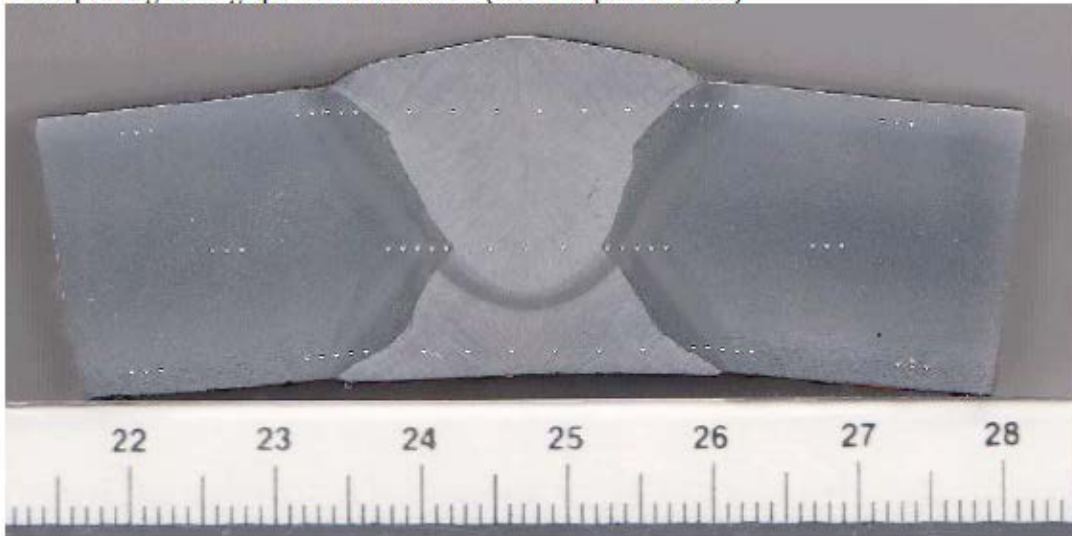
Sketch of the hardness sections.

Indentation no.	Vickers Hardness measurements									
	Hardness section no. (see figure above)									
	1 HAZ	2 BM	3 HAZ	4 BM	5 WM	6 HAZ	7 BM	8 HAZ	9 BM	10 WM
1	218	188	218	191	217	226	189	223	195	213
2	208	187	208	193	215	203	189	200	199	214
3	193	187	192	194	215	176	191	180	199	219
4	178		178		218	180		183		
5	190		198		215	189		189		
6					219					
7										
8										
9										
10										
Max.	218	188	218	194	219	226	191	223	199	219

Indentation no.	Vickers Hardness measurements				
	Hardness section no. (see figure above)				
	11 HAZ	12 BM	13 HAZ	14 BM	15 WM
1	217	197	218	203	221
2	205	195	210	205	224
3	188	196	198	204	231
4	197		212		229
5	201		217		222
6					217
7					
8					
9					
10					
Max.	217	197	218	205	231

 SINTEF SINTEF Industry Materials Testing Laboratory	VICKERS HARDNESS ON MACRO SECTION OF WELD			
	Id. TEST MACHINE Zwick/Roell ZHV	PERFORMED BY Malin Alette Lervåg	DATE 04.09.2019	PROJECT NO. 102017484-5

Corresponding macrograph with indentations. (The ruler pitch is 1 mm)

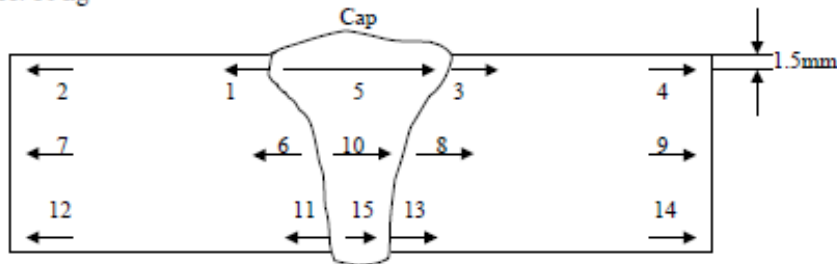


B.4 T-X65

 SINTEF SINTEF Industri Materials Testing Laboratory	VICKERS HARDNESS ON MACRO SECTION OF WELD		
	ID. TEST MACHINE Zwick/Roell ZHV	PERFORMED BY Malin Alette Lervåg	DATE 25.09.19

MACRO AND HARDNESS TESTING

Test force: 10 kg



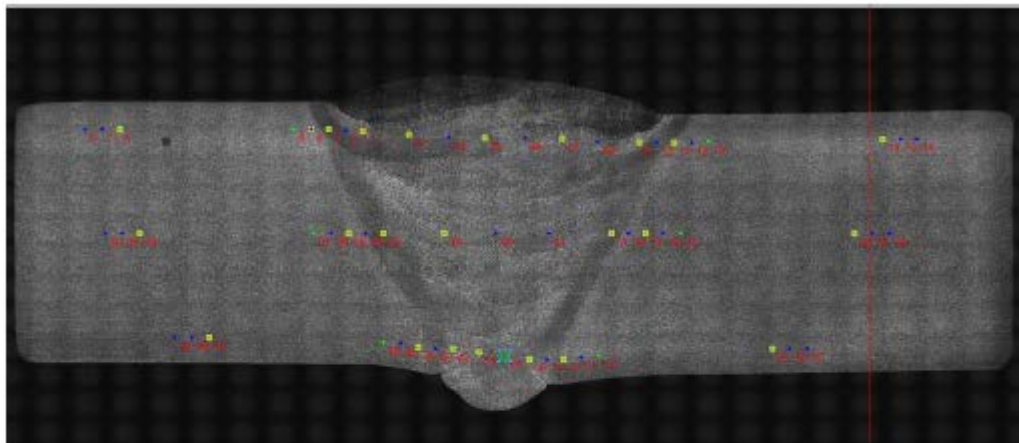
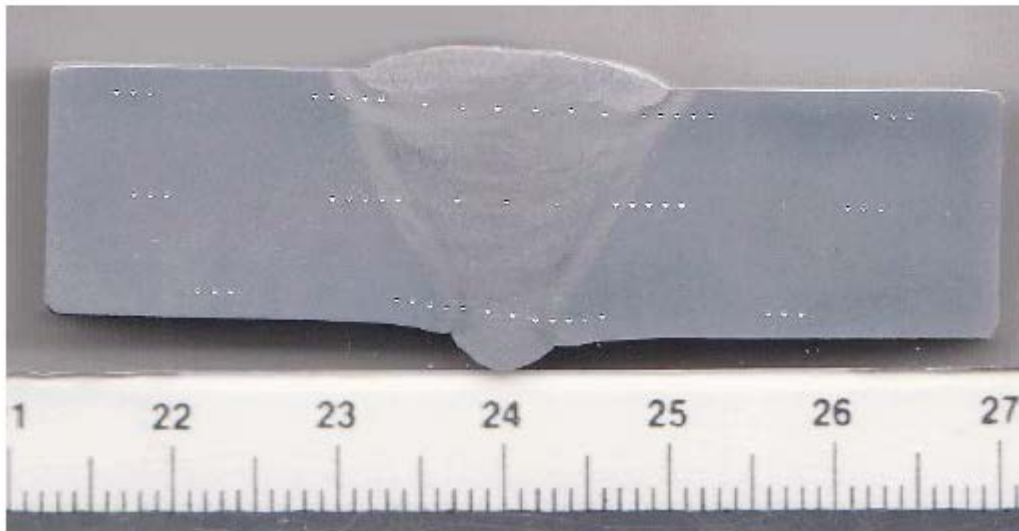
Sketch of the hardness sections.

Vickers Hardness measurements										
Indentation no.	Hardness section no. (see figure above)									
	1 HAZ	2 BM	3 HAZ	4 BM	5 WM	6 HAZ	7 BM	8 HAZ	9 BM	10 WM
1	221	183	219	183	219	184	190	180	192	199
2	208	184	194	182	206	178	184	178	190	198
3	196	183	184	182	207	185	189	196	190	204
4	181		182		215	188		199		
5	187		188		208	193		198		
6					220					
7										
8										
9										
10										
Max.	221	184	219	183	220	193	190	199	192	204

Vickers Hardness measurements					
Indentation no.	Hardness section no. (see figure above)				
	11 HAZ	12 BM	13 HAZ	14 BM	15 WM
1	206	202	201	203	205
2	200	203	202	202	205
3	204	205	193	201	
4	204		203		
5	213		209		
6					
7					
8					
9					
10					
Max.	213	205	209	203	205

 SINTEF SINTEF Industri Materials Testing Laboratory	VICKERS HARDNESS ON MACRO SECTION OF WELD		
	Id. TEST MACHINE Zwick/Roell ZHV	PERFORMED BY Malin Alette Lervåg	DATE 25.09.19

Corresponding macrograph with indentations. (The ruler pitch is 1 mm)



C TECHNIP GIRTH WELD CERTIFICATE FOR T-X65 MATERIAL

NEPTUNE ENERGY		Welding Procedure Specification				TechnipFMC																					
Project name		Fenja		WPS No.		075688C001-ONT-FEN-GLGI-LC1-WPS10A																					
Project No.		075688C001		Position		PH/5G Joint type 25° V																					
Procedure description		Onshore Tie-in and Cut Out		Supporting WPQR		068047C001-O-ONT-OSE-GI-WPQR10 Rev. 0																					
Client		Neptune Energy		Client spec		TR1096 Rev. 5.02																					
Process description		Manual GTAW		Test Code		DNV-OS-F101 Rev. 2013																					
Base Material	Material A		Material B																								
	Grade		DNV SMLS 450 SFPDU		DNV SMLS 450 SFPDU																						
	Supply / Delivery Condition		Q- Quenched & Tempered		Q- Quenched & Tempered																						
	Steel Supplier		Nippon Steel & Sumitomo Corporation		Nippon Steel & Sumitomo Corporation																						
	Nominal Inner Diameter		ID [mm] 242,30	ID [inch] 9 1/2	ID [mm] 242,30	ID [inch] 9 1/2																					
	Nominal Outer Diameter		OD [mm] 273,10	OD [inch] 10 3/4	OD [mm] 273,10	OD [inch] 10 3/4																					
	Nominal Wall Thickness		WT [mm] 15,40	WT [inch] 3/5	WT [mm] 15,40	OD [inch] 3/5																					
	DNV OS-F101:2013- Pipe Tolerance [mm]		ID 240,9 - 243,7	W.T. 13,86 - 16,94	ID 240,9 - 243,7	W.T. 13,86 - 16,94																					
	Chemical Composition WPS material [wt%]		P _{CMn} 0,15	C: 0,06	P _{CMn} 0,15	C: 0,06																					
	Chemical Composition Qualified Max [wt%]		P _{CMn} 0,17	C: 0,08	P _{CMn} 0,17	C: 0,08																					
Consumable	Consumable 1		Consumable 2		Consumable 3																						
	Make		ESAB																								
	Brand		OK Tigrod 13.23																								
	Batch		as per wirelist																								
Gas	Gas 1		Gas 2		Gas 3																						
	Gas Type		Shielding Gas																								
	Classification and Designation		ISO 14175 - 11 (99,998)																								
	Mixture		Ar 4.8 (99.998 % Ar)																								
Nozzle Diameter [mm]		15-20																									
Flow rate [L/min]		17-20																									
Details	Clamp Type		External Clamp		Removal of Bullets/Tacks		Earliest after HP completion																				
	Cont. Tip to W. D. [mm]		N/A		Oscillation Rate [BPM]		N/A																				
	Cont. Tube to W. D. [mm]		N/A		Weave Width [mm] *		8,5																				
	S.W.D.T.		N/A		Electrical Stick-out		N/A																				
	Software		N/A		Synergy pGMAW		N/A																				
	CMT Synergy		N/A		Min preheat [°C]		100 (Propane)																				
	Number of welders		2		Max T before cool [°C]		350 (Forced air/water)																				
	Electrode		2.4 mm Tungsten, WT20		Flux		N/A																				
	Max HILLO:				Welding Equipment		Root / Hot Pass / Fill / Cap Lincoln Square Wave TIG 355 or Lincoln Precision TIG 375																				
					Maximum interpass [°C]		250																				
				Time between R & HP		Welding Cont.																					
				Dual / Single Torch		N/A																					
Weld sketch	Weld Preparation				Pass Sequence																						
					<table border="1"> <thead> <tr> <th>Layer</th> <th>1</th> <th>2</th> <th>3</th> <th>4</th> <th>5</th> <th>6</th> <th>7</th> <th>8</th> <th>Tot</th> </tr> </thead> <tbody> <tr> <td>Height of each layer, indicative</td> <td>2,0</td> <td>1,5</td> <td>1,5</td> <td>4</td> <td>5</td> <td>6</td> <td>7</td> <td>8</td> <td>15,4</td> </tr> </tbody> </table>				Layer	1	2	3	4	5	6	7	8	Tot	Height of each layer, indicative	2,0	1,5	1,5	4	5	6	7	8
Layer	1	2	3	4	5	6	7	8	Tot																		
Height of each layer, indicative	2,0	1,5	1,5	4	5	6	7	8	15,4																		
Parameters	Pass No.	Weld Process / Direct.	Arc Characteristic	Consumable	Gas	Polarity	Current [A]		Volts [V]	Travel Speed [mm/s]	Wire Feed Speed [m/min]	Heat Input [KJ/mm]															
					Shield	Purge	min	max	min	max	min	max	avg														
	Root	141 ↑		Cons. 1	Gas 1		DC -ve	100 - 157	8,4 - 10,4	0,8 - 1,4	-	1,0 - 1,5	1,3														
	Hot Pass	141 ↑		Cons. 1	Gas 1		DC -ve	140 - 236	8,5 - 10,9	1,4 - 1,7	-	0,9 - 1,4	1,1														
	1st Fill	141 ↑		Cons. 1	Gas 1		DC -ve	163 - 240	8,6 - 11,7	1,6 - 2,0	-	1,0 - 1,5	1,2														
	Fill	141 ↑		Cons. 1	Gas 1		DC -ve	190 - 278	9,0 - 12,8	1,4 - 2,1	-	1,3 - 1,9	1,6														
Cap	141 ↑		Cons. 1	Gas 1		DC -ve	163 - 249	9,0 - 12,7	1,3 - 2,1	-	1,1 - 1,6	1,4															
Notes	<ol style="list-style-type: none"> All starts and stops ground for all passes. * Max stringer/weave to transition is 3 x electrode diameter (7,2) Consumable batch according wire list Any moisture to be removed with clean rags soaked in solvent before welding WPS qualified from 068047C001-O-ONT-OSE-GI-WPQR10 (Weld no. WP10-01) 20% HI included in WPS, ref Method Statement - Calculation of Heat Input, OSB-M518-01 																										
	TechnipFMC						TechnipFMC																				
	Prepared by						Approved by																				
	OSB Welding Engineer						OSB Engineering Manager																				
	Hilde Skauge						MARI SKAUGE																				
	Date: 15/11/19						Date: 13/11/19																				
Welding Engineer						OSB Safety																					
TechnipFMC						TechnipFMC																					
Neptune Energy/3. party						Date, Sign:																					
Welding Procedure Specification 075688C001-FEN-10°-GLGI-LC1-WPS- Rev 0																											



Technology for a better society

www.sintef.no